Conformations and Interactions of Star-Branched Polymeric Systems

Inaugural–Dissertation
zur
Erlangung des Doktorgrades der
Mathematisch-Naturwissenschaftlichen Fakultät
der Heinrich-Heine-Universität Düsseldorf

vorgelegt von

ARBEN JUSUFI

aus Ratingen

Düsseldorf, 4. Februar 2002

Gedruckt mit Genehmigung der
Mathematisch-Naturwissenschaftlichen Fakultät
der Heinrich-Heine-Universität Düsseldorf

Referent: Prof. Dr. H. Löwen
Koreferent: Hochschul-Doz. C. N. Likos, PhD

Tag der mündlichen Prüfung: 24. Mai 2002

This thesis is based on the following original papers:

Chapter 3 and Appendix C:

A. Jusufi, C. N. Likos, and H. Löwen,
Conformations and interactions of star-branched polyelectrolytes,
Physical Review Letters **88**, 018301 (2002).

A. Jusufi, C. N. Likos, and H. Löwen,
Counterion-induced entropic interactions in solutions of strongly stretched, osmotic polyelectrolyte stars,
The Journal of Chemical Physics **116**, 11011-11027 (2002).

Chapter 4:

A. Jusufi, J. Dzubiella, C. N. Likos, C. von Ferber, and H. Löwen,
Effectice interactions between star polymers and colloidal particles,
Journal of Physics: Condensed Matter **13**, 6177-6194 (2001).

J. Dzubiella, A. Jusufi, C. N. Likos, C. von Ferber, H. Löwen, J. Stellbrink,
J. Allgaier, D. Richter, A. B. Schofield, P. A. Smith W. C. K. Poon, and P. N. Pusey,
Phase separation in star polymer-colloid mixtures,
Physical Review E **64**, 010401(R) (2001).

J. Dzubiella and A. Jusufi,
Star-polymer-colloid mixture,
Condensed Matter Physics **5**, Vol. 2 (30) (2002).

Appendix A:

C. von Ferber, A. Jusufi, C. N. Likos, H. Löwen, and M. Watzlawek,
Triplet interactions in star polymer solutions,
European Physical Journal E **2**, 311-318 (2000).

Abstract

We examine the conformations and effective interaction potentials for two classes of star-branched polymeric materials. The work consists essentially of two parts: the investigation of the interaction potential between two polyelectrolyte stars (PE-stars), and between an uncharged star polymer and a hard colloidal particle of varying curvature. While in the latter case we can take use of wide knowledge of pure star polymers in terms of their conformations, in the case of PE-stars we have to develop a convenient theoretical model to study conformational properties of an isolated PE-star. We observe a strong "trapping"-effect of the inhomogeneously distributed counterions within the PE-star, as well as significant counterion condensation along the chains, which are almost fully stretched. We use these one-star results, also confirmed by monomer-resolved Molecular Dynamics computer simulations with explicit consideration of counterions, for an extension of the theory to the two-star case. Based on variational free energy calculations we compute, in addition to conformational properties, the effective interaction potential between two PE-stars. In this context, we have to account for the strongly inhomogeneous charge distribution of PE-stars, and the possibility of counterion condensation. As a result, we obtain a non-linear ultra-soft repulsion between two PE-stars, induced mainly by the entropic contribution of the counterions. We compare these theoretical results with data obtained from Molecular Dynamics simulations of two stars for a wide range of parameter combinations, including the addition of salt. We also propose an analytical expression for the effective pair potential between two PE-stars for all distances and physical parameters: a combination of a power-law repulsion at close separations and a Yukawa decay at larger distances. In the case of star-polymer-colloid mixture, we start with a consideration of a star polymer at a hard wall and expand the model to that of a star polymer at a spherical colloid, considering a wide range of size ratios between the two. The mean force acting on the star has been compared with results from Molecular Dynamics simulations. As in pure star polymer solutions for low arm numbers, we obtain again two parts for the effective interaction between a star and a wall or a sphere: a logarithmic repulsion at close separations, and a Gaussian decay at distances beyond overlap. In both cases, for PE-stars as well as for a star-polymer-colloid mixture, we obtain very good agreement between theory and simulation, enabling future work on the systems considered, concerning the structural and phase properties of many-body systems consisting of such macromolecules.

Zusammenfassung

Die vorliegende Arbeit befaßt sich mit der Bestimmung der effektiven Wechselwirkung in komplexen Systemen, verdeutlicht an zwei Beispielen aus der aktuellen Forschung auf dem Gebiet der weichen Materie. Zum einen berechnen wir das effektive Wechselwirkungspotential zwischen zwei sternförmigen Polyelektrolyten (PE-Sterne), zum anderen bestimmen wir dieselbe Größe zwischen einem ungeladenen Sternpolymer und einem harten kolloidalen Teilchen. Während letzteres, aufbauend auf Erkenntnissen detaillierter theoretischer und experimenteller Untersuchungen, analysiert werden kann, sind wir im Fall von PE-Sternen, aufgrund unzureichend vorhandener Ergebnisse auf diesem Gebiet, gezwungen ein theoretisches Modell zu entwickeln, um zunächst genauere Einsichten über ihre Konformation zu erhalten. Mithilfe von Molekular Dynamik Simulationen eines isolierten PE-Sterns mit expliziter Berücksichtigung der Gegenionen, ist es möglich Theorie- und Simulationsergebnisse direkt miteinander zu vergleichen. Wir beobachten eine inhomogene Gegenionenverteilung im Bereich des Inneren des Sterns, sowie eine deutliche Gegenionenkondensation entlang der fast völlig gestreckten Ketten. Auf diesen Erkenntnissen der Ein-Stern-Studie basierend, erweitern wir das Ein-Stern-Modell auf ein Zwei-Sterne-Modell um die effektive Wechselwirkung zu bestimmen. In diesem Zusammenhang berücksichtigen wir die stark inhomogene Ladungsverteilung der Sterne, sowie die Möglichkeit der Gegenionenkondensation; die Behandlung dieser Aspekte stellt ein Novum bei der Untersuchung dieser Systeme dar. Mit Hilfe der Variation der freien Energie wird das effektive Wechselwirkungspotential zwischen zwei PE-Sternen gewonnen und mit Daten aus unseren Molekur Dynamik Simulationen verglichen. Als Ergebnis beobachten wir ein nichtlineares, extrem weiches Abstossungspotential zwischen den Sternen, hauptsächlich verursacht durch die Gegenionenentropie. Diese Voraussage stimmt sehr gut überein mit unseren Simulationsdaten, und zwar für eine weite Auswahl von Parameterkombinationen, wobei die Betrachtung eines salzhaltigen Systems eingeschlossen ist. Zudem geben wir einen aus zwei Anteilen bestehenden analytischen Ausdruck für das effektive Paarpotential zwischen zwei PE-Sternen an: ein extrem weiches Potenzgesetz für kleine Abstände, und ein Yukawa-Abfall für Abstände jenseits der Überlappung der Sterne. Die Abstoßung ist zwar auf absoluter Skala größer gegenüber neutralen Sternen, sie fällt jedoch "weicher" ab. Im Falle der Sternpolymer-Kolloid Mischung berechnen wir zunächst die mittlere Kraft, die ein Stern in der Nähe einer harten Wand erfährt. Anschließend erweitern wir das Modell auf ein Sternpolymer an einem sphärischen Kolloidteilchen. In beiden Fällen ist das Ergebnis für die Paarwechselwirkung änhlich der der Wechselwirkung zweier Sternpolymere kleiner Armzahl: ein ultra-weiches logarithmisches Wechselwirkungspotential für kleine Abstände, und ein Gauss'scher Abfall jenseits der Überlappung. In beiden in dieser

Arbeit vorgestellten Fällen, sowohl für Polyelektrolytsterne, als auch für die Sternpolymer-Kolloid-Mischung, erhalten wir eine sehr gute Übereinstimmung zwischen Theorie und Simulation. Wir eröffnen mit der Angabe eines analytischen Ausdrucks für die effektive Wechselwirkung die Möglichkeit für künftige Untersuchungen, wie beispielsweise das Studium des Phasenverhaltens oder der strukturellen Eigenschaften dieser Makromoleküle.

Contents

1 Introduction **1**

2 Conformations and Effective Interactions of Polymers **7**
2.1 Conformations of polymers 7
2.1.1 Ideal and real chain models 10
2.1.2 The solvent effect 12
2.1.3 The charge effect 14
2.1.4 Experimental methods 18
2.2 The concept of the effective interaction 19
2.2.1 The effective Hamiltonian 19
2.2.2 The effective interaction potential 22
2.2.3 The measurement of the effective Hamiltonian 24

3 Star-shaped Polyelectrolytes **26**
3.1 Dilute solutions: sizes and conformations of isolated PE-stars 27
3.1.1 The simulation model 28
3.1.2 The density profile 31
3.1.3 Theory of isolated polyelectrolyte-stars 32
3.1.4 An isolated star with added salt 40
3.2 Concentrated solutions: effective interactions between PE-stars 41
3.2.1 Theory 42
3.2.2 Results for the effective interaction 47
3.2.3 Interacting stars in the presence of added salt 54
3.3 Summary and concluding remarks 55

4 Effective Interaction between Star Polymers and Colloids **57**
4.1 Theory 58
4.1.1 A star polymer and a flat wall 59
4.1.2 A star polymer and a spherical colloid 63
4.2 Simulation 66
4.2.1 The simulation model 66
4.2.2 Star-wall and star-colloid interactions 67

4.3 Revised star-star interaction for small arm numbers 74
4.4 Summary and concluding remarks 76

5 Conclusions and Outlook **78**

List of Abbreviations **82**

Appendix

A Triplet interactions in star polymer solutions **83**
A.1 Theoretical predictions for three stars 84
A.2 Comparison with simulation results 85
A.3 Conclusions 88

B The Lekner method **90**

C Electrostatic potential for a chopped sphere **93**
C.1 Calculation of the electrostatic potential Φ_{in} 93
C.2 Calculation of the electrostatic potential Φ_{out} 98

Bibliography **99**

Acknowledgement **107**

Chapter 1

Introduction

The concept of effective interaction is one of the most important tools in statistical physics. Especially for the study of complex fluids the knowledge of the effective interaction between the involved particles opens a gate for further investigations. To understand this one should be aware on the characteristics of complex fluids and the problems which arise in studying those systems.

Complex fluids are, in contrast to so-called simple fluids, multicomponent systems. The involved particles can disperse in size and in other physical quantities like charges. Geometrical asymmetries itself increase the complexity due to ensuing different length and time scales, on which the system has to be considered. Consider for example charged colloids in a salted solution, there are at least three different length scales: the microscale of the solvent, the nanoscale of the counter- and coions, some typical electrostatic quantities like the Debye length on nanoscale as well, and finally the size of the colloidal particle itself on mesoscale (1nm-1μm). In addition all mentioned particles have different timescales as well, since, e.g., their diffusion times differ in similar orders of magnitudes as the associated length scales. In computer simulations, like in Molecular Dynamics (MD) or Monte Carlo (MC) simulations, one has to deal with timesteps, typically in femtosecond scale, in order to regard the movement of the smallest particles in the convenient way. For investigations of large-scale phenomena of the colloidal particle over times of milliseconds, even special techniques like multiple-timestep methods [1, 2], cannot effort the required simulation expenses. It is therefore desireable and beneficial to develop a method which can bridge the ensuing length and time scales in order to enable a systematic study of large-scale phenomena, like structural correlations or the phase behavior of the complex fluid.

The basic idea of the mentioned concept of effective interaction is to "trace" out the microscopic degrees of freedom of all particles except of the particle we are interested for. In the above mentioned example we integrate out the degrees of freedom of the solvent molecules, the counter- and coions, in order to obtain a so-called effective interaction between the colloidal particles only. This effective interaction include in contrast to the "bare" interactions of the colloids all interaction components of the smaller particles implicitely.

For example, in the so-called Asakura Oosawa (AO) model of a colloid-polymer mixture [3], where colloids are hard spheres, i.e. their "bare" interaction is infinite at contact and zero elsewhere, further hard-core interactions between the polymers and the colloids, but no interaction at all between polymers, the so-called depletion effect occurs. By tracing out the degrees of freedom of the polymers one obtains the effective interaction between the colloids. In fact one coarse-graine the system in this way. The colloids even acquire an attractive contribution in their effective interaction potential. The knowledge of the effective interaction between the colloids enables then a structural analysis of the colloidal system, i.e. one investigate the system on mesoscopic lengthscales. In this way, one bridge existing lengthscales of the polymers to the lengthscale of the colloids.

Another example of complex fluids are polymer solutions themselves. They are complex and provide a multicomponent system in nature, even though the solvent is considered to be "only" a "smeared" background. Polymers have an internal conformation, formed by chains of so-called monomers. Here, the microscopic degrees of freedom, the monomer coordinates and momenta, result from the monomers, which are themselves the constituent of the colloidal particle, the polymer. Hence, a formulation of the effective interaction between the polymers requires the knowledge of the conformation of the polymer. Polymers with globule shapes may have different interaction potentials than coil-shaped polymers. The different polymer phases appears due to their behavior in solution. This leads to the question of the flexibility of the chain, which determines the polymer conformation, and finally the effective interaction between the polymers. The above mentioned AO model treats the polymers as non-interacting particles, but this is not always true. In fact, one obtains a Gaussian interaction potential [4], based on a conformational analysis of isolated chains. On the other side, polymers show also an ultra-soft logarithmic potential at close separations for self-avoiding chains, i.e. in good solvents [5]. It is also important to know which parameters influence the flexibility of the chain, and therefore the conformation. Two examples for such parameters are the solvent quality and, eventually charges in the case of charged polymers, so-called polyelectrolytes (PEs).

In this work we consider a special architecture of polymeric systems, so-called star-branched polymers. In contrast to linear polymers, which are studied extensively [6, 7, 8, 9, 10] just in the past years star polymers have been subject of wide interest in soft matter physics, (for a review see e.g. [11]). Star polymers are systems of linear polymers that are grafted at a common microscopic core. By tuning the arm number or the functionality, f, they build an important link between linear polymers ($f = 1, 2$) and steric-stabilized colloids ($f \gg 1$), as depicted in Fig. 1. Star polymer solutions find applications as stabilization components in colloidal systems, due to their steric repulsion against the van der Waals attraction acting between the star polymer cores, at which the chains are grafted. They are also applied as viscoelastic fluid in oil industry. But even in basic research they are of large interest. Star polymers have been studied by theoretical methods [12, 5], experiments [13, 14, 15, 16, 17] and computer modeling [18, 19, 20, 21, 22, 23], concerning their static

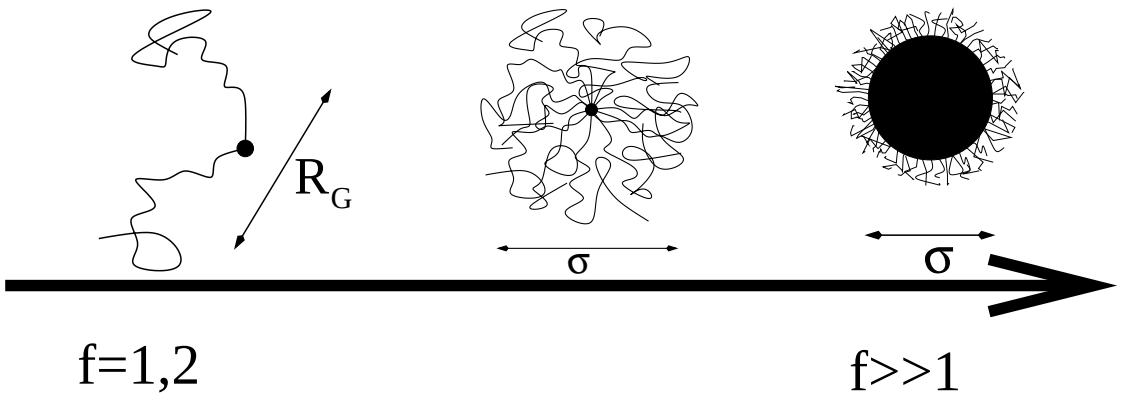

Figure 1.1: Illustration of a star polymer (in the middle) providing a link between linear polymers (left sketch) and steric stabilized colloids (right sketch). The sizes are denoted by the radius of gyration R_g or the diameter σ.(Courtesy of Martin Watzlawek.)

properties as well as in relation to their dynamical properties [24, 25, 26]. They belong to the class of ultra-soft interacting particles [27, 28, 29, 30] and provide a comprehensive phase behavior with exotic crystal symmetries [31, 32]. Due to their internal structure they constitute a challenge in formulation of an effective interaction potential. With the help of scaling theory [12, 5] it was possible to develop an effective interaction [27, 28] and to take it as a starting quantity for further investigations like their phase behavior [31, 32, 33].

In contrast to pure star polymer solutions (in the sense that there are no other colloidal particles in the solution), mixtures of star polymers with truly hard colloids have only been investigated quite recently. In realistic systems star polymers often occur in a mixture with colloidal particles. Again, a theoretical prediction of the phase behavior of this binary mixture is enabled by constructing an effective interaction between the involved particles [34, 35, 36]; the development of the effective interaction between star polymers and colloidal particles is part of this work.

A further and more challenging star-like system are polyelectrolyte stars (PE-stars), i.e., star polymers containing monomers along the chains, which dissociate so-called counterions into the solution; the whole system is electrical neutral. The challenge consists of the fact that those systems establish a link between soft matter systems with internal structure on one side, and an electrostatic system with strongly inhomogeneous charge distribution on the other. The coupling of statistical mechanics and electrostatics results in some interesting effects, like the so-called counterion (Manning-)condensation [37], where the electrostatic attraction between the counterions and the oppositely charged monomers wins against its competitive counterion entropy. This kind of effect and the variation of the additional parameter "charge" lead to interesting conformational phase behaviors of the star, expected

to range from fully stretched chains up to collapsed globules. A rich phase diagram has been proposed by Schiessel et al. in the case of linear polyelectrolyte solutions [38]. A similar behavior for stars can be expected.

Analogously to neutral star polymers, PE-stars provides a link between linear PEs ($f = 1, 2$) and charged colloids, ($f \gg 1$), according to Fig. 1. Since the charge offers an additional tuning parameter PE-star solution can be more efficient in terms of their stability against coagulation than "usual" steric- or charged stabilized colloids. Moreover, star-branched PEs can be viewed as a combination of steric- and charged stabilized colloidal particles. It can be expected that not only the repulsion between PE-stars is higher, than for example the DLVO repulsion between charged colloids [39, 40], also their strength can be tuned by more parameters like by the functionality f, by the charge fraction along the chains, as well as by the salt concentration.

In contrast to neutral star polymers, their charged counterparts have not been understood in full detail. An experimental investigation requires a convenient sample, which is relativly difficult to prepare chemically. In addition one has to take account of the counterions, which can disturb a bare observation of the stars only. Recently there have been carried out some X-ray scattering of a dilute PE-star solution [41]. Similar objects like colloidal polyelectolyte brushes, are also subject of recent research interest in this field [42, 43, 44]. From the theoretical point of view there have been studies of the internal structure of isolated PE-stars [45, 46, 47, 48]. Pincus considered two of such stars but could only give somewhat qualitative predictions for the effective interaction between PE-stars [49]. He proposed that the counterions, which guarantee the neutrality of the whole system, are playing the major role for the interaction potential, and he predicted a constant force between the stars. Since there have not exist computer simulations or experimental studies on this matter, this prediction could not been verified yet.

The difficulty for a detailed study of PE-stars arises again from the ensuing different length scales: there are the microscopic length scales, like the monomer- and counterion diameter, the extension size of the star, and there are also charge-induced length scales. Although in the neutral stars the first two length scales also exist, their treatment was enabled by tracing out the microscopic degrees of freedom of the monomers, whereas in the charged case this is not possible anymore, due to ensuing long-ranged Coulomb interactions. The associated length scales, like the Debye screening length, cannot be handled straightforward. Scaling concepts, as used for neutral systems, are not convenient methods for calculating conformational properties quantitatively. Hence, it is not surprising that much more difficulties exist for the calculation of an effective interaction and conventional scaling concepts fail. Therefore the gate for further theoretical investigation of large scale phenomena in PE-star solutions remained closed.

In addition computer simulation of PE-stars are missing, since they require large computational effort, resulting in a long CPU time. Although the simulation of linear PEs has progressed in the past years [50, 51, 52] there is a lack of results in the case of star-branched

PEs. In this work we present both a theory and a simulation study of star-branched PEs, enabling a straightforward comparison between both methods.

The work starts with Chapter 2 as a prelimenary part of the main subjects. Chapter 2 begins with a short review of some common terms in polymer theory. The main focus lies in the description of the reasons for the flexibility of polymer chains, and their influencing parameters, like the solvent quality and the charge effect. In this context we stress the reason for conformational properties of star-like systems, considered in Chapter 3. Another important part of Chapter 2 concerns the effective interaction. Following Ref. [53] we give a formal statistical mechanical justification for the concept of the effective interaction. We also show the link between theory and computer simulation relating to the measurement of the interaction potential in computer simulations, which is quite relevant for verifying theoretical predictions. The mentioned link between theory and simulation is a very important aspect for all studied systems in this work for which we compare theoretical models with simulation results.

The main focus of the work lies in Chapter 3, where the study of PE-stars in terms of their theoretical treatment and of their computer modeling is presented. Both methods are applied on an isolated PE-star, and on two stars. The results were published recently [54, 55] and are shown in this work. The Chapter is shared in two parts. In the first Section an isolated PE-star is considered in a Wigner-Seitz cell, based on an idea of Klein Wolterink et al. [48]. However, our theoretical model has to be distinguished from the model of Klein Wolterink et al. in terms of two main features: first, we consider an inhomogeneous charge distribution within the star; second, we distinguish three counterion states, one of this states counts for condensed counterions. Both features provide a novum in the calculation of PE-stars, and have not been taken into account in previous works [45, 46, 47, 48, 49], although they are crucial for the development of the effective interaction potential. A variational free energy calculation were done in order to obtain values for the radius of the star, and for the numbers of the counterions in their three states. A comparison with results for this conformational properties obtained from monomer-resolved Molecular Dynamics simulations with explicit counterion consideration shows a very good agreement, for the salt-free case as well as in the added salt case. In the second part of Chapter 3 we expand the one-star model to a two star model. Here, two stars are considered at separation D and all free energy contributions contain a D-dependence. The free energy calculation yield a interaction potential for the stars. The main result is that the interaction potential is essentially induced by the counterion entropy, and only indirectly by the electrostatic repulsion of the chains, as was already predicted qualitatively by Pincus [49]. However, the repulsive force is not constant, as he proposed; moreover, it is a non-linear decay, softer concerning its curvature than in the case of neutral star polymers [27], but larger in its absolute value, depending on the charge fraction. The theoretical results are compared with simulation data with excellent agreement, also for the case of added salt. We also present an analytical expression for the interaction potential for all distances and parameter combinations, in order to

give stimulation for further experimental investigations and large scale studies of PE-star solutions.

Chapter 4 deals with the calculation of the effective interaction between a neutral star polymer and a colloidal particle, as was published recently in Refs. [35, 56]. The procedure starts with a calculation of the osmotic pressure of a star at a hard wall, based on an idea of Pincus [49]. The next step is the modification of the theoretical model of a star close to a spherical colloid. The resulting effective forces are verified and confirmed by monomer-resolved Molecular Dynamics simulation data. Furthermore, a modified version of the star-star potential which is valid for very low arm numbers, $f \lesssim 10$ is presented. The proposed analytical expression for the effective interaction potential between the star and a colloid has been used as a input quantity in liquid state theory [57] in order to calculate the phase behavior of a star polymer colloid mixture [34, 36, 56].

The two last mentioned Chapters are self-contained and at the beginning and at the end of each Chapter a short introduction and a summary, respectively, to the topic dealt are given. After a conclusion and an outlook of the work in Chapter 5 three Appendices follow. In Appendix A the effect of triplet interaction in star polymer solutions is shortly presented, based on Ref. [30]. It is an example for many-body contributions mentioned in Section 2.2, and justifies the use of the pair potential approximation for the considered star-like systems, since it has only minor contributions to the total force. The other Appendices deal with some technical information: in Appendix B about the Lekner method for the treatment of long-ranged Coulomb forces in computer simulations [58]. In Appendix C some technical details for the calculation of the electrostatic potential of two fused spheres are presented. The results are used for the calculations of two PE-stars in Section 3.2.

Chapter 2

Conformations of Flexible Polymers and their Effective Interactions

As a preparation for the later investigations into star-like systems, a short overview of some important terms within polymer theory is given in this chapter. The main focus lies in the consideration of static properties of flexible polymers. The analysis of the conformation of polymer systems is important for the understanding of the physical behavior of polymers. A detailed study of the conformation is often a prerequisite for the formulation of a theory that can bridge the gap between a microscopic and a macroscopic description of polymeric matter.

One way of predicting macroscopic properties such as phase behavior is to put forward an effective interaction potential between colloidal particles like star polymers. Knowledge of the form of effective interaction potential allows it to be used as an input quantity in liquid integral equation theory and/or computer simulations in order to calculate structure factors of colloidal systems. Therefore, effective interaction provides an important link between theory, computer simulation and experiment.

In this chapter we adopt a similar procedure to that of Refs. [59] and [53]. We begin with a description of the conformation of linear polymer chains and the parameters that are responsible for their flexibility and consequently for the conformations of the chains. The second part of the chapter is largely based on Ref. [53] and provides a statistical mechanical derivation of the effective interaction in a multi-component system. It is shown that the concept of the effective interaction can be defined exactly within the framework of statistical mechanics. Furthermore, it is presented how the effective interaction potential can be measured in computer simulations.

2.1 Conformations of polymers

One of the first questions concerns the reason of the flexibility of a single polymer chain. To answer this, one should proceed with a microscopic view at the spatial layout or the

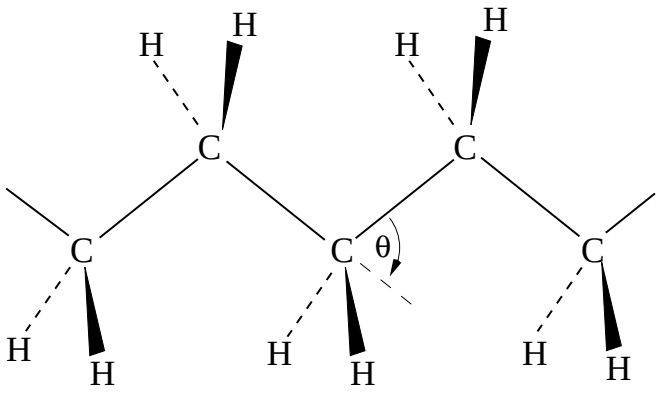

Figure 2.1: Schematic picture of a polymer chain, consisting of methylene groups. The bond angle θ between two neighbored chain segments is also depicted.

instantaneous configuration of a chain molecule.

In Fig. 2.1 we sketch a typical configuration of a chain molecule, in this case consisting of methylene groups CH_2. Although the bond length a between the methylene groups as well as the bond angle θ are fixed, there still remain degrees of freedom available to the overall configuration of the chain. This freedom manifests itself in rotating two neighbored monomers around their bond axis without affecting a and θ. The mentioned rotations around the bonds are important for the flexibility of the chain and affect the configuration of the polymer. The spatial structure of a polymer chain is given by the positions of the chain segments called monomers, which consist of a group of atoms. We will see later in this Section that one can define an effective monomer, which allows them full freedom of rotation, not only around the bond.

First we want to define two quantities describing the extension of a polymer. We consider the bond vectors $\boldsymbol{l}_i$ between the chain segment $i-1$ and i, $i > 1, 2, \ldots, N$ with N as the degree of polymerization . These bond vectors define the so called end-to-end vector

$$\boldsymbol{L} = \sum_{i=1}^{N} \boldsymbol{l}_i, \tag{2.1}$$

whereas the absolute value of $\boldsymbol{L}$ gives information about the extension of the polymer:

$$L^2 = \boldsymbol{L} \cdot \boldsymbol{L} = \sum_{i,j=1}^{N} \boldsymbol{l}_i \cdot \boldsymbol{l}_j = \sum_{i=1}^{N} l_i^2 + 2 \sum_{1 \le i < j \le N} \boldsymbol{l}_i \cdot \boldsymbol{l}_j. \tag{2.2}$$

In general, we can define the distance between two monomers M_i and M_j as

$$L_{ij}^2 = \sum_{i'=i+1}^{j} l_{i'}^2 + \sum_{i \le i' < j' \le j} \boldsymbol{l}_{i'} \cdot \boldsymbol{l}_{j'}. \tag{2.3}$$

Similar to the end-to-end vector $\boldsymbol{L}$, the radius of gyration s is another quantity that provides a measure of the spatial extension of the chain as well. s is defined as the mean

squared value of the distance vectors $\boldsymbol{s}_i, i = 0, 1, 2, \ldots, N$ of the monomer positions and the position of the polymer's center of mass.

$$s^2 = \frac{1}{N+1} \sum_{i=0}^{N} s_i^2. \tag{2.4}$$

Because of $\boldsymbol{L}_{ij} = \boldsymbol{s}_i - \boldsymbol{s}_j$ one obtains

$$s^2 = \frac{1}{(N+1)^2} \sum_{0 \le i < j \le N} L_{ij}^2 \tag{2.5}$$

Actually, one needs the mean values of the quantities because one measures in experiments usually the quantities of a huge number of configurations.

This leads to the definition

$$R_{\mathrm{ce}}^2 \equiv \langle L^2 \rangle = Na^2 + 2 \sum_{i<j} \langle \boldsymbol{l}_i \cdot \boldsymbol{l}_j \rangle \tag{2.6}$$

for the average squared end-to-end distance, and to

$$R_{\mathrm{g}}^2 \equiv \langle s^2 \rangle = \frac{1}{(N+1)^2} \sum_{0 \le i < j \le N} \langle L_{ij}^2 \rangle \tag{2.7}$$

for the average squared radius of gyration. The brackets $\langle \ldots \rangle$ denote the average of all configurations in the undisturbed case, i.e. without external forces acting on the polymers.

Both quantities calculated in Eqs. (2.6) and (2.7) are very important, since they are measurable in experiments as well as in computer simulations, and allow a straightforward comparison with theoretical predictions.

The task of the theory is to model the polymeric system in a convenient way. There are some simple chain models that describe the behavior of a chain, and which enable a calculation of (2.6) and (2.7) [9, 59, 53]. Those models seem to be somewhat simplified, nevertheless they offer a concrete basis for comparisons with real chains in order to obtain some qualitative results.

As already mentioned above, it should be noted that the flexibility of the chains has its microscopic origin at the existence of various choices every monomer has to orient itself with respect to the preceding one in the chain sequence. Though these possible orientations are not all equally favorable energetically, thermal fluctuations constantly change the instantaneous orientations of successive monomers, thus giving rise to the flexibility of the chain. There are different parameters that influence the flexibility of a polymer chain and thereby the extension of the polymer. For such cases one has to find a convenient model. One of the important parameters is the solvent quality. Due to internal effective interactions between the monomers themselves as well as with the solvent, the solvent quality influence the polymer conformation indirectly, as we will see in Section 2.1.2.

2.1.1 Ideal and real chain models

Before we cater to the solvent quality in more detail we come back to the chain segments, the so called monomers. A monomer consist in general of one or more molecules and has in fact, depending on the number of molecules, direct influence to the size of the monomer. This size could be in the same order of magnitude of the persistence length l_p. The persistence length is defined through the correlation function between the bond vectors $\boldsymbol{l}_i$. Usually, the bond vectors of linear polymers loose already at short distances their correlation and the correlation function $\langle \sum_{i,j} \boldsymbol{l}_i \cdot \boldsymbol{l}_j \rangle$ can be described by an exponential decay [8], where the correlation function has the value 1 at zero separation. The persistence length is now defined by the length at which the correlation function has decayed on the value of e^{-1}. The physical meaning of this definition is that the correlation between a particular bond $\boldsymbol{l}_i$ and another bond $\boldsymbol{l}_j$ at distances $L_{ij} > \lambda_p$ is essentially lost. It is reasonable to group all molecules within the radius l_p from molecule M_i as one particle called "monomer" or "Kuhn segment".

It is reasonable to treat monomers in such a way, especially for very long chains. It enables us to consider the system on a larger length scale, thereby reaching the mesoscopic regime, where atomistic or quantum mechanical properties become irrelevant. Furthermore it enables to simulate polymeric system within a manageable cost of calculation and CPU time, and even in a sufficient accuracy, of course depending on what quantities one is interested for. In most cases typical quantities, like the radius of gyration, are calculated sufficiently accurate.

The simplest picture of a flexible chain is the so-called ideal or Gaussian chain, where a model of the chain is provided by the random walk (RW). Here we assume that every bond vector $\boldsymbol{l}_i$ is undisturbed in his motion by all other bond vectors. In this way the inner product $\boldsymbol{l}_i \cdot \boldsymbol{l}_j$ in Eq. (2.6) is uniformly distributed in the interval $[-a^2, a^2]$ and its expectation value vanishes. It should be noted that this deviates from the discussion about the flexibility mentioned in the beginning of the Section according to the condition of fixed bond lengths and bond angles. This condition is not necessary anymore within the picture of a polymer chain consisting of monomers.

We obtain in the Gaussian (RW) model for the expectation value of the end-to-end distance in Eq. (2.6) a scaling behavior

$$R \equiv R_{ce} = aN^{1/2} \tag{2.8}$$

The scaling exponent $\nu_0 = 1/2$ suggest the name Gaussian chain. The name of ideal chain stems from the fact that this model allows overlapping of the monomers: they do not 'feel' each other. In order to calculate the free energy associated with ideal chains the central limit theorem is useful [53].

Since the bond vectors are independent the end-to-end distance R follow a normal distribution. This implies that the quantity $W_0(R)$, where $W_0(R)\mathrm{d}R$ denotes the total number of ideal chains with end-to-end distance lying between R and $R + \mathrm{d}R$, has the Gaussian

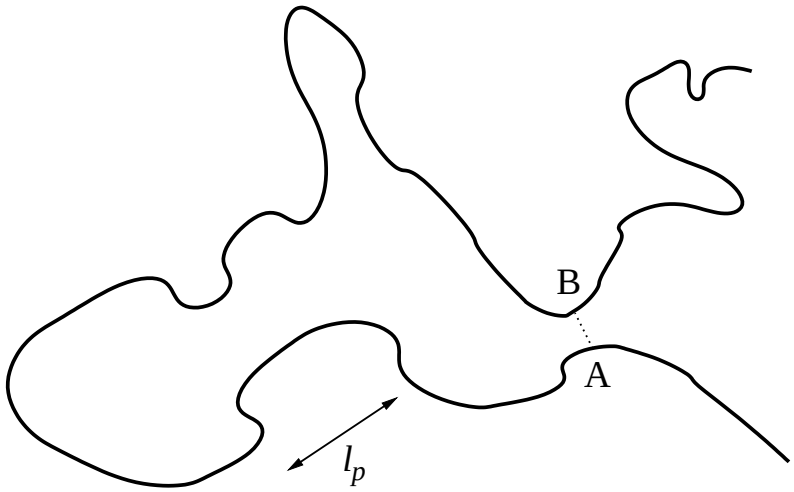

Figure 2.2: A self-avoiding polymer chain. The repulsion between the polymer segments A and B is denoted by the dotted line. Although their distance along the chain is much bigger than l_p A and B are correlated due to their repulsion. (Courtesy of Christos N. Likos.)

form [9, 10]

$$W_0(R) \sim R^2 \exp\left(-\frac{3R^2}{2Na^2}\right). \tag{2.9}$$

The prefactor R^2 on the right hand side of Eq. (2.9) above arises from geometrical reasons while the exponent corresponds to the Boltzmann factor in the partition function of the chain. This leads to an elastic free energy F_0 of the ideal chain, which is entropic in nature, and reads as [7]

$$F_\mathrm{el} = F(0) + \frac{3k_\mathrm{B}TR^2}{2Na^2}. \tag{2.10}$$

$F(0)$ is an unimportant constant while the last term can be identified as an elastic spring with the spring constant $3k_\mathrm{B}T/Na^2$.

Related to the scaling behavior for the end-to-end distance in Eq. (2.8), it should be emphasized that real chains show a larger extension due to the prohibited overlapping of the monomers, hence yielding a different scaling exponent $\nu > \nu_0 = 1/2$. In contrast to the ideal chains, the real chains follow a so-called self-avoiding walk. The microscopic reason for the self avoidance lies in the steric repulsion between the monomers, which is short-ranged in nature but nevertheless induces a long-range effect for the whole chain, irrespectively of the persistence length l_p. Since the chains are very long, monomers from different sequences can approach each other and their repulsion enforces a correlation in their positions, as Fig. 2.2 illustrates.

In order to describe the self-avoiding effect in a manageable manner, Edwards used an

ansatz for the so-called excluded volume interaction, approximated by a δ-function [10, 60, 61]

$$v_{\rm mm}(\boldsymbol{r}_i, \boldsymbol{r}_j) = v_0 k_{\rm B} T \delta(\boldsymbol{r}_i - \boldsymbol{r}_j). \tag{2.11}$$

Here, $\boldsymbol{r}_i$ denotes the position of the ith monomer along the chain and v_0 is the so-called excluded volume parameter. A quantitative analysis of the excluded volume effects was first proposed by Flory [6]. The free energy of a self-avoiding polymer chain is taken to be given by the sum of the elastic free energy of Eq. (2.10) and an interaction free energy $F_{\rm int}(R)$ due to the excluded volume effects. Assuming a uniform distribution of monomers within the coil of radius R, and neglecting correlations, we obtain an estimation for $F_{\rm int}(R)$ from Eq. (2.11) [10, 7]

$$F_{\rm int} \simeq v_0 k_{\rm B} T \frac{N^2}{2R^3}. \tag{2.12}$$

Adding both contributions to the free energy $F_{\rm el}(R)$ in Eq. (2.10) and $F_{\rm int}(R)$ in Eq. (2.12), and minimizing the resulting total free energy with respect to R, yielding the size R^* of the chain

$$R^* = (v_0 a^2)^{1/5} N^{3/5} \sim N^{3/5}. \tag{2.13}$$

The scaling exponent $\nu = 3/5$ is the so-called Flory exponent. Despite this simple formulation the exponent is in excellent agreement with the "exact" value $\nu = 0.588$, which is calculated through renormalization-group methods [62] and computer simulations [63]. Note that the above value for ν are results valid in three dimensions.

In both the ideal and self-avoiding chain, the number of the monomers N and the radius of the polymer coils are connected by scaling laws of the form $R(N) \sim N^\nu$ where ν is 1/2 and 3/5 for the Gaussian chain and for the self-avoiding chain, respectively. The scaling law $R(N) \sim N^\nu$ is *universal* in the sense that it holds irrespectively of the chemical blocks of the polymer. Finally, we remark that these scaling laws remain valid when the end-to-end distance of the chain is replaced by another characteristic length which measures the macroscopic size of the chain, such as the radius of gyration R_g in Eq. (2.7), as long $R_g \gg a$, or an equivalent mesoscopic length fulfill this condition.

2.1.2 The solvent effect

Since the polymers are always found in solution they are under the influence of the solvent. In what follows, we present for the sake of simplicity a lattice model, to account for the solvent effect and introduce the notion of solvent quality [9]. This model is depicted in Fig. 2.3.

If the polymers have a high affinity to the solvent molecules, the polymers are easy solutable and the chain extends with respect to the ideal state. In this case there are good solvent conditions for the polymer. In the reverse case there are poor solvent conditions and the polymers contract. This behavior, extension and contraction, points to a correlation between the excluded volume effect and the polymer interaction with the solvent.

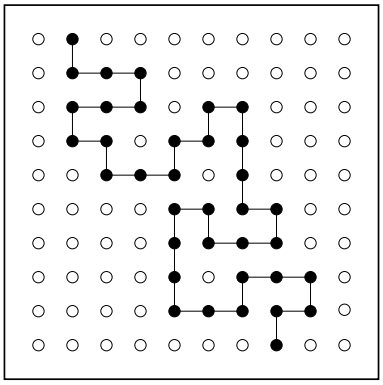

Figure 2.3: A lattice model of a chain in a solvent. The monomers are denoted by the black circles and the solvent molecules by the white ones. For the case of simplicity, these two species are taken to have the same size.(Courtesy of Christos N. Likos.)

To investigate this behavior,we distinguish the interaction energy between monomers among each other $\epsilon_{\rm mm}$, the monomers and the solvent molecules $\epsilon_{\rm ms}$, and the solvent molecules among each other $\epsilon_{\rm ss}$. We define the energy loss associated with bringing two polymer segments close to each other,

$$\Delta\epsilon = \frac{1}{2}(\epsilon_{\rm mm} + \epsilon_{\rm ss}) - \epsilon_{\rm ms}. \tag{2.14}$$

Referring to Eq. (2.12) for the interaction contribution to the free energy, $F_{\rm int}$ has to be modified, which was done by mean-field calculation [9]. The result is a different excluded volume parameter v_0:

$$v_0 \to v(T) = v_0(1 - 2\chi). \tag{2.15}$$

Here, χ is a parameter defined as

$$\chi \equiv \frac{z\Delta\epsilon}{k_{\rm B}T}, \tag{2.16}$$

with z being the coordination number of the lattice, see Fig. 2.3. As can be seen in Eq. (2.15), the excluded volume parameter $v(T)$ is temperature-dependent. The origin of the nearest-neighbor interaction modeled by the parameters $\epsilon_{\mu\nu}$ (μ, ν =m,s) is usually the dispersion force between the molecules, and is in general attractive. These van-der-Waals attractions correspond to a proportionality between $\epsilon_{\mu\nu}$ and the products of the atomic polarizabilities α_μ, α_ν, i.e., $\epsilon_{\rm mm} = k\alpha_{\rm m}^2, \epsilon_{\rm ss} = k\alpha_{\rm s}^2$ and $\epsilon_{\rm ms} = k\alpha_{\rm m}\alpha_{\rm s}$, with some positive proportionality constant k. Substituting these expressions into the definition of the quantity $\Delta\epsilon$, Eq. (2.14), we obtain

$$\Delta\epsilon = \frac{k}{2}(\alpha_{\rm m} - \alpha_{\rm s})^2 > 0, \tag{2.17}$$

which implies, through Eq. (2.16), that $\chi > 0$ as well. The effect of the solvent is, in general, to decrease the bare excluded volume parameter and to bring the segments closer to each

other. Whether this only effects the constant of proportionality in the Flory scaling law (2.13) $R^* \sim N^{3/5}$ or changes the exponent itself, depends on the magnitude of χ. The latter can be externally controlled by the temperature. We examine three distinct cases below.

- *Good solvent*: This corresponds to the case $(1-2\chi) > 0$ and occurs physically for high temperatures. According to Eq. (2.15), in this case the renormalized excluded volume parameter $v(T)$ remains positive. The size of the chain still scales according to Flory's law $R^* \sim N^{3/5}$ and the interaction between the monomers can effectively described as purely repulsive. In the high-temperature regime, $k_{\mathrm{B}}T \gg \Delta\epsilon$, the solvent effects are in fact completely suppressed, the temperature plays no role and this solvent is called *athermal*.

- *Poor solvent*: This corresponds to the case $(1-2\chi) < 0$ and occurs at sufficiently low temperature T. The excluded volume parameter becomes negative and the chain collapses into a compact coil, thus following a scaling law with a different exponent $R^* \sim N^{1/3}$. The monomers minimize the interface with the solvent and their interaction among each other has effectively an attractive part.

- Θ-*solvent*: This corresponds to the intermediate case $(1-2\chi) = 0$, where the excluded volume interaction vanishes. The chain behaves macroscopically as ideal, following the scaling law of a Gaussian chain $R^* \sim N^{1/2}$. The particular value of the temperature when this occurs, is called the Θ-temperature and is given, according to Eq. (2.16), by the expression

$$T_\Theta = \frac{2z\Delta\epsilon}{k_{\mathrm{B}}}. \tag{2.18}$$

In rising the temperature from values corresponding to a poor solvent to those corresponding to a good solvent the chain undergoes a so-called coil-to-globule transition, which has been observed experimentally [64]. Hence, the solvent quality has a strong effect on the flexibility of a chain. We will see as next that another parameter, the charge on chain sites, influences the flexibility of a chain even in a stronger way than the solvent.

2.1.3 The charge effect

Polymers that carry charges on some of their sites are called *polyelectrolytes* [49]. Along the polymer chain there are ionizable groups which dissociate counterions into the solution. The charges along the chain are in most cases of the same sign. Polymers carrying charges of both signs either are called *polyampholites* [65].

In contrast to the neutral polymers, the electrostatic interaction is dominating in comparison to the excluded volume interaction. In the simplest case of screened Coulomb interaction by homogeneous distributed charges, the interaction can be described by the Debye-Hückel (DH) potential V_{DH} [65]

$$V_{\mathrm{DH}}(r) \sim \frac{\exp(-r/\lambda_{\mathrm{D}})}{r}. \tag{2.19}$$

The range of this interaction is determined by the Debye length λ_D which is correlated with the salt concentration[1] ρ_s in the solution and/or the ionic strength I through the relation $1/\lambda_D \sim \sqrt{\rho_s} \sim \sqrt{I}$ [65]. Therewith a new relevant length scale shows up in addition to the previously mentioned lengths, and can be as large as the whole chain or longer. Because of this additional length, a simple estimation of the exponent ν is not possible anymore. In the case of fully screened Coulomb potential, e.g. caused by a high salt concentration ρ_s, the case of the self avoiding chain is achieved. In the opposite case, the charges feel the undisturbed Coulomb potential and repel each other, leading to stretched chains. This stretching effect manifests itself in the radius of gyration

$$R \simeq \left(\frac{(qe)^2 a^2}{k_B T} \right)^{1/3} N, \tag{2.20}$$

where q denotes the mean number of elementary charges e per site (multivalence case: $q > 1$). In contrast to the neutral polymers (see Eqs. (2.8) and (2.13)) , the chain size is linearly dependent on the degree of polymerization N ($\nu = 1$). However, the relation (2.20) has not been confirmed neither by simulations nor by experiments. The reason is that the counterions which are in the solution as well, cause a charge screening. Under certain circumstances, they can even condense on the chain and can decrease the effective charge which leads to a contraction effects of the chain. This phenomenon is called *Manning condensation* [37, 66].

A further length scale, which was described in previous Sections, is the persistence length l_p. In contrast to neutral polymers the persistence length is not anymore in the order of magnitude of the bond length a. Because of the stretching effect the persistence length is much larger than the bond length and can even be larger than the whole chain.

In general, one assumes, that the persistence length l_p consists of an intrinsic part (given by the structure of the chemical segments) l_0 and an electrostatic part l_e, resulting from the charges, in an additive way: $l_p = l_0 + l_e$ [67, 68]. The theoretical predictions for the relation between l_e and λ_D with $l_e \sim \lambda_D^y$ are contradictory for the value of the exponent y, which are between $y = 1$ and $y = 2$. Even computer simulations give values between $y = 0.5$ and $y = 2$. Hence, the concept of the persistence length within a Debye-Hückel theory for such systems is doubtful.

The reason for this lies on the assumption of weak variations in the counterion density and neglected fluctuation effects. That is why the Debye-Hückel theory cannot describe the above mentioned Manning condensation either. This effect appears because of the competition of the translational entropy of the counterions and their electrostatic attraction with the chain.

A first adequate model is the infinite, charged rod (a stiff polyelectrolyte) with a line charge density $\rho = e/a$, with a charge separation a along the rod. For the behavior of the counterions, there is an argument of Onsager[2]: by increasing the cylinder volume for the counterions around the rod with radius r_1 to a larger radius r_2 it yields for the electrostatic

[1] Nearly all real polyelectrolyte systems are found in salted solutions.

[2] Private communication to G.S. Manning (see Ref. 13 in [37])

contribution to the free energy of the counterions

$$F_{\mathrm{el}} \sim 2k_{\mathrm{B}}T\frac{Tl_{\mathrm{B}}}{a}\ln\left(\frac{r_2}{r_1}\right), \tag{2.21}$$

and for the entropic part

$$F_{\mathrm{S}} \sim 2k_{\mathrm{B}}T\ln\left(\frac{r_2}{r_1}\right). \tag{2.22}$$

$l_{\mathrm{B}} = e^2/(\epsilon k_{\mathrm{B}}T)$ is the Bjerrum length and is a scale for the strength of the electrostatic interaction, and ϵ denotes the dielectrical constant. At the so-called critical Manning value $l_{\mathrm{B}}/a = 1$ both contributions are equal. For $l_{\mathrm{B}}/a > 1$ the electrostatic dominates, and the counterions condense along the chains, i.e. they are localized within a cylinder around the chain. While for the opposite case $l_{\mathrm{B}}/a < 1$, the so-called *Alexander criteria*, the counterions are more or less 'free' in the whole space.

Although this arguments are contended, especially for flexible polyelectrolytes, we will see in the next chapter that this theory, applied on star-shaped polyelectrolytes, is quite reasonable. We will compare theoretical predictions for such systems with computer simulations in which we consider the full Coulomb potential, resulting from discrete ions along the chain and explicit simulated counterions. With this model we are able to sample the large scope of validity for the Onsager theory.

In order to clarify the flexibility of the chains we discuss Fig. 2.4, in which a diagram of states of a dilute solution of polyelectrolyte chains is shown. The phase diagram is calculated using scaling arguments and is determined by two parameters, the excluded volume parameter v and the Bjerrum length l_{B} [38]. It shows the conformation of single chains, if one vary the solvent quality, and the electrostatic coupling by varying the temperature. The systems are modeled using the blob picture. Due to the charges one has in addition to the thermal blobs [7], the so-called electrostatic blobs.

A detailed review about linear polyelectrolytes regarding their theoretical as well as experimental investigations can be found in Ref. [65].

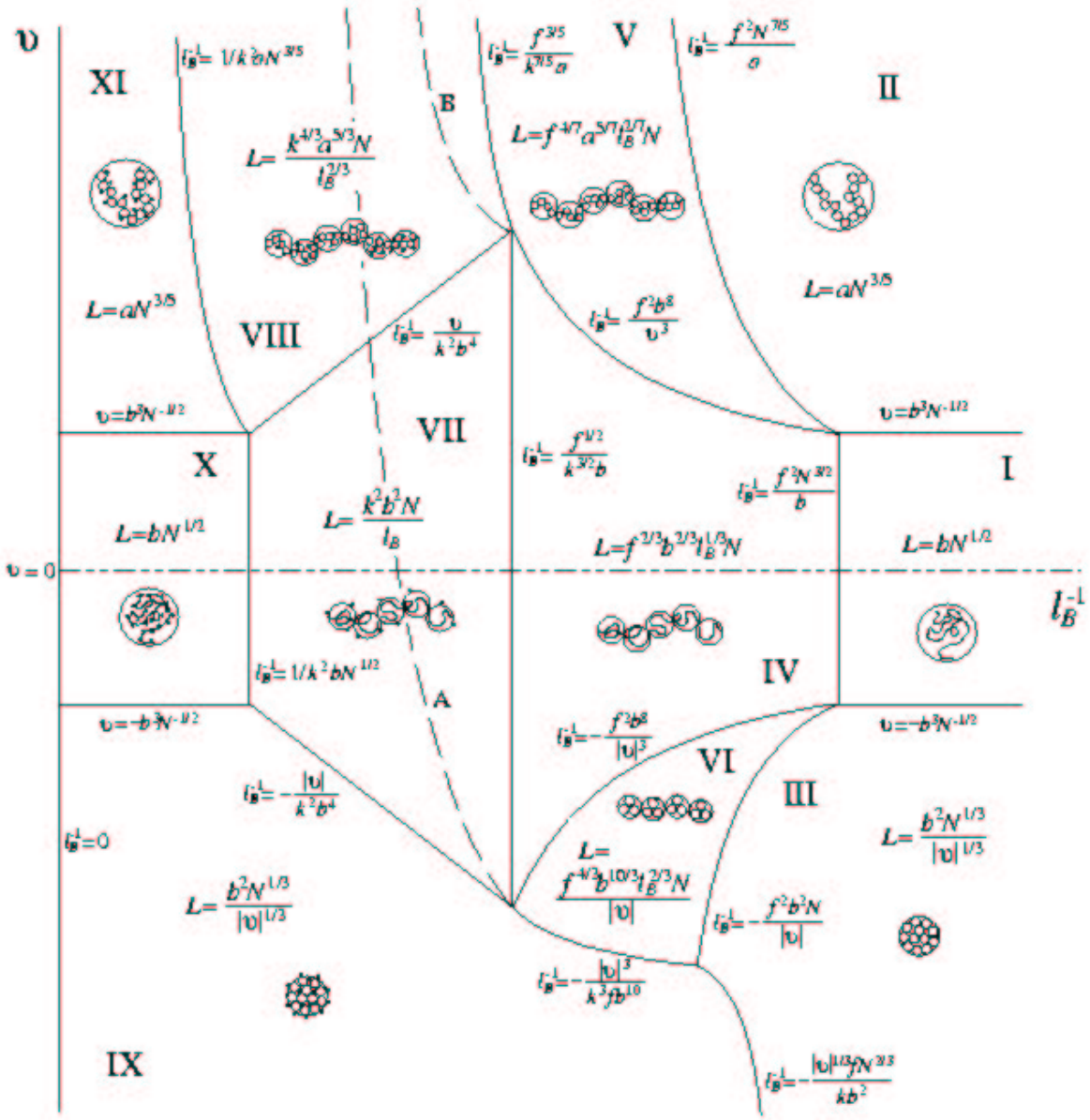

Figure 2.4: Phase diagram of a dilute solution of linear polyelectrolytes. The diagram is taken from Ref. [38], where different symbols were used (here: $b \sim (a^5/v)^{1/2}$, $f \equiv \alpha$ charge fraction, k is a constant). Each regime (I-XI), defined by different equations according to v and l_B corresponds to a certain conformation of the single chain, as depicted in the according regime. Quantitatively the different states are given by the scaling relations for the chain sizes L. At high temperatures in the regimes I-III, corresponding to small Bjerrum length l_B, the chains are unperturbed by the electrostatics. While in the regimes I-VI all counterions are released, in regimes VII-XI they are condensed (schematically depicted as dots). In the Θ-regimes I, IV, VII, and X the Gaussian behavior is valid within electrostatic blobs (see also text). In the regimes II, V, VIII, and XI (good solvent conditions) the blobs are swollen, whereas in regimes III, VI, and IX (poor solvent conditions) the blobs are collapsed. By courtesy of H. Schiessel.

2.1.4 Experimental methods

To build up a link with experiments we describe shortly some common methods in investigations of polymer solutions. The most often used methods are small-angle light-, neutron-, or X-ray-scattering experiments, SALS, SANS or SAXS, respectively. In the latter cases the transmitted momenta are small, i.e., the associated wavelength is large. The atomistic details are not resolved and one can observe the global structure of the polymers. The scattered intensity of the wave from a incident radiation of wavelength λ at a certain scattering angle θ is given by [69, 11, 70]

$$I(Q) = \int \rho(\boldsymbol{r'})\rho(\boldsymbol{r}-\boldsymbol{r'}) \exp(\mathrm{i}\boldsymbol{Q}\cdot\boldsymbol{r})\mathrm{d}\boldsymbol{r}\mathrm{d}\boldsymbol{r'}, \tag{2.23}$$

where $Q = 4\pi \sin(\theta/2)/\lambda$ is the scattering vector and $\rho(\boldsymbol{r})$ denotes the spatial distribution of scattering density in dependence of the position vector $\boldsymbol{r}$. When scattering from a very dilute solution is performed, $I(Q) \sim P(Q)$ [11], the so-called form factor of the object, which contains information about its molecular weight, size and mass distribution. Indeed, in the limit of $Q \to 0$, the probe is too coarse to detect anything else but the number of scatterers in the sample and hence it delivers information about the average density or, equivalently, the molecular weight of the polymer. At larger scattering vectors, $Q \simeq R_g^{-1}$ the polymers can be viewed as diffuse, spherical objects of size R_g, and hence information about the radius of gyration R_g is gained.

The form factor can also be measured in a standard simulation. For a system of point masses, $P(Q)$ can be given as a sum over all monomers of the polymer

$$P(Q) = \frac{1}{N^2}\sum_{i=1}^{N}\sum_{j=1}^{N}\langle \exp[\mathrm{i}\boldsymbol{Q}\cdot(\boldsymbol{r}_i-\boldsymbol{r}_j)]\rangle \tag{2.24}$$

$$= \frac{1}{N^2}\left\langle \left|\sum_{i=1}^{N}\exp[\mathrm{i}\boldsymbol{Q}\cdot\boldsymbol{r}_i]\right|^2 \right\rangle . \tag{2.25}$$

Informations for structural correlations are obtained by the static structure factor $S(Q)$, which measures the density-dependent center-to-center correlations of the polymers [57]. Assuming, that the form factor $P(Q)$ of labeled polymers is density independent, $I(Q)$ can be related to $S(Q)$:

$$I(Q) = N_s P(Q) S(Q). \tag{2.26}$$

Here, N_s denotes the total number of scattering centers. Obviously, N_s can be connected to the polymer volume fraction Φ and the weight-averaged molar polymer volume V_W of the labeled scattering centers by $N_s = V_W\Phi$. For vanishing polymer density ρ, only single polymer behavior is measured due to vanishing inter-polymer correlations. Thus, $P(Q)$ can be determined by extrapolation of the measured scattering intensities $I(Q)$ to vanishing density. This procedure enable the extraction of the structure factor in further measurements.

Since the structure factor is one of the important quantities in describing structural correlations in polymer solutions, it gives rise to formulate a theory which is able to predict the effective interaction of the particles in a microscopic model. If one can propose an expression for an effective interaction between two colloidal particles, one can use the interaction potential in liquid state theories [57, 71] in order to calculate structure factors $S(Q)$ of those particles. In this way a microscopic model can predict macroscopic properties of the system. The role of the effective interaction will be discussed in more detail in the next Section. The above described procedure was already applied on star polymer solutions [27].

2.2 The concept of the effective interaction

In the last Section we saw that the polymeric systems have different types of particles like the polymers, the solvent particles, the counterions and the salt ions. In fact it is a multicomponent system, which is called '*complex fluids*" considered at mesoscopic lengthscales. In performing experiments with soft matter systems one usually focusses the attention on the static and dynamical properties of the large particles only (e.g. the polymers are the large particles, whereas the solvent and salt particles are small), i.e., one looks at the system at length scales where only the larger particles are visible and the rest plays the role of a background. The scattering profiles have to be then interpreted by means of an effective interaction between the considered large particles, which indirectly includes all the effects of the remaining constituents.

From the theoretical point of view, the large number and the large asymmetries between the species comprising the complex fluid, render a full theoretical treatment of the statistical-mechanical system as a mixture practically impossible. The introduction of an effective interaction and the ensuing reduction to a one-component system simplifies the theoretical approach considerably. The last argument is also crucial for simulation modeling of complex systems. The concept of the effective interaction reduces the CPU time significantly.

We note that the consideration of the effective interaction of only the large particles is due to the interest of their properties only. It depends always on the quantities of a certain particle type (like their pair-correlation function) which we are interested for in order to justify the "neglect" of the other particles in the system. Nevertheless, we will show in the next Subsections that the concept of the effective interaction is exact, as far as all many-body terms are considered. The derivations that are to be presented follow the ideas of Ref. [53].

2.2.1 The effective Hamiltonian

We start with the full description of a multicomponent system and reduce it to a one-component system by tracing out all the degrees of freedom but the ones we are interested in.

For the sake of simplicity we consider a classical system, i.e., the considered length

scales, in the order of typical interparticle distances a of all components, are larger than the de Broglie wavelength Λ_α associated to a component α ($\alpha = 1, 2, \ldots \nu$) of a ν-component system, although the following approach is applicable for quantum-mechanical systems as well. Λ_α is defined as

$$\Lambda_\alpha = \sqrt{\frac{h^2}{2\pi m_\alpha k_{\rm B} T}}, \tag{2.27}$$

where h denotes Planck's constant, and is much smaller than the typical interparticle distance a in the many body system.

In order to simplify the development of an effective Hamiltonian we focus now on two types of particles only ($\nu = 2$) without loss of generality. We consider two kinds of particles, "large" ones ($\alpha = 1$), and "small" ones ($\alpha = 2$). The goal is to eliminate the small particles from the picture.

Let us assume that the system contains N_1 large particles at positions $\boldsymbol{R}_i(t)$ ($i = 1, 2, \ldots N_1$), and N_2 small particles at positions $\boldsymbol{r}_j(t)$ ($j = 1, 2, \ldots N_2$), at time t in a macroscopic volume Ω at the temperature T. The corresponding partial number densities of the two components are $\rho_{1,2} = N_{1,2}/\Omega$. Accordingly the momenta of the particles are denoted by the sets $\{\boldsymbol{P}_i\}$ and $\{\boldsymbol{p}_j\}$. The two-component Hamiltonian $\mathcal{H}$ consists of three terms:

$$\mathcal{H} = \mathcal{H}_{11} + \mathcal{H}_{22} + \mathcal{H}_{12}, \tag{2.28}$$

where $\mathcal{H}_{\alpha\beta}$ contains the interaction between the species α and species β only. If we assume that the interactions are pairwise additive and radially symmetric, the three terms in Eq. (2.28) read as

$$\mathcal{H}_{11} = \sum_{i=1}^{N_1} \frac{\boldsymbol{P}_i^2}{2M} + \sum_{i=1}^{N_1} \sum_{j=i+1}^{N_1} v_{11}(|\boldsymbol{R}_i - \boldsymbol{R}_j|), \tag{2.29}$$

$$\mathcal{H}_{22} = \sum_{i=1}^{N_2} \frac{\boldsymbol{p}_i^2}{2m} + \sum_{i=1}^{N_2} \sum_{j=i+1}^{N_2} v_{22}(|\boldsymbol{r}_i - \boldsymbol{r}_j|) \tag{2.30}$$

and

$$\mathcal{H}_{12} = \sum_{i=1}^{N_1} \sum_{j=1}^{N_2} v_{12}(|\boldsymbol{R}_i - \boldsymbol{r}_j|). \tag{2.31}$$

In Eqs. (2.29)-(2.31) above, M and m denote the masses of the large and small particles, respectively, and $v_{\alpha\beta}(r)$ are the potential energy between the particles of species α and β at the center-to-center separation r. To facilitate the presentation, we introduce some shorthand notations

$$V_{11}(\{\boldsymbol{R}\}) = \sum_{i=1}^{N_1} \sum_{j=i+1}^{N_1} v_{11}(|\boldsymbol{R}_i - \boldsymbol{R}_j|), \tag{2.32}$$

$$V_{22}(\{\boldsymbol{r}\}) = \sum_{i=1}^{N_2} \sum_{j=i+1}^{N_2} v_{22}(|\boldsymbol{r}_i - \boldsymbol{r}_j|) \tag{2.33}$$

and

$$V_{12}(\{\boldsymbol{R}\},\{\boldsymbol{r}\}) = \sum_{i=1}^{N_1}\sum_{j=1}^{N_2} v_{12}(|\boldsymbol{R}_i - \boldsymbol{r}_j|), \tag{2.34}$$

where $\{\boldsymbol{R}\}$ and $\{\boldsymbol{r}\}$ are shorthands for $(\boldsymbol{R}_1, \boldsymbol{R}_1, \ldots \boldsymbol{R}_{N_1})$ and $(\boldsymbol{r}_1, \boldsymbol{r}_1, \ldots \boldsymbol{r}_{N_2})$, respectively.

We now turn our attention to the statistics and choose for this purpose a canonical ensemble to trace out the degrees of freedom of the small particles. The double trace over any quantity $\mathcal{O}$ that depends on all coordinates and momenta, is defined in this ensemble as

$$\mathrm{Tr}_1\mathrm{Tr}_2[\mathcal{O}] = \frac{h^{-3N_1}}{N_1!}\frac{h^{-3N_2}}{N_2!}\int \mathrm{d}\boldsymbol{P}^{N_1}\int \mathrm{d}\boldsymbol{p}^{N_2}\int \mathrm{d}\boldsymbol{R}^{N_1}\int \mathrm{d}\boldsymbol{r}^{N_2}\mathcal{O}(\{\boldsymbol{P}\},\{\boldsymbol{p}\},\{\boldsymbol{R}\},\{\boldsymbol{r}\}), \tag{2.35}$$

where Tr_α denotes the multiple integral over the positions and momenta of all degrees of freedom of particles of species α ($\alpha = 1, 2$), the prefactor $h^{-3N_\alpha}/(N_\alpha!)$ being included. The canonical partition function $Q(N_1, N_1, \Omega, T)$ is the double trace over the Boltzmann factor $\exp(-\beta\mathcal{H})$, and using the definitions (2.28) and (2.27):

$$\begin{aligned} Q(N_1, N_1, \Omega, T) &= \frac{h^{-3N_1}}{N_1!}\frac{h^{-3N_2}}{N_2!}\int \mathrm{d}\boldsymbol{P}^{N_1}\int \mathrm{d}\boldsymbol{p}^{N_2}\int \mathrm{d}\boldsymbol{R}^{N_1}\int \mathrm{d}\boldsymbol{r}^{N_2}\mathrm{e}^{\mathcal{H}_{11}+\mathcal{H}_{22}+\mathcal{H}_{12}} \\ &= \frac{(\Omega\Lambda_1^{-3})^{N_1}}{N_1!}\frac{(\Omega\Lambda_2^{-3})^{N_2}}{N_2!}Z(N_1, N_1, \Omega, T), \end{aligned} \tag{2.36}$$

where $\beta = 1/(k_\mathrm{B}T)$. In Eq. (2.35) the shorthand $\int \mathrm{d}\boldsymbol{R}^{N_1}$ has been used for $\int\int\ldots\int \mathrm{d}\boldsymbol{R}_1\mathrm{d}\boldsymbol{R}_2\ldots\mathrm{d}\boldsymbol{R}_{N_1}$ and analogously for the $\{\boldsymbol{r}\}$-coordinates and the momenta. In Eq. (2.36) we carried out the integration over the momenta and we defined the configurational part of the partition function, $Z(N_1, N_1, \Omega, T)$, which reads as

$$Z(N_1, N_1, \Omega, T) = \frac{1}{\Omega^{N_1}}\int \mathrm{d}\boldsymbol{R}^{N_1}\mathrm{e}^{-\beta V_{11}(\{\mathbf{R}\})}\frac{1}{\Omega^{N_2}}\int \mathrm{d}\boldsymbol{r}^{N_2}\mathrm{e}^{-\beta[V_{22}(\{\mathbf{r}\})+V_{12}(\{\mathbf{R}\},\{\mathbf{r}\})]}. \tag{2.37}$$

By integrating out the degrees of freedom of the small particles, and keeping simultaneously the positions $\boldsymbol{R}_1, \boldsymbol{R}_2, \ldots \boldsymbol{R}_{N_1}$ fixed, we obtain a partial partition function $Q_2(\{\boldsymbol{R}\})$ as

$$\begin{aligned} Q_2(\{\boldsymbol{R}\}) &= \frac{\Lambda_2^{-3N_2}}{N_2!}\int \mathrm{d}\boldsymbol{r}^{N_2}\mathrm{e}^{-\beta[V_{22}(\{\mathbf{r}\})+V_{12}(\{\mathbf{R}\},\{\mathbf{r}\})]} \\ &= \frac{(\Omega\Lambda_2^{-3})^{N_2}}{N_2!}Z_2(\{\boldsymbol{R}\}), \end{aligned} \tag{2.38}$$

with the partial configurational part $Z_2(\{\boldsymbol{R}\})$. For the sake of brevity we dropped the dependence of quantities on N_1, N_2, Ω, T from the argument list. The physical meaning of the quantity $Q_2(\{\boldsymbol{R}\})$ is now clear: it represents the partition function of the small particles in an external field generated by the large particles, whose positions are held fixed at $\boldsymbol{R}_1, \boldsymbol{R}_2, \ldots \boldsymbol{R}_{N_1}$. A comparison between Eqs. (2.38) and (2.36) shows that the partition function of the system can also be expressed as

$$Q = \mathrm{Tr}_1[\mathrm{e}^{-\beta\mathcal{H}_{11}}Q_2(\{\boldsymbol{R}\})]. \tag{2.39}$$

At this point we are now in the position to define the *effective Hamiltonian* $\mathcal{H}_{\text{eff}}$, which depends on the momenta and on coordinates of the large particles only:

$$\mathcal{H}_{\text{eff}} = \mathcal{H}_{11} - k_{\text{B}}T \ln Q_2(\{\boldsymbol{R}\}). \tag{2.40}$$

An equivalent definition is

$$\exp(-\beta\mathcal{H}_{\text{eff}}) = \text{Tr}_2[\exp(-\beta\mathcal{H})], \tag{2.41}$$

which brings forward the fact that $\mathcal{H}_{\text{eff}}$ is a mixture between the pure Hamiltonian and a free energy of the small particles in the instantaneous environment of the large ones, hence, reduced the original problem to a simpler one.

We now can continue with the usual way in the statistical mechanics in order to get measurable quantities and calculate the expectation value $\langle\mathcal{O}\rangle$ of any observable $\mathcal{O}(\{\boldsymbol{P}\},\{\boldsymbol{R}\})$ whose value depends on the momenta and coordinates of the large particles only. We start with the Hamiltonian of the original system, tracing out the degrees of freedom of the subsystem 2 first and end up with the expression of the average in the effective system:

$$\begin{aligned}
\langle\mathcal{O}\rangle &= \frac{\text{Tr}_1\text{Tr}_2[\mathcal{O}(\{\boldsymbol{P}\},\{\boldsymbol{R}\})\exp(-\beta\mathcal{H})]}{\text{Tr}_1\text{Tr}_2[\exp(-\beta\mathcal{H})]} \\
&= \frac{\text{Tr}_1[\mathcal{O}(\{\boldsymbol{P}\},\{\boldsymbol{R}\})\text{Tr}_2[\exp(-\beta\mathcal{H})]]}{\text{Tr}_1[\text{Tr}_2[\exp(-\beta\mathcal{H})]]} \\
&= \frac{\text{Tr}_1[\mathcal{O}(\{\boldsymbol{P}\},\{\boldsymbol{R}\})\exp(-\beta\mathcal{H}_{\text{eff}})]}{\text{Tr}_1[\exp(-\beta\mathcal{H}_{\text{eff}})]}.
\end{aligned} \tag{2.42}$$

The last line follows by the definition of Eq. (2.41). As far as the properties of the large particles are concerned, the description in terms of the effective Hamiltonian is completely equivalent to the original one and no information has been lost.

2.2.2 The effective interaction potential

Although the definition of the effective Hamiltonian in Eq. (2.40) is exact so far, it is in practice only in few special cases possible to trace out the small degrees of freedom exactly. Therefore one has to use approximate schemes, in order to come up with a reasonable and manageable expression for this quantity.

Having in mind that we are interested in the effective interaction of the big particles in our considered system, we have at first to look into some of the characteristic features of $\mathcal{H}_{\text{eff}}$ in order to analyze the structure of the effective Hamiltonian.

We use Eq. (2.29) to decompose Eq. (2.40) in the following terms

$$\begin{aligned}
\mathcal{H}_{\text{eff}} = &\sum_{i=1}^{N_1}\frac{\boldsymbol{P}_i^2}{2M} + \sum_{i=1}^{N_1}\sum_{j=i+1}^{N_1} v_{11}(|\boldsymbol{R}_i - \boldsymbol{R}_j|) \\
&+ \tilde{V}(\{\boldsymbol{R}\}; N_1, N_2, \Omega, T) + k_{\text{B}}T\Omega\rho_2[\ln(\rho_2\Lambda^3) - 1]
\end{aligned} \tag{2.43}$$

with

$$\begin{aligned}\tilde{V}(\{\boldsymbol{R}\};N_1,N_2,\Omega,T) &= -k_\mathrm{B}T\ln\left\{\frac{1}{\Omega^{N_2}}\int \mathrm{d}\boldsymbol{r}^{N_2}\mathrm{e}^{-\beta[V_{22}(\{\mathbf{r}\})+V_{12}(\{\mathbf{R}\},\{\mathbf{r}\})]}\right\}\\ &= -k_\mathrm{B}T\ln Z_2(\{\boldsymbol{R}\}).\end{aligned} \tag{2.44}$$

The last term in Eq. (2.43) is the ideal gas contribution from the kinetic degrees of freedom of the second component, $F_\mathrm{id}^{(2)}$, while $\tilde{V}$ contains all the non-trivial contributions arising from the interactions of the small particles.

Now we follow a procedure developed by Dijkstra et al. by expanding the term $\ln Z_2(\{\boldsymbol{R}\})$ in the following way [72, 73, 74]:

$$-k_\mathrm{B}T\ln Z_2(\{\boldsymbol{R}\}) = \tilde{V}_0+\tilde{V}_1+\tilde{V}_2+\tilde{V}_3+\ldots,$$

where

$$\tilde{V}_0 = \Omega\tilde{v}_0(\rho_1,\rho_2,T), \tag{2.45}$$

$$\tilde{V}_1 = \sum_{i=1}^{N_1}\tilde{v}_1(\{\boldsymbol{R}\};\rho_1,\rho_2,T), \tag{2.46}$$

$$\tilde{V}_2 = \sum_{i=1}^{N_1}\sum_{j=i+1}^{N_1}\tilde{v}_2(|\boldsymbol{R}_i-\boldsymbol{R}_j|;\rho_1,\rho_2,T), \tag{2.47}$$

$$\tilde{V}_3 = \sum_{i=1}^{N_1}\sum_{j=i+1}^{N_1}\sum_{k=j+1}^{N_1}\tilde{v}_3(|\boldsymbol{R}_i-\boldsymbol{R}_j|,|\boldsymbol{R}_j-\boldsymbol{R}_k|,|\boldsymbol{R}_k-\boldsymbol{R}_i|;\rho_1,\rho_2,T), \tag{2.48}$$

$$\tag{2.49}$$

and so on. The functions $\tilde{v}_m$ represent m-body effective interactions between the particles. The fact that all terms depend in addition to the coordinates of the large particles (except of the first term) on thermodynamic variables (densities and temperature) as well, allows us to "tune" the effective interaction by controlling some external parameters.

The extensitivity of the term $\tilde{V}_0$ follows from the requirement of extensitivity of the total free energy. This term and the kinetic contribution of the second component in Eq. (2.43) constitute the so-called *volume terms* F_0 of the effective Hamiltonian:

$$\begin{aligned}F_0 &= k_\mathrm{B}T\Omega\rho_2[\ln(\rho_2\Lambda^3)-1]+\Omega\tilde{v}_0(\rho_1,\rho_2,T)\\ &= \Omega f_0(\rho_1,\rho_2,T).\end{aligned} \tag{2.50}$$

Moreover, the term $\tilde{V}_1$ represents a sum of one-body potentials. However, the original problem has full translational symmetry which is apparently violated by this term. We conclude that it has to vanish:

$$\tilde{V}_1 = 0.$$

The remaining terms are sums of pair-, triplet- and higher-order interactions. Their series is usually truncated at second order, thus yielding a system interacting effectively in terms of

pair potentials only. This constitutes the *pair-potential approximation*. There is very little evidence of a breakdown of the pair-potential approximation [75], though many-order effects may be "hidden" in parameters of the effective potential [76]. In general, problems with the pair-potential picture are to be expected at very high concentrations of macroparticles only. We will show in Appendix A that exactly this happens for star polymer systems at high concentration and we will see the deviation of the interaction potential regarding triplet forces from the pair-potential approximation.

The choice to trace out the small particles in favor of the larger ones could have been reversed, because nothing in the formalism prevents us from tracing out the larger particles. However, from the stage, where the approximation comes into the game, it should be physically clear that the pair-potential approximation is a very poor one for the small particles in the presence of the large ones.

Gathering now the results for Eqs. (2.43)-(2.50) we find that *in the pair-potential approximation* the effective Hamiltonian reads as

$$\mathcal{H}_{\text{eff}} = \sum_{i=1}^{N_1} \frac{\boldsymbol{P}_i^2}{2M} + \sum_{i=1}^{N_1} \sum_{j=i+1}^{N_1} V_{\text{eff}}(|\boldsymbol{R}_i - \boldsymbol{R}_j|; \rho_1, \rho_2, T) + \Omega f_0(\rho_1, \rho_2, T), \tag{2.51}$$

where the *effective interaction potential* V_{eff} is given by

$$V_{\text{eff}}(r; \rho_1, \rho_2, T) = v_{11}(r) + \tilde{v}_2(r; \rho_1, \rho_2, T),$$

i.e., it is a sum of direct interactions and those influenced by the smaller particles. In the above definition we used the notation for the large particle separation $r = |\boldsymbol{R}_i - \boldsymbol{R}_j|$. We further note that in contrast to the "usual", truly microscopic Hamiltonians, the effective Hamiltonian consists not only of a kinetic and a potential part, but also of the volume term $\Omega f_0(\rho_1, \rho_2, T)$.

It is one of the important tasks of this work to derive effective interactions for star-shaped polymer systems and to compare the theoretical results with computer simulations, or, if available, with experiments. We will see in the next Subsection how the effective potential can be measured.

2.2.3 The measurement of the effective Hamiltonian

Up to this point we have introduced the effective Hamiltonian as a theoretical concept which facilitates the analysis of complex fluids, by reducing the original, many-component problem to an effective one-component one. The task for the theorist is now to find a reasonable approximation for the effective potential. The validity of such approximations has to be tested, before it can be used for the next step in calculating thermodynamical properties like structural correlations for the effective one-component system. The mentioned test can be done by experiment or by computer simulations.

There are experimental methods by which the force between two colloidal particles can be measured using a surface force apparatus (SFA) [77, 78, 79] or atomic force microscopy

(AFM) [80]. A different technique used is total internal reflection microscopy (TIRM) [81, 82, 83, 84], which can measure the effective interaction directly [85]. However, in all these methods, one measures the effective potential only [86]. They do not offer the possibility to measure the volume term $\Omega f_0(\rho_1, \rho_2, T)$.

A different approach to test a theoretical prediction for the effective potential are computer "experiments", like Monte-Carlo (MC) or Molecular Dynamics (MD) simulations [2, 1]. As can be seen from Eq. (2.40), the effective Hamiltonian is the sum of the direct Hamiltonian $\mathcal{H}_{11}$ and the free energy of the small degrees of freedom in the external field of the large particles. It is a well-known fact that in a standard simulation only averages of operators can be calculated [2, 1]; the calculation of a partition function, such as $Q_2(\{\boldsymbol{R}\})$, requires the use of special techniques, such as thermodynamic integration [86]. Hence, a straightforward simulation cannot yield the effective Hamiltonian directly. Instead, one resorts to the calculation of other quantities: In a MC simulation one can calculate the second virial coefficient of the system, which contains the effective pair potential in the Boltzmann factor. Or one calculate the pair-correlation function $g(r)$ and obtain from the relation $g(r) = e^{-\beta V_{\text{eff}}}$ the effective pair potential. A different, straightforward way is the calculation of the force $\boldsymbol{F}_i$ acting on the macroparticle i [86, 28], instead of the potential:

$$\boldsymbol{F}_i = -\nabla_{\boldsymbol{R}_i} \mathcal{H}_{\text{eff}}(\{\boldsymbol{R}\}). \tag{2.52}$$

Using Eq. (2.43) and (2.44) we find

$$\begin{aligned} \boldsymbol{F}_i &= \sum_{j\neq i} [-\nabla_{\boldsymbol{R}_i} v_{11}(|\boldsymbol{R}_i - \boldsymbol{R}_j|)] \\ &\quad + \frac{1}{Z_2(\{\boldsymbol{R}\})} \int \mathrm{d}\boldsymbol{r}^{N_2} [-\nabla_{\boldsymbol{R}_i} V_{12}(\{\boldsymbol{R}\}, \{\boldsymbol{r}\})] \mathrm{e}^{-\beta[V_{22}(\{\mathbf{r}\}) + V_{12}(\{\mathbf{R}\},\{\mathbf{r}\})]} \\ &= \sum_{j\neq i} [-\nabla_{\boldsymbol{R}_i} v_{11}(|\boldsymbol{R}_i - \boldsymbol{R}_j|)] + \left\langle -\nabla_{\boldsymbol{R}_i} V_{12}(\{\boldsymbol{R}\}, \{\boldsymbol{r}\}) \right\rangle_2, \end{aligned} \tag{2.53}$$

which shows that the effective force is the sum of the direct force and the average over the small degrees of freedom of the forces exerted from the small particles to the large one, denoted by $\langle \ldots \rangle_2$. MD simulations are suitable for calculations of statistical averages. The force can be measured in a straightforward way and can be compared with theoretical expressions for the effective potentials. Once more, the volume terms cannot be measured in this way; their gradient with respect to any coordinate vanishes identically.

The expression in Eq. (2.53) is very important for the further considerations, because it justifies the comparison of simulation results for the effective force with the theoretical predictions. This method has already been applied for star polymers [28] and in this work it is also applied for star-shaped polyelectrolytes, as will see in the next chapter.

Chapter 3

Star-shaped Polyelectrolytes

Polyelectrolytes (PEs) are polymer chains carrying ionizable groups along their backbone. Upon solution into a polar (aqueous) solvent, these groups dissociate into the solvent, leaving behind a charged polymer in coexistence with its dissolved counterions. The problem of the structure of PE-solutions is a challenging one from the theoretical point of view, because it combines the complexities of polymer physics, chain connectivity and self-avoidance, and of the long-range Coulomb interaction between the charged monomers. At the same time, there exists vivid interest on these molecules, due to their numerous biological and technological applications. Typical PE-biomolecules are DNA and proteins; sulfonated polystyrene and polyacrylic acid, the key ingredient in diapers, are some of the most common commercially used polyelectrolytes. The structure of PE solutions, the conformational properties of the constituent macromolecules in the same, as well as the questions of counterion condensation and chain collapse have been the subject of many recent investigations [87, 88, 38, 89, 90, 91, 92, 93, 94, 95] employing a variety of theoretical and computational approaches. [96]

When polyelectrolytes are grafted on surfaces they form a polyelectrolyte-brush. Considerable progress towards a theoretical understanding of the properties of *planar* brushes has been made through the use of scaling theory, self-consistent field (SCF) calculations, and computer simulations. [97, 98, 99, 100, 101] Much less is known about spherical PE-brushes. These result by grafting PE's of contour length L on spherical colloidal particles of radius b. In the limit $L \gg b$, one obtains the star-branched polyelectrolytes or simply PE-stars. These are systems of great physical and practical importance: grafting of PE chains on colloidal particles dissolved in polar solvents greatly enhances their stability against flocculation; [102, 42] PE brushes are models of block copolymer micelles formed by hydrophobically modified PEs in aqueous solutions; [48] and they have considerable potential in industrial applications due to the increased need for water-supported systems. [103, 104] Pincus was the first to present a theory on the interactions of PE-stars, based on scaling ideas. [102] The two fundamental ingredients in Pincus' approach are the retraction of the chains of the stars as they approach each other (no interdigitation) and the domination of the force acting between them by the entropic contribution of the trapped counterions. PE-stars that have

the property of absorbing most of the counterions are called *osmotic*. [47] Based on these assumptions, Pincus predicted that the force between two PE-stars should be independent of their separation. Borisov *et al.* put forward a scaling theory, together with SCF calculations to study the conformations of isolated PE stars. [47, 48, 46]

In a recent Letter, [54] we proposed an analytical theory for the conformations and interactions of PE-stars and compared its predictions with the results from Molecular Dynamics computer simulations. In this Chapter, we give a detailed account of the theoretical model, which is valid for both isolated and interacting stars, and present more extensive comparisons with simulations for both salt-free and salt-containing solutions. We have investigated the sizes, conformations and interactions of PE-stars for high charging fractions $\alpha \geq 1/6$. We find a stretching of the chains and significant counterion condensation. For the force between two stars, our results are quantitatively different than the early predictions of Ref. [102], in that we find the force to be dependent on the star-star separations. Qualitatively, however, we confirm Pincus' prediction, [102] stating that the interaction is dominated by the entropic effects of the counterions and not by the electrostatic contribution. Simple, analytical expressions for the effective interactions between PE-stars for given arm numbers and charging fractions are also put forward.

The rest of the Chapter is organized as follows: in Section 3.1 we examine the conformations of isolated stars, and in particular: in Section 3.1.1 we introduce the simulation model, in Section 3.1.2 we discuss the obtain density profiles from simulations, which are used as input to the theory presented in Section 3.1.3. The conformations of PE-stars with added salt are discussed in Section 3.1.4. In Section 3.2 we turn our attention to the effective interactions between two PE-stars. The theory is presented in Section 3.2.1, and the results and comparisons to simulations in Section 3.2.2 for the salt-free case and in Section 3.2.3 for the case of added salt. In Section 3.3 we summarize and conclude the Chapter. As the theoretical model involves the calculation of electrostatic potentials for unusual geometries, we present this technical part in the Appendix C.

3.1 Dilute solutions: sizes and conformations of isolated polyelectrolyte-stars

In a very dilute solution of PE-stars, the interactions between the macromolecular aggregates are very weak. Therefore, in scattering experiments the total scattering intensity gives information about the *form factor* of the star, i.e., about the size, shape, and density distributions of the monomers around the star center. [69] In this Section, we present the results of MD simulations and theory regarding the density profiles, sizes and counterion distributions of isolated stars.

3.1.1 The simulation model

We begin with the description of the simulation model, valid for both a single star polyelectrolyte and two star polyelectrolytes. We performed monomer-resolved Molecular Dynamics (MD) simulations using the model of Kremer *et al.* for single polyelectrolyte chains. [51, 18, 20] In our considerations we have f chains with N monomers per chain, all chains coupled at a common core, whose size $R_{\rm d}$ is much smaller than the extension of the star-shaped macromolecule. The introduction of the core is necessary to accommodate the chains close to the center, where the monomer density is high.

The polyelectrolyte chains are modeled as bead-spring chains of Lennard-Jones (LJ) particles. The idea of this method was first applied on neutral linear polymers and on a single star polymer. [18, 20] For good solvent conditions, a shifted LJ potential is used to describe the purely repulsive excluded volume interaction between all Nf monomers:

$$V_{\rm LJ}(r) = \begin{cases} 4\varepsilon_{\rm LJ}\left[\left(\frac{\sigma_{\rm LJ}}{r}\right)^{12} - \left(\frac{\sigma_{\rm LJ}}{r}\right)^{6} + \frac{1}{4}\right] & \text{for } r \le 2^{1/6}\sigma_{\rm LJ}; \\ 0 & \text{for } r > 2^{1/6}\sigma_{\rm LJ}. \end{cases} \tag{3.1}$$

Here, r is the distance of the interacting beads, $\sigma_{\rm LJ}$ is the microscopic length scale of the beads and $\varepsilon_{\rm LJ}$ sets the energy scale. In accordance with previous work, [28] we have chosen for the temperature $T = 1.2\varepsilon_{\rm LJ}/k_{\rm B}$, where $k_{\rm B}$ is the Boltzmann constant.

The connectivity of the bonded monomers is assured by a finite extension nonlinear elastic (FENE) potential:

$$V_{\rm FENE}(r) = \begin{cases} -\frac{1}{2}k_{\rm FENE}\left(\frac{R_0}{\sigma_{\rm LJ}}\right)^2 \ln\left[1 - \left(\frac{r}{R_0}\right)^2\right] & \text{for } r \le R_0; \\ \infty & \text{for } r > R_0, \end{cases} \tag{3.2}$$

where $k_{\rm FENE}$ denotes the spring constant and is set to $k_{\rm FENE} = 7.0\varepsilon_{\rm LJ}$. This interaction diverges at $r = R_0$, which determines the maximal relative displacement of two neighboring beads, as can be seen from the plot in Fig. 3.1. The energy $\varepsilon_{\rm LJ}$ is the same as in Eq. (3.1), whereas for the length scale R_0 we have chosen the value $R_0 = 2.0\,\sigma_{\rm LJ}$.

The interactions between the monomers and the central particle mentioned above are modeled as follows. All monomers have a repulsive interaction $V^c_{\rm LJ}(r)$ of the truncated and shifted Lennard-Jones type with the central particle,

$$V^c_{\rm LJ}(r) = \begin{cases} \infty & \text{for } r \le R_{\rm d}; \\ V_{\rm LJ}(r - R_{\rm d}) & \text{for } r > R_{\rm d}, \end{cases} \tag{3.3}$$

whereas the innermost monomers in the chain experience an additional attractive potential $V^c_{\rm FENE}(r)$ of the FENE type with this chain, namely

$$V^c_{\rm FENE}(r) = \begin{cases} \infty & \text{for } r \le R_{\rm d}; \\ V_{\rm FENE}(r - R_{\rm d}) & \text{for } r > R_{\rm d}. \end{cases} \tag{3.4}$$

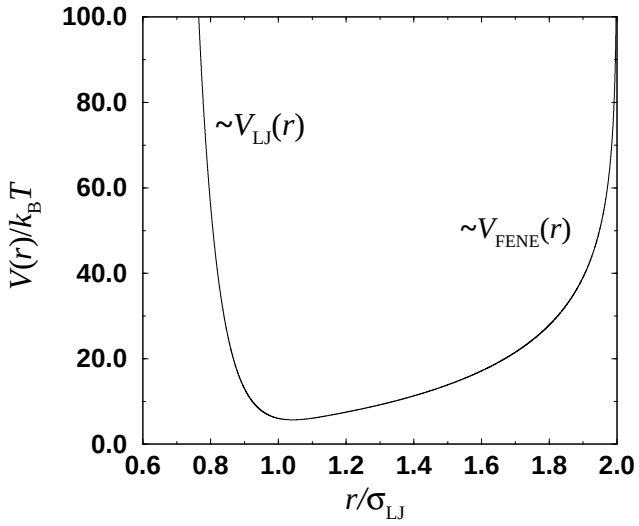

Figure 3.1: Potential energy between two bonded monomers. The energy consists of the repulsive Lennard-Jones term and a FENE contribution, Eqs. (3.1) and (3.2), respectively. The maximum distance between the bonded monomers is $r = R_0 = 2\sigma_{\mathrm{LJ}}$.

Each chain is charged by a fraction α in a periodical manner: every $1/\alpha$ bead carries a monovalent charge. For reasons of electroneutrality, the same amount of monovalent charges as the charged monomers, namely the $N_c = \alpha f N$ released counterions, are included in the simulation box. They are able to freely move in the box, thereby they are simulated explicitly. The snapshot shown in Fig. 3.2 illustrates the different kinds of particles in the system.

The full Coulomb interaction $V_{\mathrm{Coul}}(r)$ between all charged units (monomer ions and counterions) has finally to be taken into account, see also the energy plot for charged particles in Fig. 3.3::

$$V_{\mathrm{Coul}}(r_{ij}) = \frac{q_i q_j e^2}{\epsilon r_{ij}} \equiv k_{\mathrm{B}} T l_{\mathrm{B}} \frac{q_i q_j}{r_{ij}}, \tag{3.5}$$

where $q_i = \pm 1$ for the charged monomers and the counterions, respectively. The Bjerrum length l_{B} is defined as the length at which the electrostatic energy equals the thermal energy:

$$l_{\mathrm{B}} = \frac{e^2}{\epsilon k_{\mathrm{B}} T}, \tag{3.6}$$

where e is the unit charge of the interacting particles, and ϵ the permittivity of the solvent. For water in room temperature one obtains $l_{\mathrm{B}} = 7.1$Å. Unless explicitly mentioned, no salt is added. The solvent is only taken into account via the dielectric background ϵ. The Bjerrum length is fixed to $l_{\mathrm{B}} = 3.0\sigma_{\mathrm{LJ}}$. This is a realistic value for typical polyelectrolytes, such as the hydrophobic sodium poly(styrene-*co*-styrene sulfonate) (NaPSS) or the hydrophilic poly(acrylamide-*co*-sodium-2-acrylamido-2-methylpropane-sulfonate). [105] The long-ranged Coulomb forces are calculated via the Lekner method [58]. The details of the methods are presented in App. B.

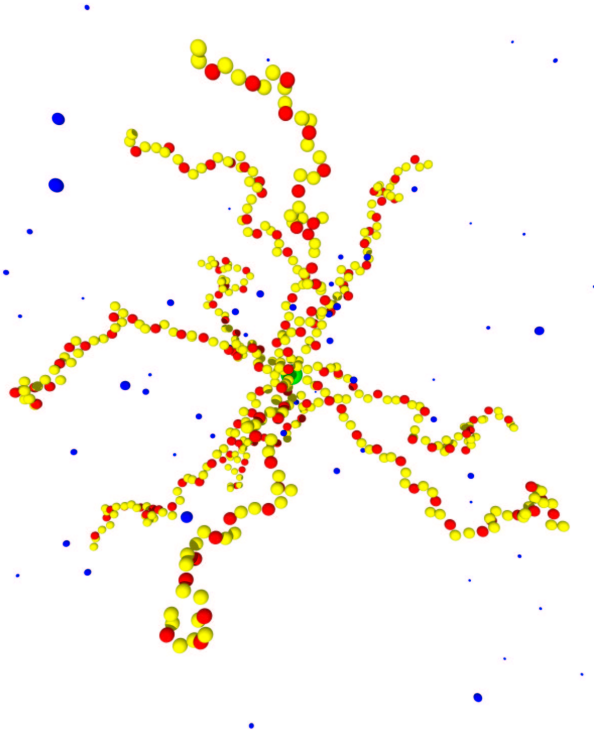

Figure 3.2: Snapshot of a star-branched polyelectrolyte with $f = 10$, $N = 50$ and $\alpha = 1/3$. The bright gray balls are the neutral monomers, the dark spheres along the chains indicate the charged monomers (every third ball). The counterions are the small, dark spheres around the star.

The single polyelectrolyte star was simulated in a cubic box with a typical edge length of $L_b = 90\sigma_{\mathrm{LJ}}$ with periodic boundary conditions, emulating a dilute PE-star solution. The box size was varied as well, in order to investigate the influence of the long-ranged Coulomb forces and of the density on the single-star conformations.

The core of the star was located at the box center and remained fixed during the simulation run. The time step was typically $\Delta t = 0.002\tau$ with $\tau = \sqrt{m\sigma_{\mathrm{LJ}}^2/\varepsilon_{\mathrm{LJ}}}$ being the associated time unit and m the monomer mass. The counterions were taken to have the same mass and size as the charged monomers.

After a long equilibration time ($150\,000 - 200\,000$ time steps), different static quantities were calculated during simulation runs lasting between $500\,000 - 1\,300\,000$ time steps, namely the center-to-end distances R and the density profiles of the monomers, the monomer ions, and the counterions that are trapped within the star due to the attractive Coulomb interaction between them and the monomer ions. Simulations were carried out for a variety of arm numbers f ($f = 5$, 10, 18, 30, 40, 50) and charge fractions α ($\alpha = 1/6$, $1/4$, $1/3$), allowing us to make systematic predictions for the f- and α-dependencies of all theoretical parameters. In addition, we investigated the chain length dependence by varying the degree

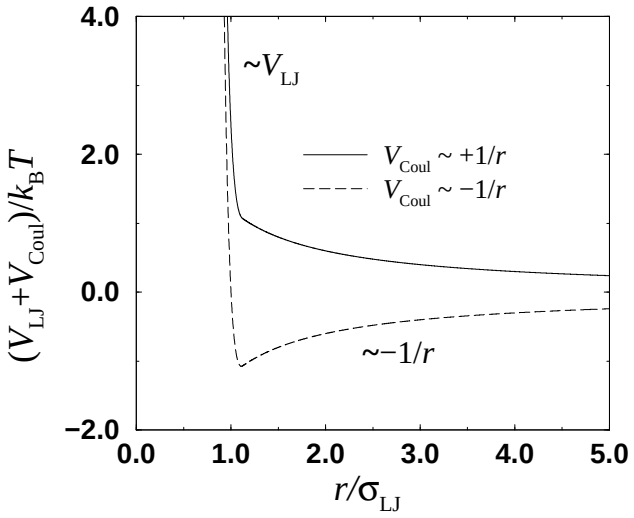

Figure 3.3: Potential energy between nonbonded charged particles (monomer ions and counterions). The energy consists of the repulsive Lennard-Jones term and the Coulomb interaction, Eqs. (3.1) and (3.5), respectively. The Lennard-Jones potential ensures that two opposite charged particles cannot fuse; the system is stable against implosion. However, due to the minimum in the energy counterion condensation is possible.

of polymerization N of the chains. The values $N = 50$, 100, 150, and 200 were considered.

3.1.2 The density profile

Let $c_{\mathrm{mon}}(r)$, $c_{\mathrm{charge}}(r)$ and $c_{\mathrm{counter}}(r)$ be the expectation values of the one-particle densities of the monomers, charged monomers and counterions as functions of the distance from the star center r, respectively. We measured all three quantities during the simulation run and investigated primarily their f- and α-dependence. In addition, we measured the fraction of trapped counterions that were condensed along the rods, by surrounding every charged monomer with a fictitious sphere of radius l_{B} and monitoring the number of counterions inside all spheres.

We focus here on the density profiles. As seen in Fig. 3.4, the monomers show a scaling behavior of their profile, a feature qualitatively similar to neutral star polymers [28, 12]. Quantitatively, however, the scaling exponent is different: in the neutral-star case, one obtains $c(r) \sim r^{-4/3}$, [12, 18, 20] in the charged-star case we obtain a power-law $c(r) \sim r^{-1.8}$, i.e., the chains are much more stretched. To demonstrate this point, we show in Fig. 3.5 snapshots of a charged and a neutral star; the stretching of the chains of the charged star is manifest.

The fully rod-like chain limit yields a monomer profile scaling as [46, 47] $c(r) \sim r^{-2}$ and hence a slope -2 in a double-logarithmic plot. This rod-like behavior has been experimen-

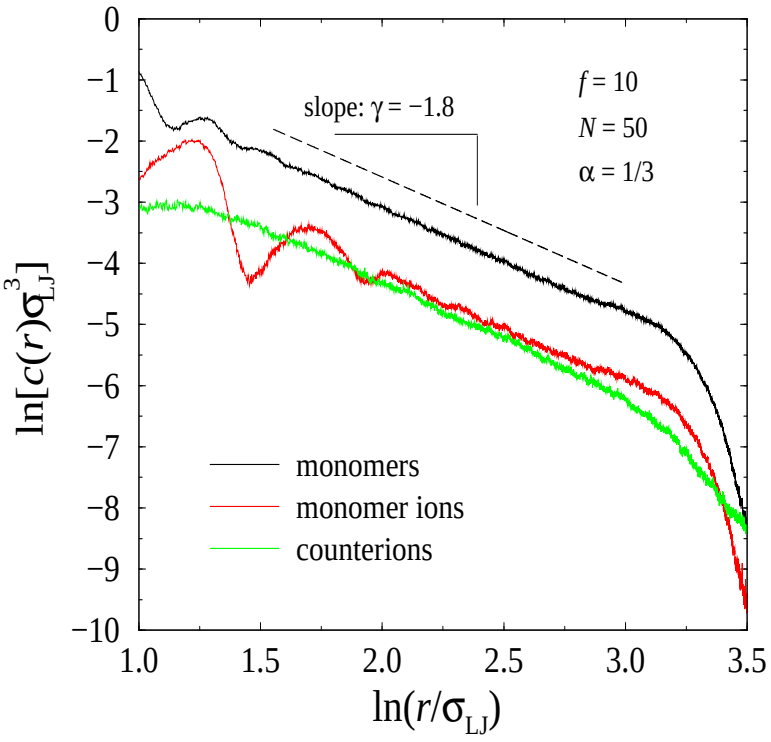

Figure 3.4: Double-logarithmic plot of the density profile of monomers, monomer ions, and counterions, for a star with $f = 10$, $N = 50$ and $\alpha = 1/3$. The slope of the scaling regime is also shown. Its value, $\gamma = -1.8$ indicates the stretching of the chains.

tally observed in neutron scattering studies of block copolymer micelles. [106] Because of small lateral fluctuations of the chains, [92, 93] the fully rod-like limit is not reached here and the slope $\gamma = -1.8$ is obtained. Nevertheless, the value indicates an almost complete stretching of the chains. The counterion density profile shows the same scaling as that of the monomers. This is a manifestation of the tendency of the counterions to achieve local charge neutrality, a feature also seen in simulations of planar polyelectrolyte brushes. [100] However, the counterions, in contrast to the monomers, are not bounded and therefore they add a high entropic contribution to the free energy of the system. This is a relevant point because many investigations on these systems are based on homogeneous distributions of the counterions within PE-stars polyelectrolytes. [46, 47, 45, 48] As we will see in Section 3.2, the inhomogeneous behavior of the counterions play a crucial role for the effective interaction between two polyelectrolyte stars.

3.1.3 Theory of isolated polyelectrolyte-stars

In the theoretical investigations, we employ a mean-field, Flory-type approach for the analysis of the large-scale properties of polyelectrolyte stars, which is akin to that of Ref. [48].

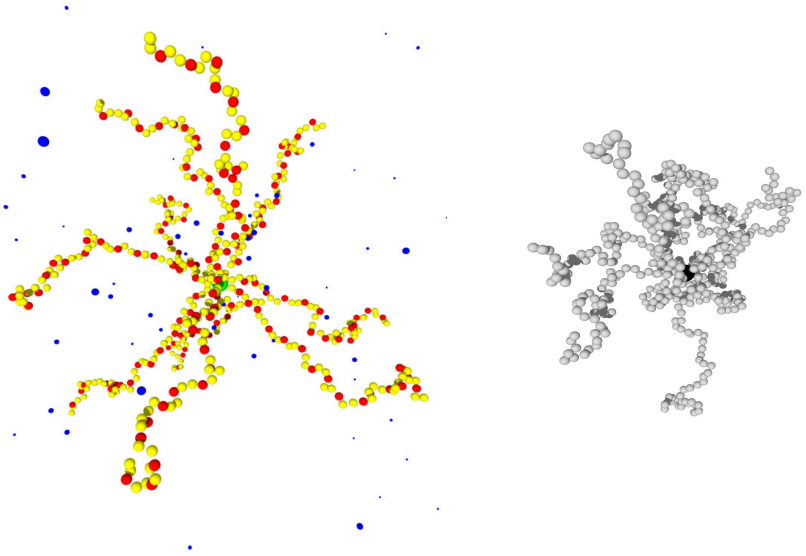

Figure 3.5: Snapshots of a polyelectrolyte star (left picture, $\alpha = 1/3$) and a neutral star polymer (right picture, $\alpha = 0$) each with $f = 10$ arms and $N = 50$ monomers per arm. The stretching of the chains in the case of the charged star, in contrast to the neutral star, can be clearly seen.

We consider a star in a dilute solution of density $\rho_{\rm st} = N_{\rm st}/V$ containing $N_{\rm st}$ PE-stars in the macroscopic volume V. We define accordingly the 'Wigner-Seitz radius' (or 'ion-sphere radius') $R_W = (4\pi\rho_{\rm st}/3)^{-1/3}$. The star is envisioned as a sphere of radius R enclosed in a cell of radius $R_W > R$; all counterions are restricted to move inside this cell. Fig. 3.6 illustrates the situation and is helpful for the further considerations.

Particular attention has to be paid to the Manning-condensation of counterions on the rod-like chains. [90, 91, 37, 67, 107] The condensation takes place when the dimensionless parameter $\xi = l_{\rm B} N\alpha/R$ exceeds unity. [37] This condition is satisfied for all our parameter combinations, see Tables 3.1-3.3. Thus, in the model, the N_c counterions are partitioned into three different states: N_1 *condensed* counterions within f tubes around the branches of the star: these are confined to move in quasi one-dimensional cylindrical domains. N_2 *trapped* counterions inside the star: these are allowed to explore the whole interior of the star. Finally, N_3 *free* counterions that move into the bulk of the solution and in the model they are located in the region $R < r < R_W$. This approach is similar to the three-state model of Kramarenko *et al.*, [108] employed for polyelectrolyte microgel particles. To specify the available volumes to the condensed and trapped counterions, we introduce tubes of length R and radius $l_{\rm B}$ surrounding each rod, and treat all counterions contained in these tubes as condensed. Thus, the interior volume $V(R) = 4\pi R^3/3$ of the star is divided as $V(R) = V_1 + V_2 + f\pi\sigma_{\rm LJ}^2 R$ with $V_1 = f\pi(l_{\rm B}^2 - \sigma_{\rm LJ}^2)R$ being the total volume of the hollow tubes, available to the condensed counterions, and V_2 the volume remaining available to the

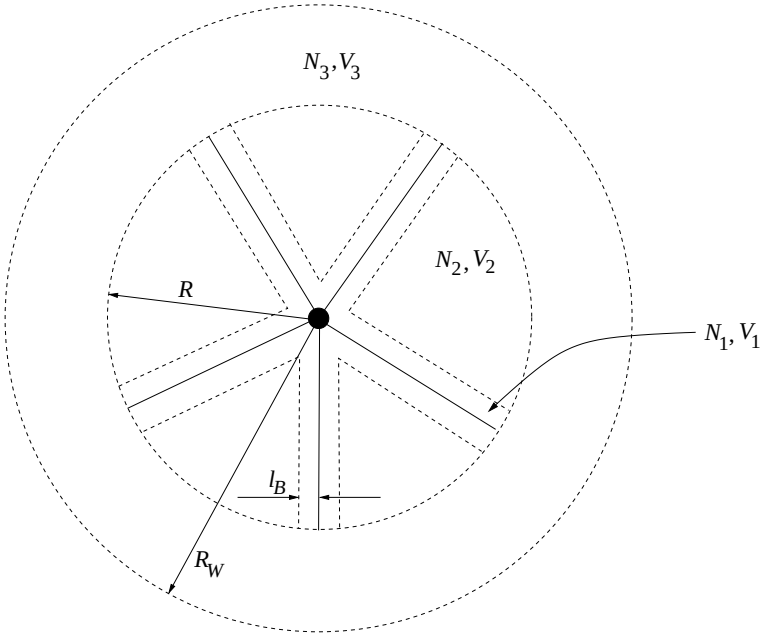

Figure 3.6: A sketch of a polyelectrolyte-star in its spherical Wigner-Seitz cell. For demonstration, five chains (solid lines) are assumed to be fully stretched and are surrounded by cylinders (dashed lines) where the condensed counterions are located. For further explanations, see text.

N_2 trapped counterions inside. Moreover, let $V_3 = 4\pi(R_W^3 - R^3)/3$ be the volume of the spherical shell for the free counterions, and $\rho_i(r)$, $i = 1, 2, 3$, the *number* densities of the three counterion types. Clearly, the number of free counterions N_3 is equal to the number of the uncompensated charges of the star Q^*/e. We emphasize that all counterions are indistinguishable particles and have been treated in this way in all considerations to follow. Particle exchanges between the three possible states constantly take place and the numbers N_i, $i = 1, 2, 3$ are simply expectation values and not prescribed occupation numbers of counterions that have been 'marked' to belong to one state or the other.

The equilibrium values for R and N_i are determined through minimization of a variational free energy which we write as

$$\mathcal{F}(R, \{N_i\}) = U_{\mathrm{H}} + U_c + F_{\mathrm{el}} + F_{\mathrm{Fl}} + \sum_{i=1}^{3} S_i, \tag{3.7}$$

where U_{H} and U_c are electrostatic contributions, F_{el} and F_{Fl} elastic and self-avoidance contributions from the chains and S_i entropic contributions from the counterions, to be described in detail in what follows.

The term U_{H} is the Hartree-type, mean-field electrostatic energy of the whole star:

$$U_{\mathrm{H}} = \frac{1}{2\epsilon} \int\int \mathrm{d}^3 r \mathrm{d}^3 r' \frac{\varrho(\boldsymbol{r})\,\varrho(\boldsymbol{r'})}{|\boldsymbol{r} - \boldsymbol{r'}|}, \tag{3.8}$$

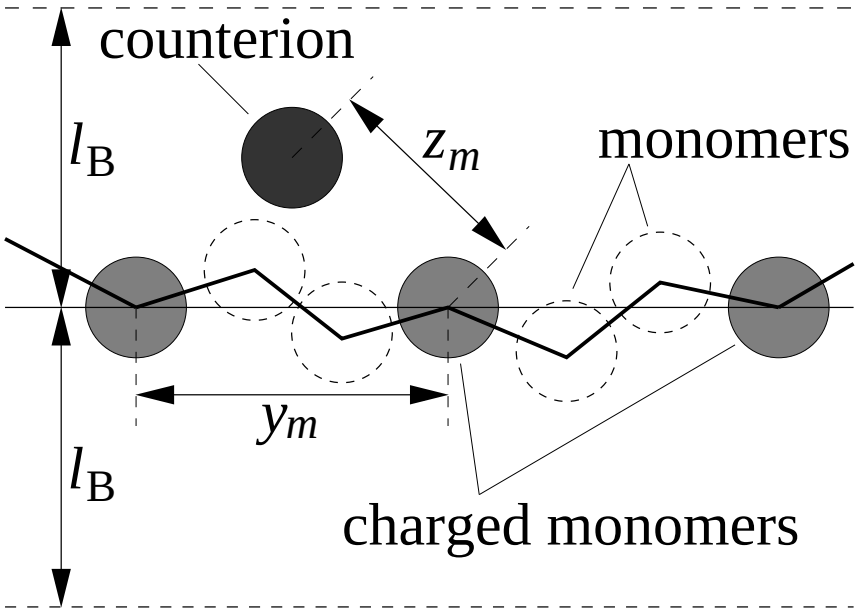

Figure 3.7: A sketch of a chain segment for the case $\alpha = 1/3$, showing monomers (dashed-lined hollow spheres), charged monomers (bright gray spheres) and a counterion (dark gray sphere). The tube radius is l_B from the central line, indicating the stretched behavior of the chain. The neutral monomers can deviate from the central line, whereas the charged monomers are situated along this line. The counterion is assumed to be placed between two charged monomers with a distance z_m to them.

with the local *charge* density $\varrho(\boldsymbol{r})$ to be defined below. The only relevant correlations arise between the condensed counterions and the charges on the chains because the average density of the trapped counterions is very low. Hence, the correlation energy U_c stems from the attractions between the rods and the condensed counterions contained in the associated tubes. To estimate the average rod–condensed counterion separation z_m, we take $z_m = (1/2)\sqrt{l_B^2 + y_m^2}$, where $y_m = R/(N\alpha)$ is the distance between two sequential charged monomers along the chain, obtaining for the correlation energy resulting from N_1 condensed counterions:

$$\frac{U_c}{k_B T} = -\frac{l_B N_1}{z_m}. \tag{3.9}$$

Fig. 3.7 illustrates the chosen value for z_m resulting from geometrical considerations. The term F_{el} is the elastic contribution of the chains, written as

$$\frac{F_{el}}{k_B T} = \frac{3fR^2}{2N}, \tag{3.10}$$

and is a Gaussian approximation of the conformational entropy of the arms of the star. For the non-electrostatic contribution of the chains F_{Fl}, arising through their self-avoidance, we

employ the Flory-type expression

$$\frac{F_{\rm Fl}}{k_{\rm B}T} = \frac{3v(fN)^2}{8\pi R^3}, \tag{3.11}$$

with the excluded volume parameter v. As usual for the case of good-solvent conditions, triplet-monomer contributions have been omitted. Finally, the terms S_i are ideal entropic contributions of the form

$$S_i = k_{\rm B}T \int_{V_i} {\rm d}^3r\, \rho_i(r) \ln \rho_i(r), \tag{3.12}$$

with $\rho_i(r) = N_i/V_i$ being the number densities of the counterions in the three possible states.

We discuss now the mean-field electrostatic and the entropic terms in more detail. The calculation of the mean-field electrostatic energy $U_{\rm H}$, Eq. (3.8), can be rewritten with the introduction of the electrostatic potential $\Phi(r)$ in the form:

$$U_H = \frac{\epsilon}{2} \int_0^{R_W} {\rm d}r \left(\frac{{\rm d}\Phi(r)}{{\rm d}r} \right)^2 r^2, \tag{3.13}$$

in spherical coordinates. Using Poisson's equation, the electrostatic field $({\rm d}\Phi(r)/{\rm d}r)$ is given by

$$-\frac{{\rm d}\Phi(r)}{{\rm d}r} = \frac{4\pi e}{\epsilon r^2} \int_0^r {\rm d}r' r'^2 \varrho(r'), \tag{3.14}$$

with the charge distribution $\varrho(r)$. Since the chains are modeled as being fully stretched, the density distributions inside the stars fall off as $\sim r^{-2}$ from the center but are uniform outside the star. We note that this is different from the approach of Ref. [48], where uniform densities inside *and* outside the star were employed. Though we obtained reasonable results for the isolated star using such trial profiles, the nonuniform ones are of paramount importance for obtaining agreement with simulation results regarding the effective interaction, as we will discuss shortly. Accordingly, we write

$$\frac{\varrho(\boldsymbol{r})}{Q^*} = \frac{\Theta(R-r)}{4\pi R r^2} - \frac{\Theta(r-R)\Theta(R_W-r)}{V_3}, \tag{3.15}$$

with the net charge $Q^* = |e|(N_c - N_1 - N_2) = |e|N_3$ and the Heaviside step function $\Theta(x)$.

Inserting Eq. (3.15) into Eq. (3.14), and integrating the result of $({\rm d}\Phi(r)/{\rm d}r)$ in Eq. (3.13), yield for the electrostatic energy

$$\frac{U_H}{k_{\rm B}T} = \frac{N_3^2 l_{\rm B}}{2R} \vartheta\left(\frac{R}{R_W}\right), \tag{3.16}$$

where the function $\vartheta(x)$ is given by

$$\vartheta(x) = 1 + \frac{5 - 9x + 5x^3 - x^6}{5(1-x^3)^2}. \tag{3.17}$$

In order to calculate the entropic contributions of the counterions in Eq. (3.12), we need to specify the number densities $\rho_i(r)$. We model the condensed counterions as having a

uniform distribution inside the tubes, an assumption supported by simulation results on single PE-chains having typical values of the ratios $\alpha l_{\rm B}/\sigma_{\rm LJ}$ considered here. [90] Thus, $\rho_1(r) = N_1/V_1$ inside the tubes and zero otherwise. Since the trapped counterions follow the profile of the charged monomers, we take $\rho_2(r) = C\, r^{-2}\Theta(R-r)$, with the proportionality constant C determined through the normalization condition

$$\int_{V_2} {\rm d}^3 r \rho_2(r) = N_2. \tag{3.18}$$

Finally, we assume a uniform distribution of the free counterions within the cell $R < r < R_W$ and take $\rho_3(r) = \Theta(r-R)\Theta(R_W - r)N_3/V_3$. Referring to ρ_2, we note that the volume which is available for the 'free' counterions inside the star is reduced by the tubes around the chains. We therefore introduce a representative sphere of radius R' having the same volume V_2 as that available to the N_2 counterions and calculate the prefactor C of ρ_2 using the normalization condition (3.18):

$$C = \frac{N_2}{4\pi R'}. \tag{3.19}$$

The reduced radius R' is determined by the equation

$$\frac{4\pi}{3}R^3 - f\pi l_{\rm B}^2 R = \frac{4\pi}{3}R'^3 \equiv V_2, \tag{3.20}$$

yielding

$$R' = R\left[1 - \frac{3}{4}f\left(\frac{l_{\rm B}}{R}\right)^2\right]^{1/3}. \tag{3.21}$$

Carrying out the integrations in Eq. (3.12), we obtain the following expressions for the entropic contributions of the counterions in their three different states:

$$\frac{S_1}{k_{\rm B}T} = N_1\left[\ln\left(\frac{N_1}{V_1}\right) - 1\right], \tag{3.22}$$

$$\frac{S_2}{k_{\rm B}T} = N_2\left[\ln\left(\frac{N_2}{4\pi R'^3}\right) + 1\right], \tag{3.23}$$

$$\frac{S_3}{k_{\rm B}T} = N_3\left[\ln\left(\frac{N_3}{V_3 - V(R)}\right) - 1\right]. \tag{3.24}$$

The Flory-term in Eq. (3.11) takes into account, in a mean-field fashion, the loss of entropy of the chains due to the *short-range*, steric repulsions of the monomers, through the effective, excluded-volume parameter v. The value of this parameter for stiff PEs has been the topic of extensive discussion in the literature. [67, 98, 102] If the chains were neutral, then a good estimate for v term would be the volume of the monomer bead, $v \cong \sigma_{\rm LJ}^3$. The presence of the condensed counterions, though, introduces monomer pairs along the backbones of the chains, whose effective diameter is $\sigma_{\rm pair} > \sigma_{\rm LJ}$. Since the condensed counterions are to be found in typical distances $l_{\rm B}$ from the chain backbone, we thereby set $\sigma_{\rm pair} = l_{\rm B} = 3\,\sigma_{\rm LJ}$ and

obtain thereby $v = \sigma^3_{\rm pair} \cong 30\,\sigma^3_{\rm LJ}$. This is the value that we employed in all our theoretical analyses. It is also in agreement with the 'screened electrostatic' estimate $v \cong l_{\rm B}\kappa^{-2}\alpha^2$ of Ref. [48], with $\kappa = \sqrt{3N_2 l_{\rm B}/R^3}$, for typical values of α, N_2 and R read off from Table 3.1.

The values R and N_i $(i = 1, 2, 3)$ are found by minimization of the free energy, i.e., through the equations

$$\left(\frac{\partial \mathcal{F}(R,\{N_i\})}{\partial R}\right)_{\{N_i\}} = \left(\frac{\partial \mathcal{F}(R,\{N_i\})}{\partial N_i}\right)_{R,\{N_j\}_{i\neq j}} = 0. \tag{3.25}$$

The results read as

$$\begin{aligned} R^3 &= \frac{N}{3f}\left\{\frac{1}{2}l_{\rm B}N_3^2\left[\vartheta(R/R_W) - \frac{R}{R_W}\vartheta'(R/R_W)\right]\right. \\ &+ 3R\left[N_2\left(1 + \frac{2}{3}\frac{\pi f l_{\rm B}^2 R}{V(R')}\right) - N_3\frac{V(R)}{V_3}\right] \\ &+ \left. N_1 R\left[1 - \left(\frac{f}{N_c}\right)^2\frac{l_{\rm B}^2}{4z_m^3}\right] + \frac{9}{8\pi}\left(\frac{fN}{R}\right)^2 v\right\}; \end{aligned} \tag{3.26}$$

$$N_3 = \frac{R}{l_{\rm B}\vartheta(R/R_W)}\left\{2 + \ln\left[\left(\frac{N_c - N_1}{N_3} - 1\right)\frac{V_3}{3V_2}\right]\right\}; \tag{3.27}$$

$$N_1 = (N_c - N_3)\left[1 + \frac{3V_2}{V_1}\exp\left(-2 - \frac{l_{\rm B}}{z_m}\right)\right]^{-1}, \tag{3.28}$$

where $\vartheta'(x) = {\rm d}\vartheta/{\rm d}x$. These three equations determine the star size R, the uncompensated charge $Q^* = N_3|e|$ inside R and the number of condensed counterions N_1 as functions of the functionality f, the degree of polymerization N, the bare charge $N_c = \alpha f N$, and the Wigner-Seitz cell radius R_W. All quantities acquire an explicit density-dependence through R_W, a usual situation for charged systems, familiar from the statistical mechanics of charged-stabilized colloids as well. [109] We calculated these quantities for different parameters and compared the results with the simulation data; the comparison is shown in Tables 3.1 and 3.2.

Referring to Table 3.1, in which the degree of polymerization is fixed to $N = 50$, we see that the radii values from theory and simulation are in very good agreement for all parameter combinations considered. Moreover, the radius is practically f-independent, a manifestation of the fact that the chains are stretched. This is one of the features that distinguish PE-stars from neutral ones, for which the scaling $R \sim f^{1/5}N^{3/5}$ holds. [28, 12] As far as the total number of trapped counterions $N_{\rm in} = N_1 + N_2$ and N_1 of condensed counterions are concerned, the following remarks can be made: both are overestimated in the theory, by an amount depending on the charging fraction α. This overestimation can be explained by the fact that we assumed a complete stretching of the chains (rod-like configuration), which results into a stronger electrostatic attraction than the true one, in which lateral chain fluctuations are present. The same mechanism is responsible for the overestimation

f	α	Q	$(R/\sigma_{\rm LJ})^1$	$(R/\sigma_{\rm LJ})^2$	$(N_{\rm in})^a$	$(N_{\rm in})^b$	$(N_1)^a$	$(N_1)^b$
5	1/3	80	26.8	26.1	47	57	27	25
10	1/6	80	23.4	23.7	42	59	22	38
10	1/4	120	25.3	25.2	77	97	46	61
10	1/3	160	27.4	26.9	110	134	72	81
18	1/6	144	24.2	25.8	91	121	60	90
18	1/4	216	26.6	26.9	156	190	107	141
18	1/3	288	28.3	28.1	217	260	159	190
30	1/4	360	27.2	28.8	278	332	213	272
30	1/3	480	28.6	29.7	384	449	309	366
40	1/3	640	29.2	30.9	531	607	392	517
50	1/3	800	29.8	32.0	668	763	514	670

Table 3.1: Comparison of conformational properties between simulation and theory for different arm numbers f. The chain length is fixed to $N = 50$, and the cell radius is $R_W = 55.83\,\sigma_{\rm LJ}$, except for $f = 40$ ($R_W = 62.04\,\sigma_{\rm LJ}$), and $f = 50$ ($R_W = 74.44\,\sigma_{\rm LJ}$).

N	Q	$(R/\sigma_{\rm LJ})^3$	$(R/\sigma_{\rm LJ})^4$	$(N_{\rm in})^a$	$(N_{\rm in})^b$	$(N_1)^a$	$(N_1)^b$
50	160	27.4	26.9	110	134	72	81
100	330	57.3	54.0	236	269	96	103
150	500	84.2	78.8	382	420	131	133
200	660	106.7	100.4	553	572	169	162

Table 3.2: Comparison of the conformational properties obtained from simulation and theory for different chain lengths N. Here the arm number is fixed to $f = 10$, the charge fraction is $\alpha \simeq 1/3$, and the cell radius is $R_W = 55.83\,\sigma_{\rm LJ}$ for $N = 50$ and $R_W = 136.48\,\sigma_{\rm LJ}$ for all other chain lengths.

of N_1. This claim is corroborated by the remark that the largest discrepancies occur for the smallest charge fraction, $\alpha = 1/6$, where the assumption of stretched chains is most questionable. On the other hand, the *ratio* of condensed to absorbed counterions appears to be almost constant, $\sim 70\%$ for all combinations considered, both in theory and simulation. With our present, minimal assumptions, we find that the theory captures quantitatively all features of the star conformations. It reproduces the tendency of the PE-stars to increase the fraction $N_{\rm in}/N_c$ of absorbed counterions as f and/or α increase, in line with the predictions of scaling theory in the 'osmotic star' regime. [46, 47]

In Table 3.2 we show the results obtained for fixed arm-number $f = 10$ and varying N. First, we observe a linear scaling of the star radius, $R \sim N$, confirming the overall stretched-chain configuration. Once again, theory and simulation are in very good agreement regarding the radius values. In order to achieve good agreement for the number of condensed

counterions, we had to gradually increase the value of the tube radius, though. As the chain length increases, so does the *absolute* value of the transverse chain fluctuations, [92] although the size of their *relative* fluctuations must remain bounded, so that the overall chain configuration is still stretched. This means that the range in which our model rod-like chains can capture counterions and condense them effectively increases. In order to estimate this enhanced range, we fixed the ratio μ of tube radius to chain length (the relative fluctuation) to its value for $N = 50$, i.e., $\mu = l_B/R(N = 50) \cong 10\%$. Thereafter, we determined the tube radius $R_{\rm tube}$ through the relation $R_{\rm tube}(N) = \mu R(N) \sim \mu N$. This change of the tube radius affects the number of condensed counterions N_1 but has otherwise only a minor effect on the other two quantities, R and $N_{\rm in}$.

Finally, we apply on our described model the aspect of the stability against implosion and explosion of the ensuing ions due to their Coulombic attractions and repulsions, respectively. The issue of stability is non-trivial, which has to be regarded carefully in all systems containing particles with a $1/r$-interaction potential [110]. The simulation model is clearly stable against implosion due to the Lennard-Jones terms in the inter-particle potential in the model, see Eq. (3.1) and Fig. 3.1. In the theoretical model implosion is avoided by the osmotic contribution to the free energy of the PE-star in Eq. (3.11) which is related to the radius with $\sim R^{-3}$. If the star becomes smaller due to electrostatic attractions the term (3.11) increase and avoid an implosion of the star. The stability against explosion is guaranteed since the system is in both models, in the theoretical as well as in the simulation model, contained in a Wigner-Seitz cell ensuring charge neutrality of the system.

3.1.4 An isolated star with added salt

The theory can also be extended to the case of added salt by the addition of entropic terms for the counter- and co-ions. With the addition of N_s salt molecules, the solution contains N_s negatively charged co-ions and N_s positively charged salt counterions, yielding a total number of $N_c + N_s$ counterions in the system. The counter- and co-ions are separated into those absorbed in the interior of the star, $N_{\rm in}^{\pm}$, and those outside: $N_{\rm out}^{+} = N_s + N_c - N_{\rm in}^{+}$ and $N_{\rm out}^{-} = N_s - N_{\rm in}^{-}$. The entropic terms of Eqs. (3.23) and (3.24) are now modified through the replacements $N_2 \to N_{\rm in}^{+} + N_{\rm in}^{-} - N_1$ and $N_3 \to 2N_s + N_c - (N_{\rm in}^{+} + N_{\rm in}^{-})$. With these changes, the theory for the salt-free case can now be carried over to the case of added salt, whereby one additional degree of freedom appears, namely the distribution of co-ions between the interior and the exterior of the star. With these modifications, the procedure remains the same and the conformational properties are determined by the requirement of minimization of the variational free energy, namely:

$$\frac{\partial \mathcal{F}(R, N_{\rm in}^{+}, N_{\rm in}^{-}, N_1)}{\partial R} = \frac{\partial \mathcal{F}(R, N_{\rm in}^{+}, N_{\rm in}^{-}, N_1)}{\partial N_{\rm in}^{\pm}} = \frac{\partial \mathcal{F}(R, N_{\rm in}^{+}, N_{\rm in}^{-}, N_1)}{\partial N_1} = 0. \tag{3.29}$$

The variational theory yields $N_{\rm in}^{-} = 0$ for all cases we considered, i.e., the prediction is that there are no co-ions penetrating the star. We have performed simulations for the salted

f	Q	N_s	c_s [mol/lt]	$(R/\sigma_{\rm LJ})^5$	$(R/\sigma_{\rm LJ})^6$	$(N_{\rm in})^a$	$(N_{\rm in})^b$	$(N_1)^a$	$(N_1)^b$
5	80	250	0.036	22.1	22.2	73	73	40	22
5	80	600	0.088	20.7	19.4	87	76	44	29
10	160	250	0.036	24.0	25.0	138	150	81	60
10	160	600	0.088	22.7	22.8	156	154	90	69
10	160	750	0.109	22.3	22.2	162	155	95	71
10	160	1000	0.146	21.9	21.3	173	156	98	74

Table 3.3: Comparison of the conformational properties between simulation and theory for two different chain numbers f and different salt concentrations c_s. The charge fraction is fixed to $\alpha \simeq 1/3$, and the cell radius is $R_W = 55.83\,\sigma_{\rm LJ}$.

case as well, finding, in full agreement with theory, that the addition of salt results into an almost complete neutralization of the PE-star with increasing salt concentration c_s, to a shrinking of its radius and to an exclusion of all co-ions from the star interior. In Table 3.3, we summarize the results obtained for different salt concentrations $c_s = N_s/V(R_W)$. First we note that the radius of the stars decreases with increasing salt concentration. This is caused by the increased osmotic pressure of the salt ions outside the star, which are in fact mostly co-ions. At the high salt concentration limit the neutral star case can be expected. The cases in which $N_{\rm in} > N_c$, seen only in the simulation results, are caused by the penetration of a small number of co-ions ($< 5\%$ of their total number) into the star interior. The theory, on the other hand, predicts that no co-ions penetrate into the star. However, in view of the fact that in simulations only a tiny fraction of co-ions are found inside the star, this discrepancy appears to be insignificant. Theory and simulation are in agreement in predicting that essentially all co-ions remain free in the exterior of the star.

3.2 Concentrated solutions: effective interactions between star-branched polyelectrolytes

In concentrated solutions, the interactions between PE-stars become important: they determine the correlations between the star centers, the intensity profiles obtained in scattering experiments and the ensuing macroscopic behavior of the solution. In order to analyze these effective interactions between the star centers theoretically, we take advantage of the facts obtained from the analysis of an isolated star. The Coulomb-interaction, the Flory contribution of the chains, and the entropy of the counterions are the physical mechanisms giving rise to the star-star interactions and hence they are the ingredients of a variational free energy for the two stars held at a distance D from one another. At the same time, all contributions to the free energy of a pair of stars acquire now an explicit D-dependence, which gives rise to the effective interaction $V_{\rm eff}(D)$, to be defined below.

3.2.1 Theory

The effective interaction $V_{\rm eff}(D)$ between two PE-stars, kept at center-to-center distance D, results after taking a canonical trace over all but the star-centers degrees of freedom and is defined as

$$V_{\rm eff}(D) = \mathcal{F}_2(D) - \mathcal{F}_2(\infty), \tag{3.30}$$

where $\mathcal{F}_2(z)$ is the Helmholtz free energy of two PE-stars at center-to-center separation z. [53] For the theoretical investigations of the force at *overlapping distances* $D \leq 2R$, we first take into consideration that, when two PE-stars overlap, the chains of each star retract, a feature already conjectured by Pincus [102] and also confirmed in all simulations that we carried out. Hence, we model the two stars as 'fused spheres', each carrying the cloud of its untrapped counterions around it, as shown in Fig. 3.8. The chains remain otherwise stretched, hence a $\sim r^{-2}$ falloff of the density profile from each star center remains. However, due to the retraction of the chains, the two profiles from each center do *not* overlap. Rather, each profile is sharply cut off as soon as the distance from the corresponding center reaches the bisecting plane located at a distance $D/2$ from the centers.

The variational free energy $\mathcal{F}_2(D)$ is written as in Eq. (3.7). Since the terms U_c, $F_{\rm el}$ and $F_{\rm Fl}$ remain unaffected by D, $V_{\rm eff}(D)$ contains only the electrostatic $U_H(D)$ and the entropic contributions $S_i(D)$, $i = 1, 2, 3$:

$$V_{\rm eff}(D) = U_H(D) + \sum_{i=1}^{3} S_i(D) = \min_{\{R,\{N_i\}\}} \mathcal{F}_2(D; R, \{N_i\}). \tag{3.31}$$

We first investigate the electrostatic part $U_H(D)$ in more detail. It is convenient to separate the total charge density $\varrho(\boldsymbol{r})$ into two contributions, $\varrho_{\rm in}(\boldsymbol{r})$ in the interior of the fused spheres ($V_{\rm in}$) and $\varrho_{\rm out}(\boldsymbol{r})$ in the eight-shaped region outside ($V_{\rm out}$). $\varrho_{\rm out}(\boldsymbol{r})$ is homogeneous and equal to $-Q^*/V_{\rm out}$. We choose a spherical polar coordinate system with its origin the center of the lower star (see Fig. 3.8). Setting $r_\theta = r\cos\theta$ and $\omega \equiv \theta - \theta_0$, we write

$$\varrho_{\rm in}(\boldsymbol{r}) = A|e|[P(\boldsymbol{r}) + P(\boldsymbol{D} - \boldsymbol{r})] \tag{3.32}$$

with the shape function:

$$P(\boldsymbol{r}) = \frac{1}{r^2}\left[\Theta(R - r)\Theta(\omega) + \Theta(D/2 - r_\theta)\Theta(-\omega)\right], \tag{3.33}$$

where the normalization factor

$$A = Q^*\{4\pi R\,[1 + \cos\theta_0(1 - \ln\cos\theta_0)]\}^{-1} \tag{3.34}$$

guarantees that $\int_{V_{\rm in}} {\rm d}^3 r\, \varrho_{\rm in}(\boldsymbol{r}) = Q^*$.

We rewrite Eq. (3.8), expressing $U_H(D)$ by using the electrostatic potential $\Phi(\boldsymbol{r})$ as

$$U_H(D) = \frac{1}{2\epsilon}\left[\int_{V_{\rm in}} {\rm d}^3 r\,(\Phi_{\rm in}(\boldsymbol{r}) + \Phi_{\rm out}(\boldsymbol{r}))\,\varrho_{\rm in}(\boldsymbol{r}) + \int_{V_{\rm out}} {\rm d}^3 r((\Phi_{\rm in}(\boldsymbol{r}) + \Phi_{\rm out}(\boldsymbol{r}))\,\varrho_{\rm out}(\boldsymbol{r})\right], \tag{3.35}$$

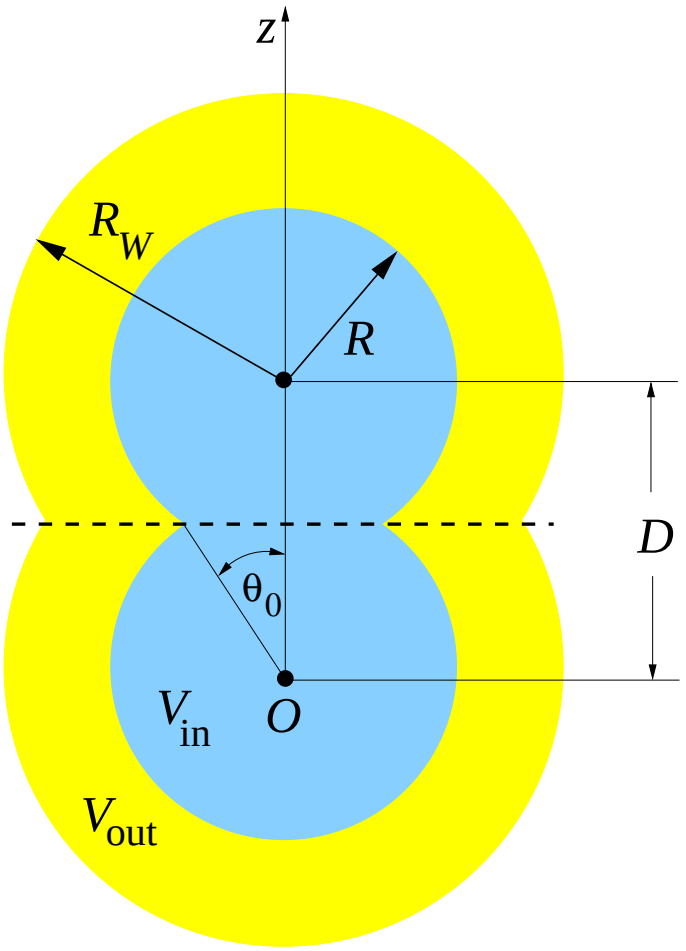

Figure 3.8: A sketch of two polyelectrolyte-stars of radius R each, held at center-to-center separation D. The dark fused spheres denote the stars and have a total volume $V_{\rm in}$. The light eight-shaped hollow region with volume $V_{\rm out}$ denotes the region in which the free counterions can move.

where $\Phi_\alpha(\boldsymbol{r})$ ($\alpha = \text{in, out}$), is the contribution of the charge density $\varrho_\alpha(\boldsymbol{r})$ to the electrostatic potential at an *arbitrary* point $\boldsymbol{r}$ in space. The calculation of $\Phi_{\rm in}(\boldsymbol{r})$ is rather technical and is shown in Appendix C.1; that of $\Phi_{\rm out}(\boldsymbol{r})$ in Appendix C.2. Unlike the single-star cases, an analytical solution is not anymore feasible and therefore numerical computations are necessary in order to determine the electrostatic energy. On dimensional grounds, $U_H(D)$ has the form

$$\begin{aligned}\frac{U_H(D)}{k_{\rm B}T} &= \frac{Z^2 l_{\rm B}}{R} h\left(\frac{R_W}{R}, \frac{D}{R}\right) \\ &= \frac{Z^2 \lambda_{\rm B}}{R}\left[h_{\rm in-in}\left(\frac{D}{R}\right) + 2h_{\rm in-out}\left(\frac{R_W}{R}, \frac{D}{R}\right) + h_{\rm out-out}\left(\frac{R_W}{R}, \frac{D}{R}\right)\right], \quad (3.36)\end{aligned}$$

where $Z = Q^*/|e|$ is the *total* number of uncompensated charges of *both* spheres and

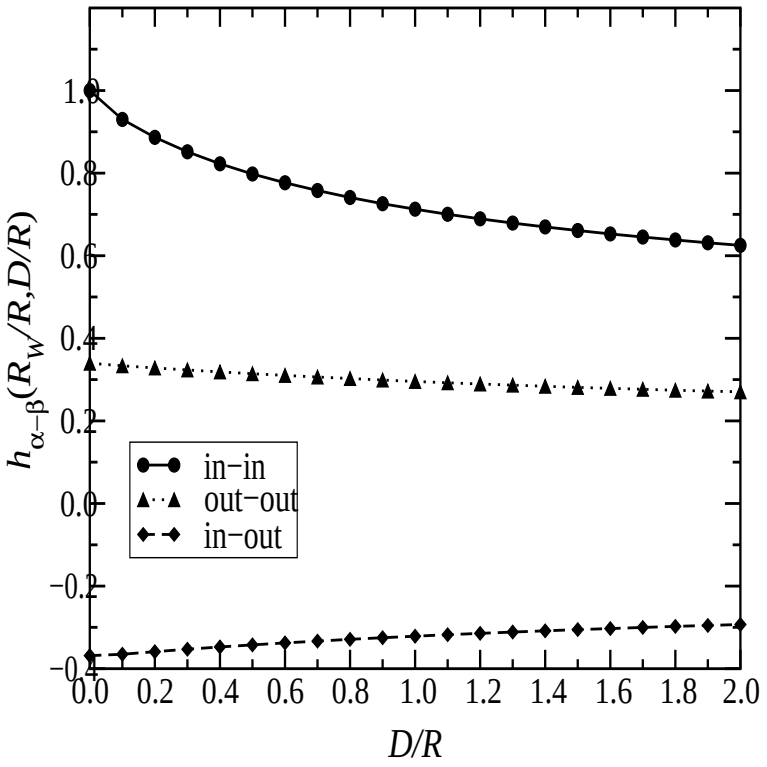

Figure 3.9: The three terms contributing to the electrostatic energy of two PE-stars, according to Eq. (3.36), as functions of the center-to-center separation D for $R_W = 1.65\,R$.

$h_{\alpha-\beta}(R_W/R, D/R)$ (α, β = in, out) are dimensionless functions arising from the integrations of the products $\Phi_\alpha(\boldsymbol{r})\varrho_\beta(\boldsymbol{r})$ in Eq. (3.35). Note that the first term, $h_{\rm in-in}$, has *no* R_W-dependence. The various contribution of the terms at $R_W = 1.65\,R$ are shown in Fig. 3.9. The strongest D-dependence arises from the integration of the term $\Phi_{\rm in}(\boldsymbol{r})\varrho_{\rm in}(\boldsymbol{r})$. The other terms are weaker, both in their energy scale and in their D-dependence.

We proceed with the calculation of the entropic terms $S_i(D)$, ($i = 1, 2, 3$), which include the D-dependent volumes of integration and their corresponding profiles $\rho_i(\boldsymbol{r})$. In particular, $\rho_1(\boldsymbol{r})$ is uniform within the $2f$ tubes and zero otherwise. The trapped counterion density $\rho_2(\boldsymbol{r})$ has the form $\rho_2(\boldsymbol{r}) = B[P(\boldsymbol{r}) + P(\boldsymbol{D} - \boldsymbol{r})]$, with the shape function $P(\boldsymbol{r})$ given by Eq. (3.33). The constant B is determined by the condition $\int_{V_2} {\rm d}^3 r\, \rho_2(\boldsymbol{r}) = N_2$, where $V_2(D) = V_{\rm in}(D) - V_1$ (here $V_1 = 2f\pi l_{\rm B}^2 R$), and reads as

$$B = \frac{N_2}{4\pi R\left[\frac{D}{2R}\left(1 - \ln\left(\frac{D}{2R}\right)\right) + 1\right]}. \tag{3.37}$$

Finally, $\rho_3(\boldsymbol{r}) = N_3/V_{\rm out}(D)$. Accordingly, we obtain the entropic contributions of the

counterions in the three different states using Eq. (3.12) as:

$$\frac{S_1}{k_\mathrm{B}T} = N_1\left[\ln\left(\frac{N_1\sigma_\mathrm{LJ}^3}{\tilde{V}_1}\right)-1\right]; \tag{3.38}$$

$$\frac{S_2}{k_\mathrm{B}T} = N_2\ln\left(\frac{N_2}{4\pi\left[1+\frac{D}{2R'}\left(1-\ln\left(\frac{D}{2R'}\right)\right)\right]}\right) + \frac{N_2}{1+\frac{D}{2R'}\left(1-\ln\left(\frac{D}{2R'}\right)\right)}\frac{D}{2R'}\ln^2\left(\frac{D}{2R'}\right)+N_2+3N_2\ln\left(\frac{R}{R'}\right); \tag{3.39}$$

$$\frac{S_3}{k_\mathrm{B}T} = N_3\left[\ln\left(\frac{N_3}{4\pi\left[\frac{1}{3}\left(\frac{R_W^3}{R^3}-1\right)+\frac{D}{4R}\left(\frac{R_W^2}{R^2}-1\right)\right]}\right)-1\right], \tag{3.40}$$

where $\tilde{V}_1 = V_1 - 2f\pi\sigma_\mathrm{LJ}^2 R$. The last term of S_2 results from the fact that the available volume for the trapped counterions is reduced by the tubes around the chains. We therefore introduce two smaller fused spheres with radius $R' \leq R$ that fulfill the condition

$$V_\mathrm{in}(R,D) - 2f\pi l_\mathrm{B}^2 R = V_\mathrm{in}(R',D), \tag{3.41}$$

with

$$V_\mathrm{in}(R',D) = \frac{4\pi}{3}R'^3\left[1+\frac{3}{2}\left(\frac{D}{2R'}\right)-\frac{1}{2}\left(\frac{D}{2R'}\right)^3\right]. \tag{3.42}$$

R' is obtained by solving Eq. (3.41) together with Eq. (3.42) and it depends additionally on D.

We emphasize that the dominant D-dependence of the two-star free energy [Eq. (3.31)] arises from the terms $U_H(D)$ and $S_2(D)$. The former is shown in Fig. 3.9 and the latter in Fig. 3.10. Three remarks are of order here: first, the number of trapped counterions $N_2 = N_\mathrm{in} - N_1$ sets the overall scale of the term $S_2(D)$ Therefore the role of the N_1 condensed counterions becomes important in 'renormalizing' the effective interaction, as we will explain shortly. Second, both $U_H(D)$ and $S_2(D)$ are non-linear functions of D, implying that the resulting effective force $F(D) = -\mathrm{d}V_\mathrm{eff}(D)/\mathrm{d}D$ is is *not* constant. This finding is at odds with the the situation in curved polyelectrolyte brushes, resulting from grafting PE-chains on a solid particle of radius b. By employing scaling arguments for the trapped counterions, Pincus predicted that in the regime $R \gg D \gg b$ the force of two porcupines is D-independent. [102] Finally, we comment on the fact that $S_2(D)$ in Fig. 3.10 shows a maximum for a small but nonzero value of the separation, $D \cong 0.1\,R$. This is an artifact of the model for the density distributions, in which we assumed a $\sim r^{-2}$-dependence of the profiles for all r. In reality, the monomer- and counterion-densities do not diverge at $r = 0$ due to the hard cores of the particles. Hence, at small separations, strong steric repulsions between the locally dense macromolecular aggregates will cause the entropy $S_2(D)$ to increase monotonically as $D \to 0$. Neither in the simulations nor in the theory, however, did we examine the effective interaction at such small separations, hence this artifact does not influence the comparisons that are to follow.

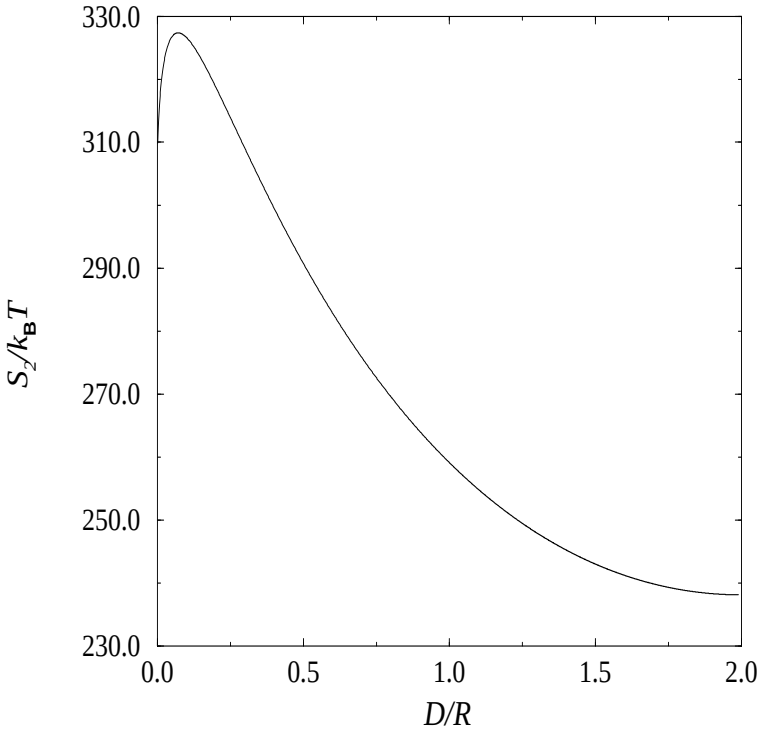

Figure 3.10: Entropic contribution of trapped counterions (here $N_2 = 100$) vs. star-star-separation D.

The effective potential $V_{\text{eff}}(D)$ is obtained by adding up the terms $S_i(D)$ and $U_H(D)$, according to Eq. (3.31) and *minimizing* the free energy $\mathcal{F}_2(D; R, \{N_i\})$ with respect to R and the N_i's for every separation $D \leq 2R$. We can simplify the problem by first taking into consideration that the star extent R is unaffected by D. Indeed, the chains are already almost completely stretched and, as confirmed during our simulation runs, R remains constant and equal to its value for the isolated star. Since the N_i's are related through $N_1 + N_2 + N_3 = N_c = \text{constant}$, only two variational parameters remain, say N_1 and N_2. In the simulations we have found that the number of condensed counterions remains, to a very good approximation, constant for all overlapping separations $D \leq 2R$, and undergoes a rather abrupt change at the crossover distance $D = 2R$. Hence, we have chosen *not* to determine N_1 through the variational calculation, but rather to treat it as a fit parameter, held constant for all D, and chosen so as to give optimal agreement with simulation results. It would be desirable to obtain this result through the full minimization; however such an attempt leads to significantly worse results than the procedure described above. On the other hand, the treatment of the net charge as a fit parameter is not at all unusual for charged systems and, in the realm of charge-stabilized colloidal suspensions, it is an oft-used approach known as *charge renormalization.* [109, 111, 112] Therefore, $\mathcal{F}_2(D, ; R, \{N_i\})$ is

only minimized with respect to N_2:

$$\left(\frac{\partial \mathcal{F}_2(D;N_2)}{\partial N_2}\right) = 0, \tag{3.43}$$

yielding

$$N_2(D) = \frac{R}{2l_{\mathrm{B}}h\left(\frac{R_W}{R},\frac{D}{R}\right)}\left\{2+\frac{D}{2R'}\frac{\ln^2\left(\frac{D}{2R'}\right)}{1+\frac{D}{2R'}\left(1-\ln\left(\frac{D}{2R'}\right)\right)}\right. \tag{3.44}$$

$$\left. + \ln\left[\left(\frac{N_c-N_1}{N_2}-1\right)\frac{\frac{1}{3}\left(\frac{R_W^3}{R^3}-1\right)+\frac{D}{4R}\left(\frac{R_W^2}{R^2}-1\right)}{1+\frac{D}{2R'}\left(1-\ln\left(\frac{D}{2R'}\right)\right)}\left(\frac{R}{R'}\right)^3\right]\right\}, \tag{3.45}$$

with R' obtained by solving Eq. (3.42). The minimizing values of $N_2(D)$ are set into $U_H(D)$ and $S_i(D)$ and enable the calculation of the effective interaction potential $V_{\mathrm{eff}}(D)$ from Eq. (3.31).

3.2.2 Results for the effective interaction

The theoretical model for the effective interaction has been tested against results of MD simulations of two star-branched polyelectrolytes. In a MD-simulation, the mean force at the center of the stars can be measured. [28, 53] For this purpose, the simulation model of an isolated star, presented in Section 3.1.1, is expanded to two stars. The microscopic interaction potentials and parameters are those presented in Section 3.1.1. The centers of the two stars were placed along the body-diagonal of the cubic simulation box with periodic boundary conditions and the mean force acting at the center of the stars was measured [28]. The effect of the periodic images can be neglected. Only for large distances D at which the periodic images of the stars are closer to their original, the force can deviate from the 'true' value, within usual computational accuracy. We checked this effect by simulating the same system without periodic images in a box with hard walls. The walls are located sufficiently far ($L_b = 120 \ldots 220\sigma_{\mathrm{LJ}}$) from the stars avoiding finite size effects. The comparison of the forces with the corresponding forces resulting from the Lekner calculations shows deviations between both methods in the order of about 15% which decays with smaller star distance D. Hence, the chosen box size of $90L_b$ are sufficiently large to neglect periodic image induced forces for our purposes on one side, and saving computational memory (RAM) space on the other side (see App. B).

Typically 120 000 time steps are used for equilibration and up to 500 000 steps were simulated to gather statistics. For deep overlaps of the stars within their radii, the periodic images of the stars have negligible effects on the effective force. We have also checked that the image charges have only a minor effect in the measured forces at bare overlaps. In Fig. 3.11, snapshots of two PE-stars at different separations D are shown, in order to illustrate the procedure and the typical conformation of the stars when they are close to one another. It is clear that the chains of each star retract from the region of overlap, i.e., there

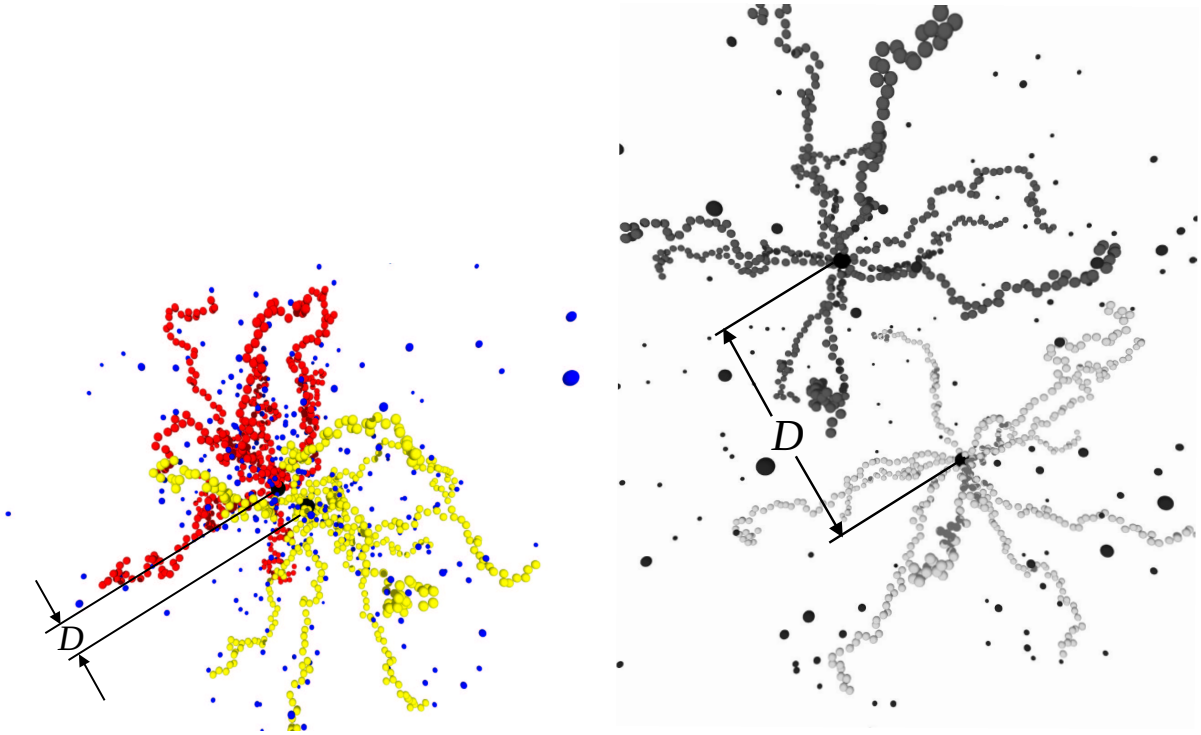

Figure 3.11: Simulation snapshots of two polyelectrolyte-stars at small center-to-center separation D (left picture) and at a larger separation (right picture). The chain length is $N = 50$ and the arm number $f = 10$.

is no interdigitation from different stars. This in the physical situation that motivates our theoretical modeling of the stars as 'chopped spheres' (see Section 3.2.1 and Appendix C.1) and it has also been employed in the scaling theory of Pincus. [102]

Consider, then, two PE-stars, $i = 1, 2$, separated by a distance D. The mean force $\boldsymbol{F}_i(D)$ acting at the center of the i-th star has two contributions, arising by the core-bonded monomers and all other non-bonded monomers acting on the core. Under these circumstances, the effective force $\boldsymbol{F}_i(D)$ acting on the i-th star center is given as a canonical average:

$$\boldsymbol{F}_i(D) = \left\langle -\vec{\nabla}_{\boldsymbol{R}_i} \left(\sum_{k=1}^{2fN} V^c_{\mathrm{LJ}}(|\boldsymbol{r}_k - \boldsymbol{R}_i|) + \sum_{l=1}^{f} V^c_{\mathrm{FENE}}(|\boldsymbol{r}_l - \boldsymbol{R}_i|) \right) \right\rangle, \tag{3.46}$$

where in the first sum the repulsive interactions of the core with *all* $2fN$ monomers in the system are considered according to Eq. (3.3) , whereas the second sum only accounts for the attractive interactions with the f innermost monomers of the chains attached to the i-th center according to Eq. (3.4). Due to symmetry, $\boldsymbol{F}_1(D) = -\boldsymbol{F}_2(D)$. In what follows, we consider thus the magnitude $F(D) = |\boldsymbol{F}_{1,2}(D)|$ of the effective force, related to the effective interaction through [53] $F(D) = -\mathrm{d}V_{\mathrm{eff}}(D)/\mathrm{d}D$.

The parameter combinations for which we performed simulations are summarized in Table 3.4. The results, compared with the theoretical predictions of Section 3.2.1, are shown

f	α	Q	(R_d/R)	N_1	ζ	$\tilde{C}$
5	1/3	80	0.01	105	0.47	0.0542
10	1/6	80	0.05	80	0.43	0.0456
10	1/4	120	0.05	147	0.45	0.0343
10	1/3	160	0.04	218	0.52	0.0265
18	1/6	144	0.06	160	0.50	0.0238
18	1/4	216	0.05	275	0.56	0.0183
18	1/3	288	0.05	400	0.59	0.0149
30	1/4	360	0.08	450	0.63	0.0114

Table 3.4: The parameters used in the simulations of two PE-stars. The degree of polymerization is $N = 50$ for all entries. R_d is the core size, scaled on the radius R obtained from Table 3.1. In the last two columns, we show in addition the parameter values for the force fit of Eq. (3.47).

in Fig. 3.12. As can be seen, there is very good agreement between theory and simulation, for all parameter combinations considered. The number of condensed counterions, N_1, lies for all curves between twice the value calculated for a star with f arms and the value for a star with $2f$ arms, which formally obtains at zero separation between the two macromolecules. The only exception is the case with $f = 5$; however, for such a low arm number, the assumption of chain retraction, and the associated cut of the density profile at the bisecting plane, are probably not valid. Nevertheless, good agreement with the simulation results is obtained with the choice $N_1 = 105$. The *shape* of the force is determined almost entirely by the entropic term S_2 and the electrostatic contribution U_H plays only a minor role, as the PE-stars are almost electroneutral. This is in full agreement with the predictions of Ref. [102]. The *magnitude* of the force is mainly determined by the amount of mobile counterions $N_2 = N_{\rm in} - N_1$ inside, hence the amount of condensed counterions plays a decisive role. Moreover, a homogeneous charge- and density-distribution inside the star leads to the erroneous prediction that the force is almost constant, hence the $\sim 1/r^2$ profiles are crucial in reproducing the shape of the force vs. distance curves.

In order to cast the effective interaction into a manageable form that should facilitate the theoretical analysis of experimental scattering data, we derive below a simple and accurate fit of the force data, which is shown in Fig. 3.13. The fit is given by

$$2R\frac{F(D)}{k_{\rm B}T} = C(f,N_c)\left[\left(\frac{D}{2R}\right)^{-\zeta} - 0.4\left(\frac{D}{2R}\right)^{1-\zeta}\right], \tag{3.47}$$

with $0.4 \lesssim \zeta \lesssim 0.63$, and a positive constant C. For the latter, we further introduce the ansatz:

$$C(f,N_c) = \tilde{C} f N_c. \tag{3.48}$$

The precise values for ζ and $\tilde{C}$ depend on f and N_c (or α) and are listed in the last two columns of Table 3.4. The exponent ζ remains always smaller than the value $\zeta_{\text{neutral}} = 1$, which obtains for neutral star polymers [28, 113] ($F \sim D^{-1}$). For neutral stars, a weakly diverging logarithmic effective interaction results [113, 27], whereas in this case the effective interaction does not diverge at the origin.

Further, the interaction beyond overlap must be determined. For this purpose, we assume that the charged monomers of one star interact with the charged monomers of the other star via a screened potential of the Yukawa form, the screening caused by the counterions surrounding the stars. Integrating these Yukawa segments on both stars, leads to a Yukawa-type tail for the effective interaction between stars at large separations as well. This is in line with the theory of effective interactions for charged colloids [109] as well as with recent results from linear-response theory applied to polyelectrolyte-stars. [114] Matching the expression valid for $D \leq 2R$, Eq. (3.47), with the expression

$$F(D) \propto -\frac{\mathrm{d}}{\mathrm{d}D}\frac{\exp(-\kappa D)}{D}, \tag{3.49}$$

valid for $D > 2R$, leads to

$$2R\,\frac{F(D)}{k_{\mathrm{B}}T} = \tilde{C} f N_c \begin{cases} \left(\frac{D}{2R}\right)^{-\zeta} - \frac{2}{5}\left(\frac{D}{2R}\right)^{1-\zeta} & \text{for } D \leq 2R; \\ \frac{3}{5}(1+2\kappa R)^{-1}(1+\kappa D)\left(\frac{2R}{D}\right)^{2}\exp[-\kappa(D-2R)] & \text{for } D \geq 2R, \end{cases} \tag{3.50}$$

where $\kappa = \sqrt{\rho_3 l_{\mathrm{B}}}$ is the inverse Debye screening length. Therefore, the full interaction potential $V_{\text{eff}}(D)$, is obtained by integration of Eq. (3.50) and reads as:

$$\frac{V_{\text{eff}}(D)}{k_{\mathrm{B}}T} = \tilde{C} f N_c \begin{cases} \frac{1}{1-\zeta}\left[1-\left(\frac{D}{2R}\right)^{1-\zeta}\right] + \frac{2}{5(2-\zeta)}\left[\left(\frac{D}{2R}\right)^{2-\zeta}-1\right] + \frac{3}{5(1+2\kappa R)} & \text{for } D \leq 2R; \\ \frac{3}{5}(1+2\kappa R)^{-1}\left(\frac{2R}{D}\right)\exp[-\kappa(D-2R)] & \text{for } D \geq 2R. \end{cases} \tag{3.51}$$

The last expression can be used in attempting to describe theoretically scattering profiles from concentrated PE-star solutions. [42, 104, 41] The effective interaction is manifestly density-dependent through the inverse Debye length κ. For the purpose of fitting experimental data, $\tilde{C}$ and ζ can be used as fit parameters, however the constraint $0 < \zeta < 1$ should always be respected.

Representative curves for the effective interaction of Eq. (3.51) are shown in Fig. 3.14(a). As can be seen from Eq. (3.51), the potential between polyelectrolyte-stars has the property of being *bounded*, i.e., its value at zero separation between the stars is finite. This is, of course, an idealization stemming from the fact that we assumed, in the theoretical modeling, that the central particle on which the chains are anchored has vanishing extent. Although in reality the effective interaction will diverge at full overlaps, the range of this divergence will be very small, typically of the order of a few Angstrom. On the other hand, the range of the interaction derived above is that of the corona radius of the stars, which can be very large, up to several microns for long chains. Hence, for a vast range of star concentrations, the macromolecules will feel only the effects of the ultra-soft interaction of Eq. (3.51) and a

theoretical analysis on the basis of the latter will be fully sufficient in capturing the physics of the correlations in the system. In this respect, the effective interaction between PE-stars belongs to a new class of potentials that have attracted considerable attention recently, the so-called *mean-field potentials*. [53, 115, 116, 117, 118, 119, 120, 121, 122, 123] Physical systems whose constituent particles interact by means of such a bounded or a slowly diverging interaction, are called *mean-field fluids*. [53, 120, 123] Typical phenomena associated with mean-field fluids are an anomalous structure factor in the fluid phase, [115, 31] reentrant melting and exotic crystal structures in the solid phase, [115, 32, 124, 125] as well as the property that at high concentrations in the uniform phase the direct correlation function of the system is, to an excellent approximation, equal to $-V_{\rm eff}(r)/(k_BT)$ $-V_{\rm eff}(r)/(k_BT)$. [115, 116, 119, 117, 118, 120]. Polymer chains, [117, 118] dendrimers, [119], as well as neutral star polymers [123] are systems that have been shown to belong to this new class. Polyelectrolyte-stars are the new member of the family.

It is pertinent to compare the effective interaction of Eq. (3.51), valid for *charged* star-polymers, with the known interaction for *neutral* stars. [27] The latter features an ultra-soft, logarithmic divergence for overlapping stars and a Yukawa-decay for nonoverlapping ones, hence it has some qualitative similarities with the interaction of PE-stars, and reads as: [27]

$$\frac{V_{\rm eff}(D)}{k_{\rm B}T} = \frac{5}{18} f^{3/2} \begin{cases} -\ln\left(\frac{D}{2R}\right) + (1+\sqrt{f}/2)^{-1} & \text{for } D \leq 2R; \\ (1+\sqrt{f}/2)^{-1}\left(\frac{2R}{D}\right)\exp\left[-\frac{\sqrt{f}(D-2R)}{4R}\right] & \text{for } D \geq 2R. \end{cases} \tag{3.52}$$

The comparison is shown in Fig. 3.14(b). Despite the potential of Eq. (3.52) diverges at the origin and that of Eq. (3.51) does not, the latter represents nevertheless much stronger repulsions at strongly overlapping configurations than the former. Although the interaction between neutral stars formally takes over at some small separation D, due to its divergence, the ultra-soft character of the latter renders this crossover value very small. Hence, polyelectrolyte-stars repel each other at overlapping separations much more strongly than their neutral counterparts. This implies that stabilization of colloidal particles against the van der Waals attraction can be achieved more efficiently by grafting of polyelectrolytes than by grafting of neutral polymer chains.

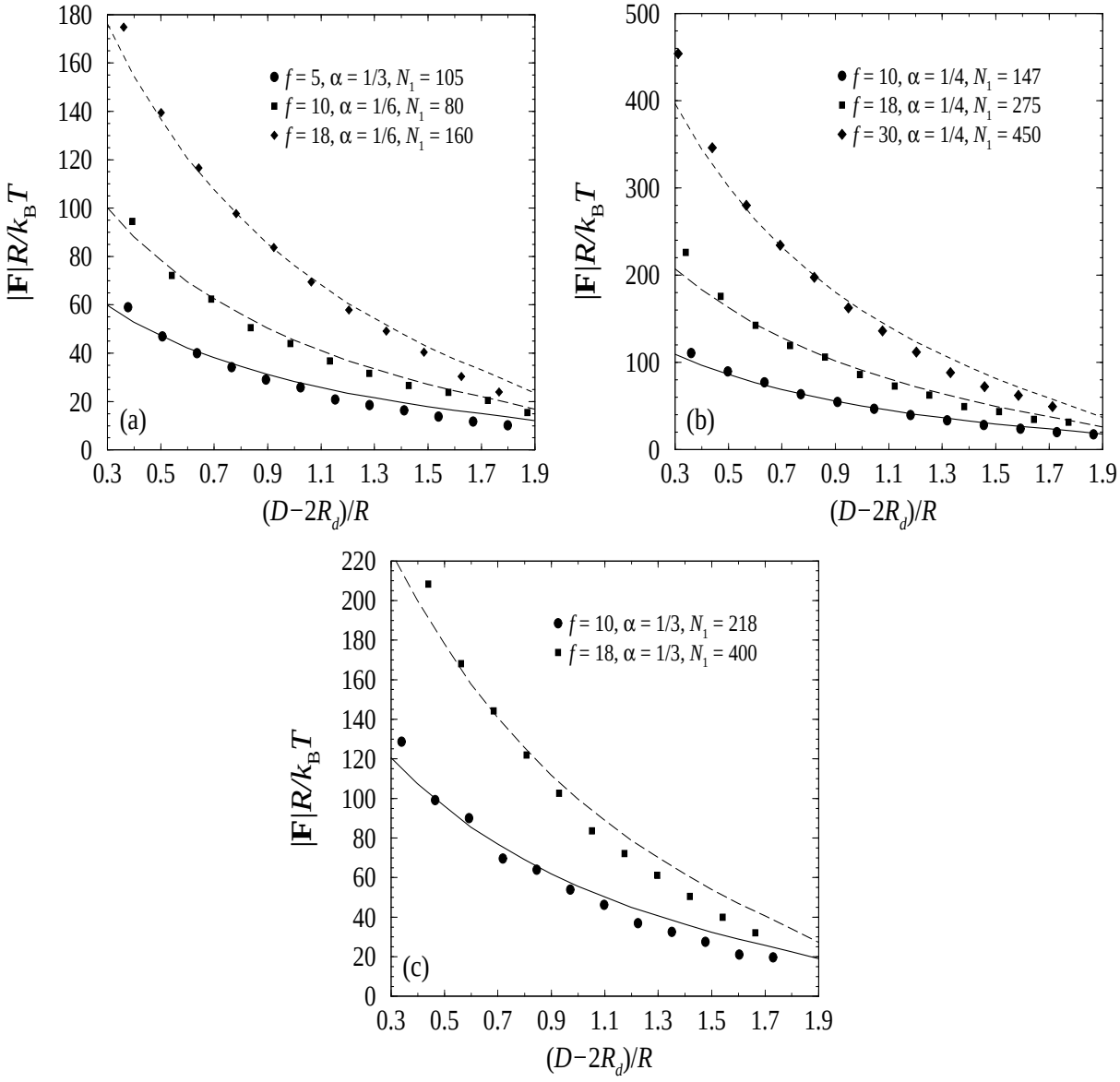

Figure 3.12: Theoretical results (lines) in comparison with simulation results (symbols) of the effective forces $|\boldsymbol{F}(D)|$ for different parameter combinations f, α and N_1. The chain length is fixed at $N = 50$. Since the theoretical model has no core, in contrast to the simulation model, the simulation data have to be displaced by the core diameter $2R_{\mathrm{d}}$.

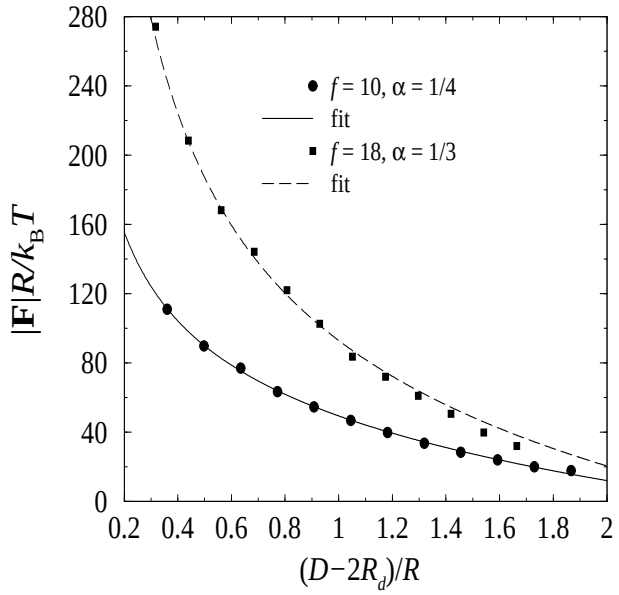

Figure 3.13: Fit (lines) of the simulation data (symbols) for the effective force between two PE-stars, according to Eq. (3.47).

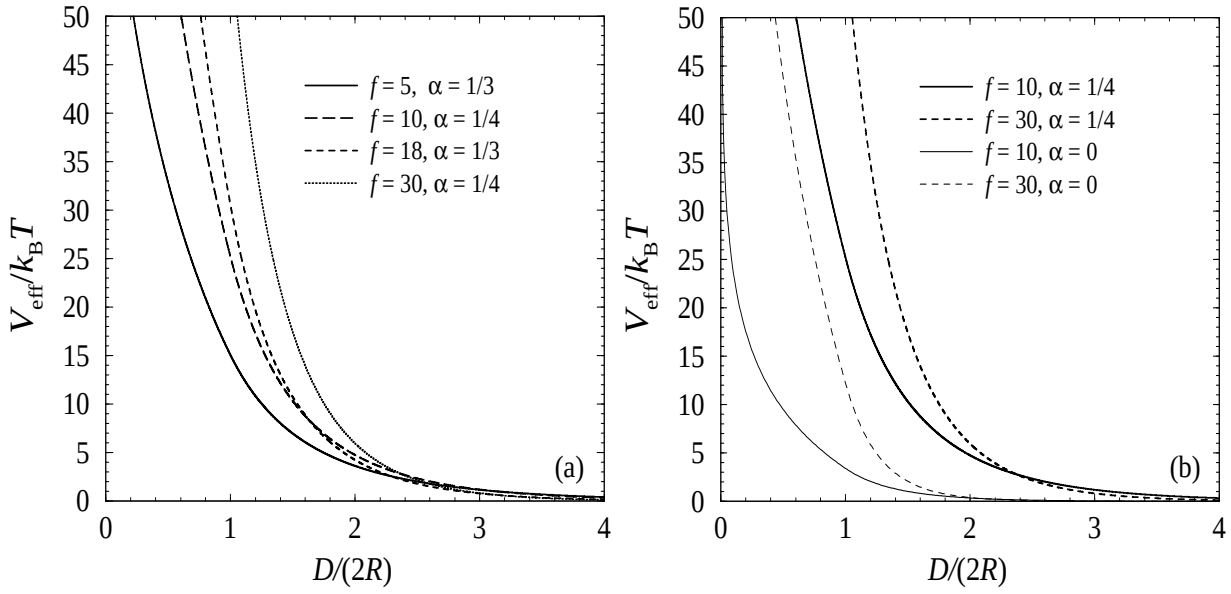

Figure 3.14: (a) The effective interaction potential $V_{\rm eff}(D)$ obtained from Eq. (3.51) for various f- and α-values. (b) A comparison between the effective interactions between charged stars (thick lines) and those for neutral stars (thin lines, obtained from Eq. (3.52)), having the same arm-number and size as the charged ones.

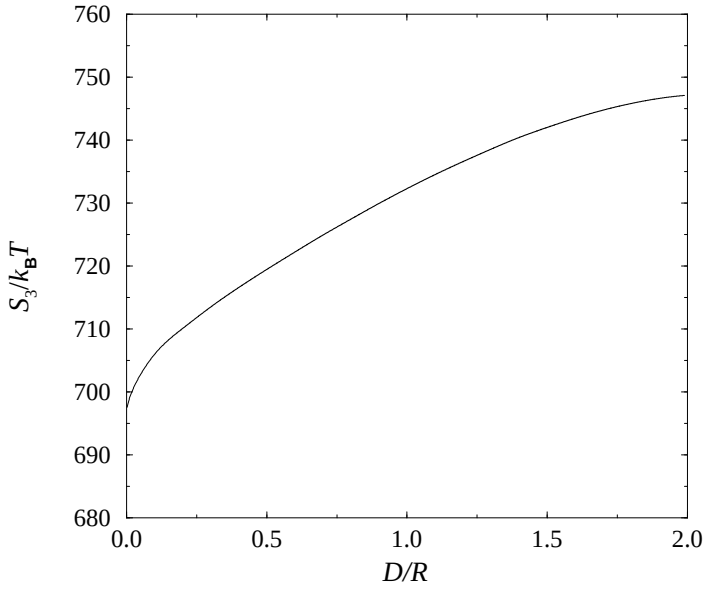

Figure 3.15: The D-dependence of the entropic contribution of the counterions and the co-ions outside the stars for the case of added salt. The parameters are $f = 10$, $\alpha = 1/3$, $N_c = 320$, with $N_s = 250$ added salt molecules. The Wigner-Seitz radius is $R_W = 55.83\,\sigma_{\rm LJ}$.

3.2.3 Interacting stars in the presence of added salt

In this Section we turn our attention to the effective interaction in the presence of added salt. As discussed in Section 3.1.4, the co-ions of the added salt remain outside the star, whereas in the salt-free case only a very small fraction of counterions can be found there. In addition, the salt counterions just supplement a small fraction to neutralize the star, hence they are also predominantly to be found in the star exterior. Therefore, we obtain in the case of added salt a drastically increased entropic contribution S_3 from the outside region, in comparison to the salt-free case. The available volume $V_{\rm out}$ to the counter- and co-ions outside the star and its dependence on the star-star separation D plays now an important role in diminishing the magnitude of the effective force between to PE-stars. Indeed, $V_{\rm out}$ increases with decreasing distances between the stars D. As the volume available to the counter- and co-ions increases with decreasing D, their entropy also grows. The dependence of the term $S_3(D)$ on D is shown in Fig. 3.15.

Since we have a large number of particles in the outside region, this entropy increase is significant and contributes to a measurable *effective attraction* to the total potential between the stars. Alternatively, one can think of the two overlapping stars in Fig. 3.8 as being hit by a large number of counterions mostly from the outside, a situation that results into an unbalanced force pushing the two stars closer to one another. This is the well-known 'depletion mechanism', [53] familiar from the classical case of colloid-polymer mixtures, [126]

in which the small polymer induces an attraction between the large, hard colloids. An important quantitative difference in the case at hand, though, is that the large stars are *not* hard but penetrable. Thus, the depletion attraction is superimposed on the repulsion caused by the trapped counterions and the total effect need not be a net attraction. Instead, a reduced repulsion between the polyelectrolyte-stars results.

The theoretical analysis of the effective interaction in the case of added salt follows the same lines presented in Section 3.2.1 above. Similarly to the single-star case, we have to make the formal substitution $N_3 = N_c - N_{\rm in} \to N_c + 2N_s - N_{\rm in}$ when N_s-salt molecules are present. Now the D-dependence of the volume $V_{\rm out}(D)$ becomes crucial in comparing with simulation results, since the size L_b of the simulation box remains constant and $V_{\rm out}(D)$ grows as D diminishes. Referring to Fig. 3.8, we see that the D-dependent Wigner-Seitz radius $R_W(D)$ can be determined by solving the equation:

$$L_b^3 = V_{\rm out}(D) + V_{\rm in}(D). \tag{3.53}$$

Solving this geometrical problem yields

$$R_W(D) = \begin{cases} \left(\frac{3}{4\pi}\right)^{1/3} L_b & \text{for } D = 0; \\ \frac{D}{2}\left[\cosh\left(\frac{\psi}{3}\right) - \frac{1}{2}\right] & \text{for } D > 0, \end{cases} \tag{3.54}$$

where ψ is given by

$$\psi = \ln\left[w + \sqrt{w^2 - 1}\right], \tag{3.55}$$

with

$$w = 1 + \frac{24}{\pi}\left(\frac{L_b}{D}\right)^3. \tag{3.56}$$

The theoretical results obtained with these modifications are shown in Fig. 3.16, and compared with simulations. Both data sets correspond to a salt concentration of $c_s = 0.036\,\mathrm{mol/lt}$. It can be seen indeed that the magnitude of the force is roughly halved in comparison with the salt-free cases of Fig. 3.12. The osmotic pressure from the outer ions has the effect of reducing the strength of the star-star-interaction for overlapping stars. For nonoverlapping stars, the same effect appears, for the well-understood reason of enhanced screening, causing an increase of the inverse Debye screening length κ in Eq. (3.51).

3.3 Summary and concluding remarks

We have analyzed the conformations, sizes, counterion distributions and effective interactions between osmotic polyelectrolyte-stars. The main findings of this work are (i) a stretching of the arms of the stars; (ii) a strong absorption of counterions in the star interior and condensation along the rod-like chains; (iii) an entropically-dominated, soft effective repulsion between PE-stars, being caused mainly by the trapped counterions; and (iv) a reduction of the strength of the repulsion in the presence of added salt.

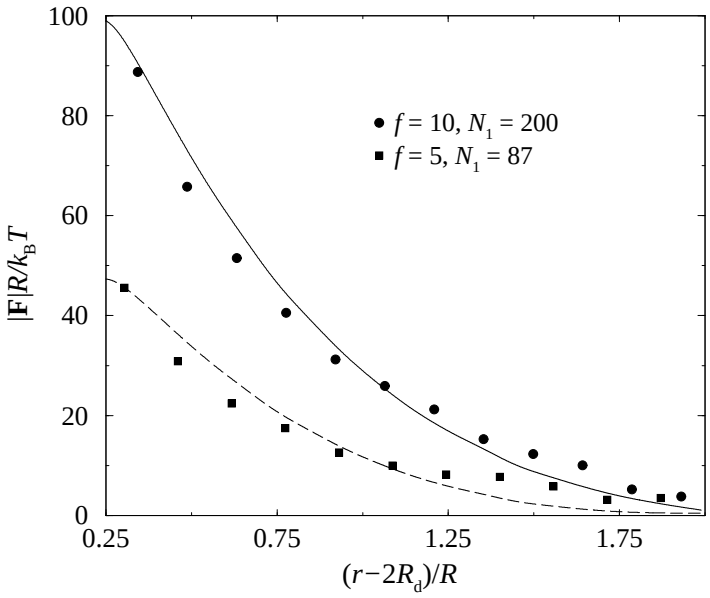

Figure 3.16: Theoretical (lines) and simulation (points) results for the force between two stars in the presence of added salt. The degree of polymerization of the chains is $N = 50$, the charging fraction $\alpha = 1/3$ and for $N_s = 250$ salt molecules in the simulation box, corresponding to a salt concentration $c_s = 0.036\,\mathrm{M}$.

The crossover of the effective interaction from a power-law form at overlaps to a Yukawa form beyond overlaps is akin to the case of neutral star polymers. Hence, it is to be expected that the anomalous structure factors found there [31] will also be seen in the case of charged stars if the concentration of the solution exceeds its overlap value. On similar grounds, an unusual phase diagram for PE-stars is also to be expected, [32] displaying exotic crystals and reentrant melting. The phase diagram will be much richer in this case, due to the addition of two more possible degrees of freedom: the charging fraction α and the salt concentration. Additional questions that should be addressed in future investigations include the effects of polydispersity [33] and many-body forces [30] in polyelectrolyte-star solutions. The latter are expected to play a minor role at reasonable concentrations, though, because the entropy argument suggests they will become important only at densities for which three PE-stars have a triplet overlap within their coronae, and higher. Finally, further work should be done to study spherical PE-brushes [42, 44] having a nonvanishing hard colloidal particle in the middle of the aggregate and a corresponding core-shell structure.

Chapter 4

Effective Interaction between Star Polymers and Colloids

Typical soft matter systems, such as polymers and colloids, almost always occur in the form of mixtures. It is the central goal of soft matter physics to offer insights into the generic phase behavior of such systems that does not depend on the detailed chemical structure of their constituents. In this respect, the study of mixtures of hard colloidal particles and non-adsorbing polymer *chains* has received a great deal of recent attention, both experimentally [127, 128, 129] and theoretically [129, 126, 130, 131]. The earliest theoretical approach to the study of colloid-polymer mixture dates back to the work of Asakura and Oosawa [3, 132], and Vrij [133], who modeled polymer chains as penetrable spheres. These models pertain mostly to Gaussian, i.e., ideal chains and are semi-quantitative. More systematic approaches have appeared in the recent years, in which self-avoiding chains are modeled and effective interactions among them are derived by means of simulations [117] or theory [131]. The gain from adopting such an alternative view is twofold: on the one hand, one has the possibility of looking at the same problem from a different angle; on the other hand, tracing out the monomers reduces the complexity of the problem by a factor N, the degree of polymerisation of the chains [134].

A physical system where the colloidal approach finds an intuitive and natural application is that of star polymers [11]. These macromolecular entities are similar to the described polyelectrolyte stars in Chapter 3 with the difference that star polymers does not carry charges. Star polymers are synthesized by covalently attaching f polymeric chains on a common center. In this way, hybrid particles between polymers and colloids can be constructed, which naturally bridge the gap between these two common states of soft matter. The number of arms f, also known as *functionality* of the stars, allows us to go from free chains ($f = 1, 2$) to stiff, spherical particles ($f \gg 1$). Effective interactions between star polymers in good [27] and Θ-solvents [135] have been recently derived and the validity of the former has been confirmed through extensive comparisons with experiments [27, 136, 17] and simulations [28, 137]. Extensions to polydisperse stars [33] as well as to many-body

forces in dense star polymer solutions [30] have also been recently carried out.

In this Chapter, we wish to carry these considerations one step further by looking at a *two-component* system of star polymers in good solvent conditions and hard, spherical, colloidal particles. Though the star-star interaction is readily available and the colloids can be modeled as hard spheres, the effective cross interaction between star polymers and colloids is still missing. It is the purpose of this Chapter to present theoretical and simulation results and to furnish analytic expressions for the force and/or the effective interaction acting between a star polymer and a spherical, colloidal particle for a large range of size ratios between the two. The theoretical approach is inspired by the earlier considerations of Pincus [49] regarding the force acting between a star and a flat wall but are made more precise here and they are also extended to include the effects of curvature. The rest of this Chapter is organized as follows: in Section 4.1 we present the general theoretical approach, both for flat and curved surfaces and derive analytic expressions for the star-colloid force which include a handful of undetermined parameters. In Section 4.2 we compare those with the results of monomer-resolved Molecular Dynamics simulations and determine the free parameters in order to achieve agreement between theory and simulation results. In Section 4.3 we present a modified version of the star-star potential which is valid for very low arm numbers, $f \lesssim 10$, and in Section 4.4 we summarize and conclude the presented Chapter.

4.1 Theory

Let us first define the system under consideration and its relevant parameters. We consider a collection of star polymers with functionality f and hard, spherical colloidal particles, the interaction between the latter species being modeled through the hard sphere (HS) potential. By considering two isolated members of each species, i.e., one star and one colloid, our goal is to derive the effective interaction between the two. The colloids have a radius $R_{\rm c}$, which is a well-defined length scale.

The stars, on the other hand, are soft, hairy balls without a sharply defined boundary and this leads to some freedom in defining length scales characterizing their spatial extent. The experimentally measurable length scale that naturally arises from small-angle neutron- or X-ray-scattering experiments (SANS or SAXS) is the radius of gyration $R_{\rm g}$ of the stars and the associated diameter of gyration $\sigma_{\rm g} = 2R_{\rm g}$. For the theoretical investigations on the subject, however, another length scale turns out to be more convenient, namely the so-called corona radius $R_{\rm s}$ of the star or the associated corona diameter $\sigma_{\rm s} = 2R_{\rm s}$. The corona radius arises naturally in the blob model for the conformation of isolated stars, introduced by Daoud and Cotton [12]. According to the Daoud-Cotton picture, the bulk of the interior of a star in good solvent conditions (and for sufficiently long arm chains), consists of a region in which the monomer density profile $c(s)$ follows a power-law as a function of the distance

s from the star center, namely:

$$c(s) \sim a^{-3} \left(\frac{s}{a}\right)^{-4/3} \bar{v}^{-1/3} f^{2/3}, \tag{4.1}$$

with the monomer length a, the excluded volume parameter v and the reduced excluded volume parameter $\bar{v} \equiv v/a^3$. Outside this scaling region, there exists a diffuse layer of almost freely fluctuating rest chains, in which the scaling behaviour of the monomer profile is not any more valid. We define the corona radius R_s of the star as the distance from the center up to which the scaling behaviour of the monomer density given by Eq. (4.1) above holds true. In what follows, we define the *size ratio* q between the stars and the colloids as:

$$q \equiv \frac{R_\mathrm{g}}{R_\mathrm{c}}. \tag{4.2}$$

In addition, the interior of the star forms a semidilute polymer solution in which scaling theory [7] predicts that the osmotic pressure Π scales with the concentration c as $\Pi(c) \sim c^{9/4}$. Combining the latter with Eq. (4.1) above, we obtain for the radial dependence of the osmotic pressure of the star within the scaling regime the relation:

$$\Pi(s) \sim k_B T \, f^{3/2} s^{-3} \qquad (s \leq R_\mathrm{s}). \tag{4.3}$$

No relation for the osmotic pressure $\Pi(s)$ for the diffuse region $s > R_\mathrm{s}$ is known to date. It is indeed one of the central points of this work to introduce an accurate ansatz for the latter, one that will allow us also to derive closed formulas for the effective force between a star and a hard object. This is the subject we examine below.

4.1.1 A star polymer and a flat wall

We begin by examining the simplest case, in which a star center is brought within a distance z from a hard, flat wall, as depicted in Fig. 4.1. Going back an idea put forward some ten years ago by Pincus [49], we can calculate the force $F_\mathrm{sw}(z)$ acting between the polymer and the wall by integrating the normal component of the osmotic pressure $\Pi(s)$ along the area of contact between the star and the wall. In the geometry shown in Fig. 4.1, this takes the form:

$$F_\mathrm{sw}(z) = 2\pi \int_{y=0}^{y=\infty} \Pi(s) \cos\vartheta \, y \mathrm{d}y. \tag{4.4}$$

Using $z = s\cos\vartheta$ and $y = z\tan\vartheta$ we can transform Eq. (4.4) into:

$$F_\mathrm{sw}(z) = 2\pi z \int_{z}^{\infty} \Pi(s) \mathrm{d}s. \tag{4.5}$$

Eq. (4.5) above implies immediately that, if the functional form for the force $F_\mathrm{sw}(z)$ were to be known, then the corresponding functional form for the osmotic pressure $\Pi(z)$ could be obtained through:

$$\Pi(z) \propto -\frac{\mathrm{d}}{\mathrm{d}z}\left(\frac{F_\mathrm{sw}(z)}{z}\right). \tag{4.6}$$

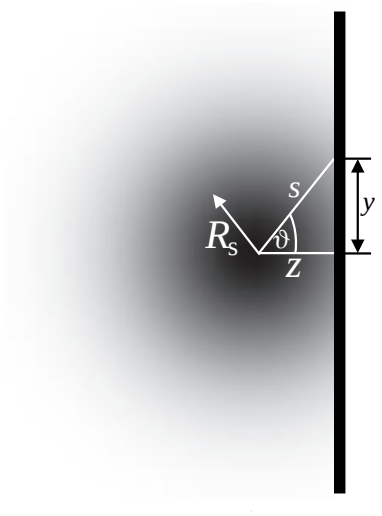

Figure 4.1: Star polymer (black-shadowed particle) interacting with a flat wall. The star polymer consists of a inner core region, where the scaling behaviour is dominant, whereas the outer regime is shadowed and indicates the exponential decay of the osmotic pressure.

To this end, we now refer to known, exact results regarding the force acting between a flat wall and a *single, ideal chain* whose one end is held at a distance z from a flat wall [138]. There, it has been established that the force $F_{\rm sw}^{\rm (id)}(z)$ is given by the relation:

$$F_{\rm sw}^{\rm (id)}(z) = k_B T \frac{\partial}{\partial z} \ln \left[\mathrm{erf}\left(\frac{z}{L}\right)\right], \tag{4.7}$$

where $\mathrm{erf}(x) = 2/\sqrt{\pi}\int_0^x e^{-t^2}\mathrm{d}t$ denotes the error function and L is some length scale of the order of the radius of gyration of the polymer. Carrying out the derivative and setting $\mathrm{erf(x)} \cong 1$ for $x \gg 1$, we obtain a Gaussian form for the chain-wall force at large separations:

$$F_{\rm sw}^{\rm (id)}(z) \cong \frac{k_B T}{L} \mathrm{e}^{-\frac{z^2}{\mathrm{L}^2}} \qquad (\mathrm{z} \gg \mathrm{L}). \tag{4.8}$$

We now imagine a star composed of ideal chains. As the latter do not interact with each other ("ghost chains") the result of Eq. (4.8) holds for the star as well. Going now to self-avoiding chains, we assert that, as the main effect giving rise to the star-wall force is the volume which the wall excludes to the chains, rather than the excluded volume interactions between the chains themselves, a relation of the form (4.8) must also hold for the force $F_{\rm sw}(z)$ between a wall and a *real* star, but with the length scale L replaced by the radius of gyration or the corona radius of the latter and with an additional, f-dependent prefactor

for taking into account the stretching effects of the f grafted polymeric chains. From Eqs. (4.6) and (4.8) it now follows that

$$\Pi(s) \propto \frac{k_B T}{L}\left(\frac{1}{s^2}+\frac{2}{L^2}\right)\mathrm{e}^{-\frac{\mathrm{s}^2}{\mathrm{L}^2}} \qquad (\mathrm{s} \gg \mathrm{L}). \tag{4.9}$$

The full expression for $\Pi(s)$ now follows by combining Eq. (4.3), valid for $s \leq R_\mathrm{s}$, with Eq. (4.9), valid for $s \gg L \cong R_\mathrm{s}$, and matching them at $s = R_\mathrm{s}$. The local osmotic pressure $\Pi(s)$ is the interior of a star polymer, as a function of the distance s from its center has hence the functional form:

$$\Pi(s) = \Lambda f^{3/2} k_B T \begin{cases} s^{-3} & \text{for } s \leq R_\mathrm{s}; \\ \left(\frac{1}{s^2}+2\kappa^2\right)\frac{\xi}{R_\mathrm{s}}\mathrm{e}^{-\kappa^2\left(\mathrm{s}^2-\mathrm{R}_\mathrm{s}^2\right)} & \text{for } s > R_\mathrm{s}, \end{cases} \tag{4.10}$$

where Λ and $\kappa = L^{-1}$ are free parameters; it is to be expected that $\kappa = O(R_\mathrm{g}^{-1})$, as we will verify shortly. On the other hand, ξ must be chosen to guarantee that $\Pi(s)$ is continuous at $s = R_\mathrm{s}$, resulting into the value:

$$\xi = \frac{1}{1+2\kappa^2 R_\mathrm{s}^2}. \tag{4.11}$$

Eq. (4.10) above concerns the radial distribution of the osmotic pressure of an isolated star. The question therefore arises, whether this functional form for the osmotic pressure can be used in order to calculate the force between a star and a flat wall also in situations where the star-wall separation is smaller than the radius of gyration of the star, in which case it is intuitively expected that the presence of the wall will seriously disturb the monomer distribution around the center and hence also the osmotic pressure. In fact, it is to be expected the osmotic pressure is a function of *both* the star-wall separation z and the radial distance s, whereas in what follows we are going to be using Eq. (4.5) together with Eq. (4.10), in which $\Pi(s)$ has no z-dependence itself. However, it turns out that this is an excellent approximation. On the one hand, it is physically plausible for large star-wall separations, where the presence of the wall has little effect on the segment density profile around the star center and the ensuing osmotic pressure profile. On the other hand, also at very small star-wall separations, the scaling form $\Pi(s) \sim s^{-3}$ continues to be valid. To corroborate this claim, we proceed with some arguments to this effect.

First, we refer once more to known, exact results concerning the radial distribution of the pressure on a hard wall arising from an ideal chain grafted on it [139], a situation similar to holding one end of a chain at a distance very close to the wall surface. The pressure $\Pi_\mathrm{id}(s)$ reads as [139]:

$$\Pi_\mathrm{id}(s) = \frac{1}{2\pi}\frac{1}{(s^2+a^2)^{3/2}}\left(1+\frac{s^2+a^2}{2R_\mathrm{g}^2}\right)\exp\left[-\frac{s^2+a^2}{4R_\mathrm{g}^2}\right], \tag{4.12}$$

with the segment length a, indicating that in the regime $a \ll s \ll R_\mathrm{g}$ indeed the scaling $\Pi_\mathrm{id}(s) \sim s^{-3}$ holds.

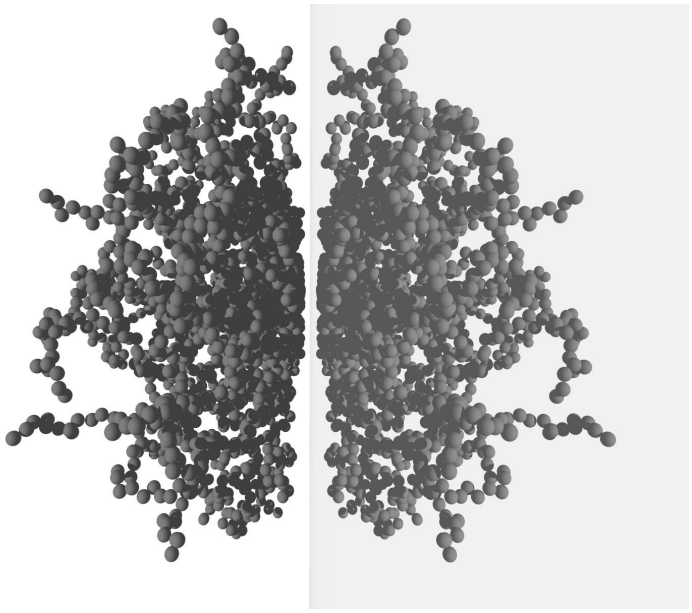

Figure 4.2: Snapshot of a simulation showing a star polymer interacting with a flat wall, at a small center-to-surface distance. The mirror-reflected image of the star, on the right, helps demonstrate that the configuration is similar to that of an isolated star with twice as many arms.

Second, we can employ a scaling argument, asserting that, on dimensional grounds, the osmotic pressure exerted by a star on a nearby flat wall and held at a distance z from it, must be of the form $\Pi(s,z) = k_B T R_{\rm g}^{-3}\, h(s/R_{\rm g}, z/R_{\rm g})$, with some scaling function $h(x,y)$; universality arguments dictate that the segment length a should not appear in the dimensional analysis and hence s, z and $R_{\rm g}$ are the only relevant length scales for this problem. Now, for small star-wall separations, $z \ll R_{\rm g}$, we replace the second argument of this function by zero. Moreover, we assert that, as the dominant contribution to the osmotic pressure for distances $s < R_{\rm g}$ comes from the first few monomers along the chains colliding with the wall, the degree of polymerisation N of the chains should be irrelevant if the chains are long. Hence, all $R_{\rm g}$-dependence of the pressure should drop out, with the implication $h(x,0) \sim x^{-3}$ for $x \ll 1$ and hence $\Pi(s) \sim s^{-3}$ in this regime.

Third, we point out that bringing a star with f arms at a small distance to a flat wall, creates a conformation which is very similar to one of an isolated star with $2f$-arms, as shown in Fig. 4.2. Hence, it is not surprising that at small star-wall separations, one recovers for the radial dependence osmotic pressure the scaling laws pertinent to an isolated star.

Finally, by inserting Eq. (4.10) into Eq. (4.5) and carrying out the integration, we find that for small star-wall distances, $z \ll R_{\rm s}$, the force scales as $F_{\rm sw}(z) \sim (k_B T)/z$, thus giving rise to a logarithmic effective star-wall potential $V_{\rm sw}(z) \sim -k_B T \ln(z/R_{\rm s})$. The latter is indeed in full agreement with predictions from scaling arguments arising in polymer theory [49, 5, 113]. This is a universal result, in the sense that it also holds for single chains, be it

real or ideal, as it can also be read off from the exact result, Eq. (4.7), using the property $\mathrm{erf}(x) \sim x$ for $x \to 0$. Thus, the proposed functional form for the osmotic pressure, Eq. (4.10), combined with Eq. (4.5) for the calculation of the effective force, has the following remarkable property: it yields the correct result both at small and at large star-wall distances and therefore appears to be a reliable analytical tool for the calculation of the effective force at *all* star-wall distances. At the same time, it contains two free parameters, Λ and κ which allow some fine tuning when the predictions of the theory are to be compared with simulation results, as we will do below. Yet, we emphasize that this freedom is *not* unlimited: on physical grounds, κ must be of the order of R_{g}^{-1} and Λ must be a number of order unity for all functionalities f, as the dominant, $f^{3/2}$-dependence of the osmotic pressure prefactor has been already explicitly taken into account in Eq. (4.10).

We are now in a position to write down the full expression for the star-wall force, by using Eqs. (4.5) and (4.10). The result reads as:

$$\frac{R_{\mathrm{s}} F_{\mathrm{sw}}(z)}{k_B T} = \Lambda f^{3/2} \begin{cases} \frac{R_{\mathrm{s}}}{z} + \frac{z}{R_{\mathrm{s}}}(2\xi - 1) & \text{for } z \leq R_{\mathrm{s}}; \\ 2\xi \exp[-\kappa^2(z^2 - R_{\mathrm{s}}^2)] & \text{for } z > R_{\mathrm{s}}. \end{cases} \tag{4.13}$$

Note the dominant, $\sim 1/z$-dependence for $z \to 0$. Accordingly, the effective interaction potential $V_{\mathrm{sw}}(z)$ between a star and a flat, hard wall held at a center-to-surface distance z from each other reads as:

$$\beta V_{\mathrm{sw}}(z) = \Lambda f^{3/2} \begin{cases} -\ln(\frac{z}{R_{\mathrm{s}}}) - (\frac{z^2}{R_{\mathrm{s}}^2} - 1)(\xi - \frac{1}{2}) + \zeta & \text{for } z \leq R_{\mathrm{s}}; \\ \zeta\, \mathrm{erfc}(\kappa z)/\mathrm{erfc}(\kappa R_{\mathrm{s}}) & \text{for } z > R_{\mathrm{s}}, \end{cases} \tag{4.14}$$

with the inverse temperature $\beta = (k_B T)^{-1}$, the additional constant

$$\zeta = \frac{\sqrt{\pi}\xi}{\kappa R_{\mathrm{s}}}\, \mathrm{erfc}(\kappa R_{\mathrm{s}})\, \mathrm{e}^{\kappa^2 \mathrm{R}_{\mathrm{s}}^2} \tag{4.15}$$

and the complementary error function $\mathrm{erfc}(x) = 1 - \mathrm{erf}(x)$. This completes our theoretical analysis of the star polymer-wall force and the ensuing effective interaction potential. The comparison with simulation data and the determination of the free parameters in the theory will be discussed in Section 4.2. We now proceed with the calculation of the effective force between a star and a spherical hard particle, where effects of the colloid curvature become important.

4.1.2 A star polymer and a spherical colloid

We apply the same idea as for the case of the hard wall: the effective force acting at the center of the objects is obtained by integrating the osmotic pressure exerted by the polymer on the surface of the colloid. In Fig. 4.3, the geometrical situation is displayed: within the corona radius of the star polymer $R_{\mathrm{s}} = \sigma_{\mathrm{s}}/2$, the osmotic pressure is determined by scaling laws; the outer regime is shadowed and signifies the Gaussian decay of the osmotic pressure.

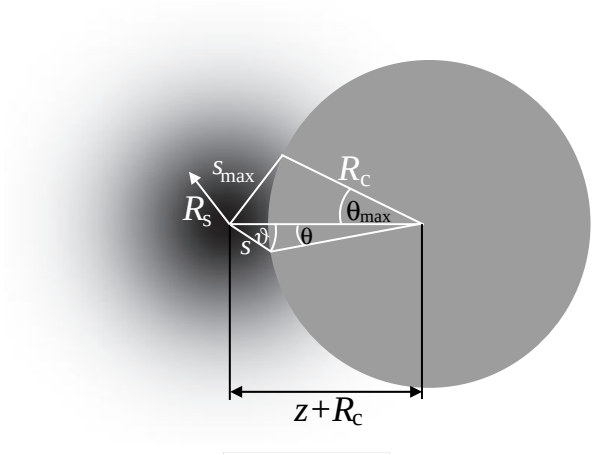

Figure 4.3: Star polymer (black-shadowed particle) interacting with a colloidal particle (grey sphere). The dark and shadowed regions of the star have the same meaning as in Fig. 4.1.

At center-to-surface distance z (center-to-center distance $r = z + R_c$), the integration of the osmotic pressure is carried out over the contact surface between star and colloid. Taking into account the symmetry of the problem, e.g., its independence of the azimuthal angle, we obtain the force $F_{sc}(z)$ between the star and the colloid as:

$$F_{sc}(z) = 2\pi R_c^2 \int_0^{\theta_{max}} d\theta \, \sin\theta \, \Pi(s) \cos\vartheta, \tag{4.16}$$

where ϑ and θ are polar angles emanating from the center of the star polymer and the colloid, respectively. The variables ϑ and θ can be eliminated in favor of the variable s, which denotes the distance between the center of the star and an arbitrary point on the surface of the colloid. This elimination is achieved by taking into consideration the geometrical relations (see Fig. 4.3):

$$s \, \sin\vartheta = R_c \sin\theta \tag{4.17}$$

and

$$s \, \cos\vartheta + R_c \cos\theta = R_c + z. \tag{4.18}$$

Eqs. (4.16), (4.17) and (4.18) yield for the star-colloid effective force the transformed integral:

$$F_{sc}(z) = \frac{\pi R_c}{(z+R_c)^2} \int_z^{s_{max}} ds \left[(z+R_c)^2 - R_c^2 + s^2\right] \Pi(s) \tag{4.19}$$

The maximum integration distance, $s_{\max}$, depends geometrically on $\theta_{\max}$, as well as on the distance z of the star polymer to the surface of the colloid and on R_c. The relation reads as

$$\begin{aligned} s_{\max} &= \sqrt{[z + R_c(1 - \cos\theta_{\max})]^2 + (R_c \sin\theta_{\max})^2} \\ &= \frac{1}{q}\sqrt{[qz + R_g(1 - \cos\theta_{\max})]^2 + (R_g \sin\theta_{\max})^2}. \end{aligned} \tag{4.20}$$

By introducing Eq. (4.10) into Eq. (4.19), an analytic expression for the effective force follows, which reads as

$$\frac{F_{sc}(z)}{k_B T} = \frac{\Lambda f^{3/2} R_c}{(z + R_c)^2} \begin{cases} [(z + R_c)^2 - R_c^2]\left[\frac{1}{2z^2} - \frac{1}{2R_s^2} + \Psi_1(R_s)\right] - \\ \quad \ln(\frac{z}{R_s}) + \Psi_2(R_s) & \text{for } z \le R_s; \\ [(z + R_c)^2 - R_c^2]\,\Psi_1(z) + \Psi_2(z) & \text{for } z > R_s. \end{cases} \tag{4.21}$$

Here, the functions $\Psi_1(x)$ and $\Psi_2(x)$ are given by:

$$\Psi_1(x) = \frac{\xi}{R_s} e^{\kappa^2 R_s^2}\left[\frac{1}{x} e^{-\kappa^2 x^2} - \frac{1}{s_{\max}} e^{-\kappa^2 s_{\max}^2}\right], \tag{4.22}$$

and

$$\Psi_2(x) = \frac{\xi}{R_s} e^{\kappa^2 R_s^2}\left[\frac{\sqrt{\pi}}{\kappa}\left[\mathrm{erf}\,(\kappa s_{\max}) - \mathrm{erf}\,(\kappa x)\right] + x e^{-\kappa^2 x^2} - s_{\max} e^{-\kappa^2 s_{\max}^2}\right], \tag{4.23}$$

where ξ is given by Eq. (4.11). Note that, for small distances, both regimes of the osmotic pressure contribute to the integral, whereas for larger distances, $z > R_s$, only the Gaussian decay does so. Due to the additional dependence of $s_{\max}$ on the distance z, [see Eq. (4.20)], an analytical expression for the effective potential $V_{sc}(z)$, analogous to Eq. (4.14) for the flat-wall case, is not possible here.

Some remarks regarding $F_{sc}(z)$ are necessary. First, for small separations z, the force scales as $F_{sc}(z) \sim (k_B T)/z$, the same behaviour found for the flat-wall case. Once more, we obtain the universal result mentioned above, which has been shown to be also valid for an ideal chain whose one end is held at a distance z from the surface of a hard sphere. Indeed, for this case the force is given by the exact relation [140]:

$$F_{sc}^{(id)}(z) = k_B T \frac{\partial}{\partial z} \ln\left[1 - \left(\frac{R_c}{z + R_c}\right) \mathrm{erfc}\left(\frac{z}{L}\right)\right], \tag{4.24}$$

with L being a length scale of order R_g. Eq. (4.24) above, yields $F_{sc}^{(id)}(z) \sim (k_B T)/z$ for $z \to 0$.

Second, let us consider the limit of small size ratios $q = R_g/R_c$. As can be seen from Eq. (4.20), the upper integration limit $s_{\max}$ scales as R_g/q, whereas the decay parameter κ is of the order R_g^{-1}. Hence, $\kappa s_{\max} \sim q^{-1}$, with the implication that for small enough q's, the argument $\kappa s_{\max}$ in the error function and in the Gaussian in Eqs. (4.22) and (4.23) can be

replaced by infinity. As we will shortly see, this is an excellent approximation up to $q \lesssim 0.3$, as both $\mathrm{erf}(x)$ and $\exp(-x^2)$ approach their asymptotic values for $x \to \infty$ rapidly. Then, the implicit z-dependence of the force $F_{\mathrm{sc}}(z)$ through $s_{\max}$ drops out and a z-integration of the latter can be analytically carried out to obtain an effective star polymer-colloid potential $V_{\mathrm{sc}}^{\infty}(z)$ which reads as [34]:

$$\beta V_{\mathrm{sc}}^{\infty}(z) = \Lambda f^{3/2} \left(\frac{R_{\mathrm{c}}}{z + R_{\mathrm{c}}} \right) \begin{cases} -\ln(\frac{z}{R_{\mathrm{s}}}) - (\frac{z^2}{R_{\mathrm{s}}^2} - 1)(\xi - \frac{1}{2}) + \zeta & \text{for } z \leq R_{\mathrm{s}}; \\ \zeta\, \mathrm{erfc}(\kappa z)/\mathrm{erfc}(\kappa R_{\mathrm{s}}) & \text{for } z > R_{\mathrm{s}}, \end{cases} \tag{4.25}$$

with the constant ζ given by Eq. (4.15). Clearly, in the limit $R_{\mathrm{c}} \to \infty$ ($q \to 0$), corresponding to a flat wall, Eq. (4.25) reduces to the previously derived result, Eq. (4.14). It is a remarkable feature that all effects of curvature are taken into account by the simple geometrical prefactor $R_{\mathrm{c}}/(z + R_{\mathrm{c}})$, for sufficiently small size ratios q. In this respect, the above result bears close similarity to the well-known Derjaguin approximation [141].

4.2 Simulation

4.2.1 The simulation model

In order to check the theoretical prediction of the forces at hard objects, we performed a monomer-resolved Molecular Dynamics (MD) simulation and calculated the mean force at the center of the star polymer to compare the data with theory. The model is based on the ideas of simulation methods applied on linear polymers and on a single star [18, 20]. The details are already presented in Sec. 3.1.1. Different parameters are used for the FENE potential (3.2): $k_{\mathrm{FENE}} = 30.0\epsilon_{\mathrm{LJ}}$ and $R_0 = 1.5\,\sigma_{\mathrm{LJ}}$. The monomers are bonded closer to each other. However, except of the missing charges the model remains essentially the same as in the case of the polyelectrolytes.

In addition all monomers interact with the colloid or with the wall via a hard potential. We note that exactly this simulation model for star polymers was already used by Grest *et al.* in their simulations of linear and star polymers in good solvent conditions [18, 20].

The timestep is typically $\Delta t = 0.002t^*$ with $t^* = \sqrt{m\sigma_{\mathrm{LJ}}^2/\epsilon}$ being the associated time unit and m the monomer mass. After a long equilibration time (500 000 MD steps), the mean force at the core of the star whose center is held at the position $\mathbf{R}$ and its dependence on the arm number f separations, is calculated as the expectation value over all instantaneous forces acting on the star core, as already described in Sec. 3.1.1:

$$\mathbf{F}(\mathbf{R}) = \left\langle -\nabla_{\mathbf{R}} \left[\sum_{k=1}^{fN} V_{\mathrm{LJ}}^{p}(|\mathbf{r}_k - \mathbf{R}|) + \sum_{l=1}^{f} V_{\mathrm{FENE}}^{p}(|\mathbf{r}_l - \mathbf{R}|) \right] \right\rangle, \tag{4.26}$$

where the first sum is carried over all fN monomers of the star and the second only over the f innermost monomers of its chains. The direct force between the central particle and the wall

did not need to be considered, as the center-to-surface distance was always kept at values where this force was vanishingly small. Note that choosing the origin of the coordinate system on the surface of the colloidal particle or wall, at the point of nearest separation between the star center and this surface, and also the z-axis in the direction connecting this origin with the star center, we immediately obtain $R \equiv |\mathbf{R}| = z$.

We have carried out simulations for a variety of arm numbers f and size ratios q, allowing us to make systematic predictions for the f- and q-dependencies of all theoretical parameters. In attempting to compare the simulation results with the theoretical predictions, one last obstacle must be removed: in theory, the fundamental length scale characterizing the star is the corona radius $R_{\rm s}$. The latter, however, is not directly measurable in a simulation in which, instead, we can only assess to the radius of gyration $R_{\rm g}$. Yet, we have previously found that the ratio between the two remains fixed for all considered arm numbers f, having the value $R_{\rm s}/R_{\rm g} \simeq 0.66$ [28]. We now proceed with the presentation of our MD results.

4.2.2 Star-wall and star-colloid interactions

We consider at first a star polymer near a hard wall. The theoretical prediction of the effective interaction force is given in Eq. (4.13). First, we consider the limit of small separations, $z \to 0$, which allows us on the one hand to test the theoretical prediction $F_{\rm sw}(z) \cong k_B T \Lambda f^{3/2}/z$ there and on the other hand to fix the value of the prefactor Λ, which is expected to have in general a weak f-dependence. For this prefactor, some semi-quantitative theoretical predictions already exist: For $f = 1, 2$ the prefactor may be calculated from the bulk and the ordinary surface critical exponents ν, γ and γ^o, γ_1^o of the n-vector model. For $n = 0$ this results in $\Lambda(f = 1) = (\gamma - \gamma_1^o)/\nu$ and $2^{3/2}\Lambda(f = 2) = (\gamma - \gamma^o)/\nu = 1/\nu$ [142, 143]. Numerical values for the exponents are known from renormalization group theory and simulation [144, 145] and yield $\Lambda(f = 1) \approx 0.83$ and $\Lambda(f = 2) \approx 0.60$. On the other hand, for very large functionalities, $f \gg 1$, one can make an analogy between a star at distance z from a wall and two star polymers whose centers are kept at distance $r = 2z$ from each other [49]. Indeed, for very large f, the conformations assumed by two stars brought close to each other is one in which the chains of each star retract to the half-space where the center of the star lies, a situation very similar to the star-wall case. Then, one can make the approximation $F_{\rm sw}(z) \cong F_{\rm ss}(2z)$, where $F_{\rm ss}$ denotes the star-star force. For the latter, it is known [27] that it has the form:

$$F_{\rm ss}(r) = \frac{5}{18} f^{3/2} \frac{1}{r} \qquad (r \to 0), \tag{4.27}$$

implying for the coefficient Λ the asymptotic behaviour:

$$\lim_{f\to\infty} \Lambda(f) \equiv \Lambda_\infty = \frac{5}{36} \cong 0.14. \tag{4.28}$$

Since there is no theory concerning the values of Λ in the intermediate regime of f, Λ is used as fit parameter. Its value can be obtained by plotting the inverse force $1/F_{\rm sw}(z)$ against

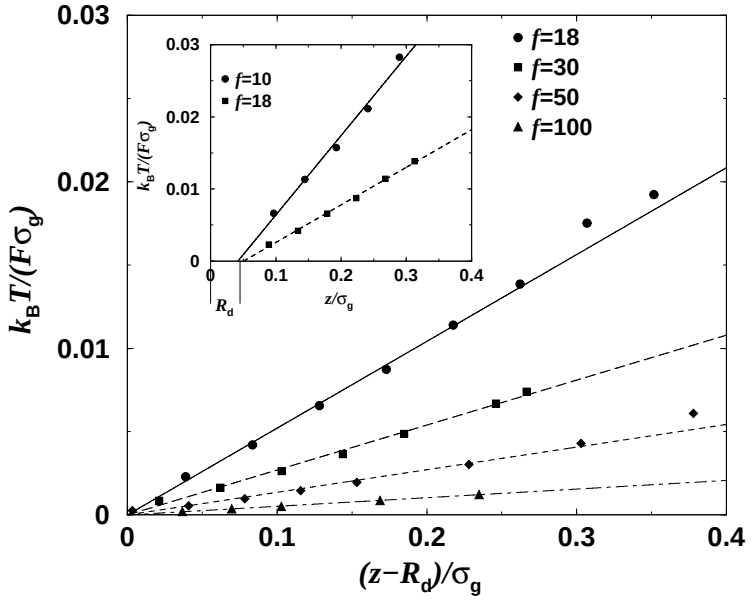

Figure 4.4: Reciprocal effective force between a star polymer and a hard flat wall plotted against the distance z between the star center to the surface of the wall for small z-values. The dependence $F(z) \sim 1/z$ is confirmed by the simulation results (symbols). The prefactor of the potential depends on f and manifests itself in the different slopes of the reciprocal forces. The inserted plot shows the divergence of the force at the distance $z = R_{\rm d}$, which is subtracted from z in the outset of the plot, to achieve divergence of the force in the origin.

z for small separations z to the hard wall. The results are shown in Fig. 4.4. Looking first at the inset, we see that, as for the earlier case of star-star interactions [28], the reciprocal force curves do not go through the origin, as a result of the finite core size, $R_{\rm d}$. Once this is subtracted, though, straight lines passing through the origin are obtained, verifying in this way the $1/z$-behaviour of the force and the associated logarithmic dependence of the effective potential at small separations. The values for $\Lambda(f)$ can be immediately read off from the slope of the curves and they are summarized in Table 4.1. There and in Fig. 4.5 we see that Λ is indeed a decreasing function of f but the asymptotic value $\Lambda_\infty = 5/36$ is still not achieved at arm numbers as high as $f = 100$.

The decay parameter κ is fixed by looking at the force at larger separations and the obtained are also summarized in Table 4.1 and shown in Fig. 4.5. As expected, κ is of the order $R_{\rm g}^{-1}$, as witnessed by the fact that the product $\kappa R_{\rm s}$ is of order unity. A monotonic increase of $\kappa\sigma_{\rm g}$ with the arm number f is observed, consistent with the view that for large f stars form compact objects with an increasingly small diffuse layer beyond their coronae [27].

With parameters Λ and κ *once and for all fixed* from the star-wall case, we now turn our attention to the interaction of a star polymer at a hard sphere of finite radius $R_{\rm c}$, equivalently size ratios $q \neq 0$. Here, the force is given by the full expressions of Eqs. (4.21), (4.22) and

f	$R_\mathrm{d}/R_\mathrm{s}$	Λ	κR_s
2	0.006	0.46	0.58
5	0.018	0.35	0.68
10	0.06	0.30	0.74
15	0.12	0.28	0.76
18	0.09	0.27	0.77
30	0.12	0.24	0.83
40	0.152	0.24	0.85
50	0.152	0.23	0.86
80	0.273	0.22	0.88
100	0.303	0.22	0.89

Table 4.1: The fit parameters arising from the comparison between theory and simulation for the star-wall and star-colloid interaction. The values of R_d shown here are not exactly the same as the input core size; they are just in the same order of magnitude, deviating only slightly from the real input value. They are still corresponding to microscopic length, and are thus irrelevant at length scales $r \sim \sigma_\mathrm{s}$. Λ is the overall prefactor and κ the inverse Gaussian decay length, both used in Eqs. (4.21) and (4.25). $\sigma_\mathrm{s} = 2R_\mathrm{s} = 0.66\,\sigma_\mathrm{g}$ denotes the corona diameter of the stars, as measured during the simulation.

(4.23); for small enough size ratios q, the approximation $\kappa s_\mathrm{max} \to \infty$ gives rise to a simplified expression for the force and to the analytical formula, Eq. (4.25) for the effective star-colloid potential. Our purpose is twofold: to test the validity of these simplified expressions as a function of q and also to find an economical way to parameterize s_max as a function of q for those values of the size ratio for which the approximation $\kappa s_\mathrm{max} \to \infty$ turns out to be unsatisfactory.

We show representative results for fixed arm number $f = 18$ and varying q in Fig. 4.6; results for different f-values are similar. It can be seen that the simplified result arising from allowing $s_\mathrm{max} \to \infty$ yields excellent results up to size ratios $q \lesssim 0.3$, see Figs. 4.6(a) and (b). However, above this value, the approximation of integrating the osmotic pressure up to infinitely large distances breaks down, as it produces effective forces that are larger than the simulation results, especially at distances z of order of the radius of gyration R_g. These are the dashed lines shown in Figs. 4.6(c)-(e). The overestimation of the force is not surprising: as can be seen from Fig. 4.3 and Eq. (4.19), we are integrating a positive quantity beyond the physically allowed limits and this will inadvertently enhance the resulting force. Hence, we have to impose a finite upper limit s_max for size ratios $q > 0.3$ in order to truncate the contribution of the Gaussian tail in the integral of the osmotic pressure in Eq. (4.19).

In Fig. 4.7 a typical snapshot of a star polymer at a colloid illustrates the situation. One can see that the main contribution of the osmotic pressure results from in the inner region of

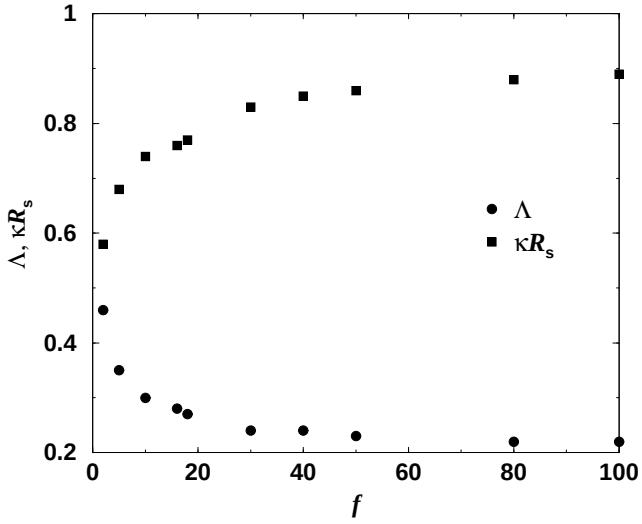

Figure 4.5: The prefactor of Λ and the decay parameter κ of Eq. (4.13) plotted against the functionality f. The value of $\Lambda = 5/36 \approx 0.14$ for $f \gg 1$ is not reached but the simulation data tend to this value very slowly. κ shows a monotonic increase with arm number f.

the star. The outer region of the chains only interact weakly with the sphere. The question now is how the value of $s_{\max}$ must be chosen. As can be seen from Eq. (4.20), this quantity is dependent on, $R_{\rm s}$, z and $\theta_{\max}$. (The latter depending on q means that $\theta_{\max}$ and q should not be treated as independent quantities.) It would be indeed most inconvenient if for every combination of these we would have to choose a different upper integration limit. Hence, we have attempted to transfer all dependence of $s_{\max}$ onto the maximum integration angle $\theta_{\max}$. We found that this is indeed possible and, in fact, the angle $\theta_{\max}(q)$ has a very weak q-dependence: starting with a value $\theta_{\max} \approx 45^{\rm o}$ at $q = 0.3$, we find that it then quickly saturates into the value $\theta_{\max} \approx 30^{\rm o}$ for all $q \gtrsim 0.35$. In this way, we are able to obtain the corrected curves denoted by the solid lines in Figs. 4.6(c)-(e), showing excellent agreement with the simulation results.

We finally turn our attention to the f-dependence of the forces for a fixed value of the size ratio, $q = 0.33$. In Fig. 4.8 we show the simulation results compared with theory for a wide range of arm numbers, $5 \leq f \leq 50$. For the theoretical fits, the values of Λ and κ from Table 4.1 were used, whereas the value of the maximum integration angle was kept fixed at $\theta_{\max} = 30^{\rm o}$ for all f-values. The agreement between theory and simulation is very satisfactory.

Thus, our conclusions for the star polymer-colloid interaction read as follows: the general, analytical expression for the *force* between the two is given by Eqs. (4.21), (4.22) and (4.23), supplemented by Eq. (4.20) in which the angle $\theta_{\max}$ has to be chosen as discussed above for $q \gtrsim 0.3$. An analytical formula for the effective *interaction potential* $V_{\rm sc}(z)$ is not possible for such size ratios. Rather, the results for the effective force have to be integrated numerically

in order to obtain $V_{\rm sc}(z)$. For size ratios $q \lesssim 0.3$ on the other hand, the approximation $s_{\rm max} \to \infty$ in Eqs. (4.21), (4.22) and (4.23) for the effective force can be made, thereby also allowing us to derive a simple, accurate, and analytic form for the interaction potential between a star polymer and a colloid, given by Eq. (4.25). These results form the basis of the statistical-mechanical treatment of star polymer-colloid mixtures in terms of standard liquid-state theories; the availability of analytical results for the pair interactions greatly facilitates the latter. A many-body theory of star polymer-colloid mixtures was put forward recently by Dzubiella *et al.* [34], who employed the above-mentioned effective interactions in order to study the fluid-fluid separation (demixing transition) in such systems. The very good agreement with experimental results obtained in that work offers further corroboration of the validity of the interactions presented here.

As the ultimate goal of the derivation of the interactions we present here is precisely to allow theoretical investigations of star polymer-colloid mixtures, we present in the next Section a short account of a revision of the star-star interactions for the case of very low arm numbers. In this way, mixtures containing stars with arbitrary arm numbers, ranging from free chains ($f = 1, 2$) to the "colloidal limit" of $f \gg 1$ can be studied in full generality.

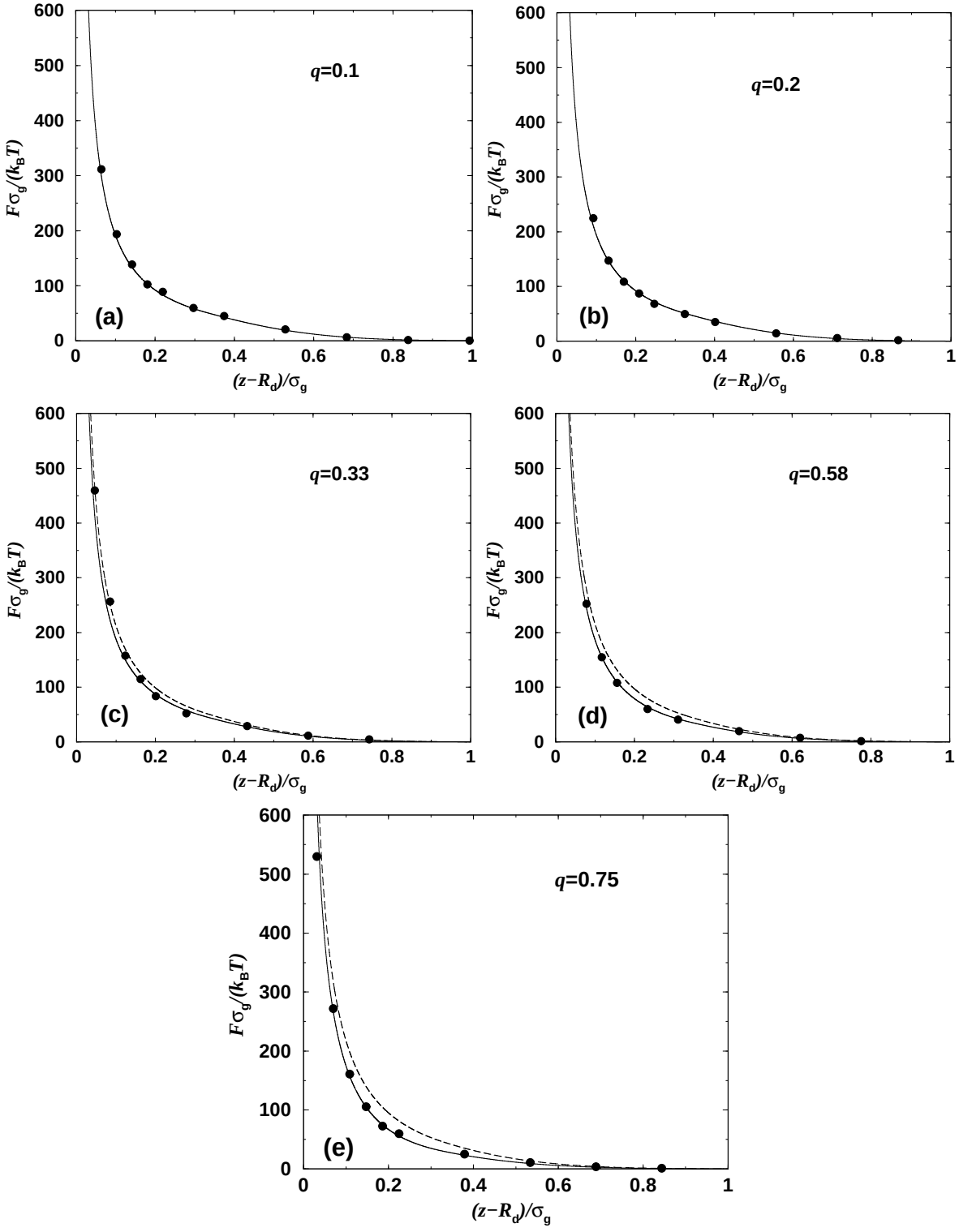

Figure 4.6: Comparison between simulation (symbols) and theoretical (lines) results for the effective force between a star polymer and a colloidal particle for different size ratios q, as a function of the center-to-surface separation z. The arm number here is $f = 18$. The solid lines in (a) and (b) are derived from Eq. (4.21) for $s_{\max} \to \infty$. In (c)-(e) the curves derived by means of this approximation are shown dashed and they increasingly deviate from the simulation results as q grows. Thereby, a finite upper integration limit has to be introduced (see the text), producing the curves denoted by the solid lines in (c)-(e) and bringing about excellent agreement with simulation.

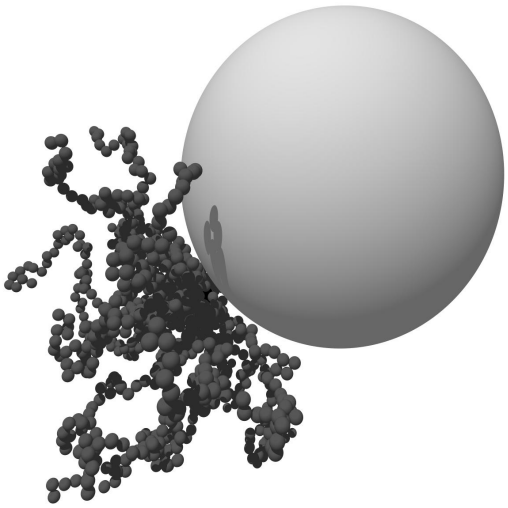

Figure 4.7: Snapshot of a typical configuration of a star polymer with $f = 18$ arms near a colloidal sphere with $q = 0.75$. One should notice that predominantly the inner region of the star interacts with the hard sphere, yielding the main contribution of the inner core regime to the osmotic pressure of a region, determined by $\theta_{\max} \approx 30^{\circ}$. Thereby, the upper integration limit $s_{\max}$ in Eq. (4.19) is limited, see also the geometrical aspects of Eq. (4.20) and Fig. 4.3.

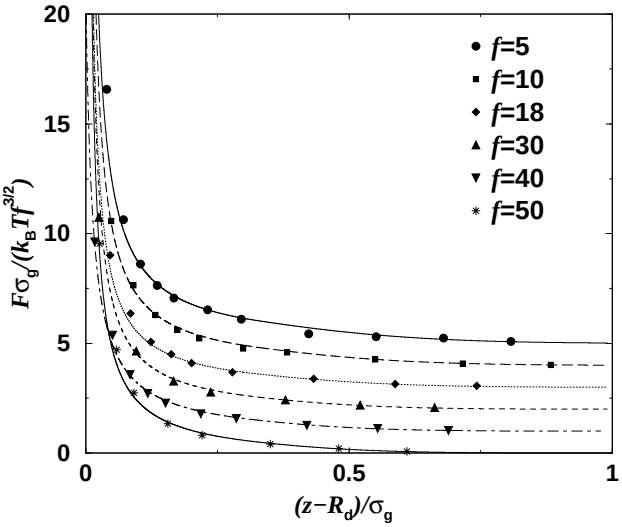

Figure 4.8: The effective force between a star polymer and a colloid for different arm numbers f and $q = 0.33$ plotted against z, the distance of the star center to the surface of the colloid. The lines are the theoretical and the symbols the simulation results. For clarity, the data have been shifted upwards by constants: $f = 10 : 1$, $f = 18 : 2$, $f = 30 : 3$, $f = 40 : 4$, $f = 50 : 5$.

4.3 Revised star-star interaction for small arm numbers

The effective interaction between two stars in a good solvent was recently derived by theoretical scaling arguments and verified by neutron scattering and molecular simulation [27, 136, 17, 28], leading thereafter to the phase diagram of the system [32, 31]. The pair potential was modeled by an ultra-soft interaction which is logarithmic for an inner core and shows a Yukawa-type exponential decay at larger distances [27, 32], as we already presented in Eq. (3.52):

$$V_{\rm ss}(r) = \frac{5}{18} k_{\rm B}T f^{3/2} \begin{cases} -\ln(\frac{r}{\sigma_{\rm s}}) + \frac{1}{1+\sqrt{f}/2} & \text{for } r \le \sigma_{\rm s}; \\ \frac{\sigma_{\rm s}/r}{1+\sqrt{f}/2} \exp(-\frac{\sqrt{f}}{2\sigma_{\rm s}}(r-\sigma_{\rm s})) & \text{for } r > \sigma_{\rm s}, \end{cases} \tag{4.29}$$

However, the theoretical approach giving rise to Eq. (4.29) does not hold for arm numbers $f \lesssim 10$, because the Daoud-Cotton model of a star [12], on which the Yukawa decay rests, is not valid for small f. In these cases, the interaction has to a shorter-ranged decay for $r > \sigma_{\rm s}$. The shortcomings of the blob model can be made evident if one considers the extreme limit $f = 1$, corresponding to free chains. There, the geometrical blob picture and the associated "cone approximation" [19] break down. It is therefore instructive to consider known results about the effective interactions between free chains in order to obtain some insight for the case at hand.

Most of the work done on chain-chain interactions concerns the effective potential between the centers of mass of the chains [117, 134, 146, 147, 148]. Theoretical approaches considering two chains [148], simulations of two chains [146, 147], as well as recent, state-of-the-art simulations of many-chain systems [117, 134] all reach the conclusion that the effective center-of-mass to center-of-mass interaction has a Gaussian form with its range set by the radius of gyration of the chains. Here, we are interested in a slightly different interaction, namely that between the end-monomer of one chain and the end-monomer of the other. However, at distances of the order of $R_{\rm g}$ or larger, whether the centers of mass or the end-monomers choice of the two chains are held fixed should not make much difference. Therefore, we assume a Gaussian decay of the star-star potential for small f-values and center-to-center distances larger than $\sigma_{\rm s}$. We emphasize that *only* the large distance decay of the interaction is affected; its form at close approaches has to remain logarithmic [113]. Accordingly, we propose the following star-star pair potential for arm numbers $f < 10$, replacing the Yukawa by a Gaussian decay:

$$V_{\rm ss}(r) = \frac{5}{18} k_{\rm B}T f^{3/2} \begin{cases} -\ln(\frac{r}{\sigma_{\rm s}}) + \frac{1}{2\tau^2\sigma_{\rm s}^2} & \text{for } r \le \sigma_{\rm s}; \\ \frac{1}{2\tau^2\sigma_{\rm s}^2} \exp\left(-\tau^2(r^2-\sigma_{\rm s}^2)\right) & \text{for } r > \sigma_{\rm s}, \end{cases} \tag{4.30}$$

where $\tau(f)$ is a free parameter of the order of $1/R_{\rm g}$ and is obtained by fitting to computer simulation results, see Fig. 4.9. For $f = 2$ we obtain the value $\tau = 1.03$ which, together

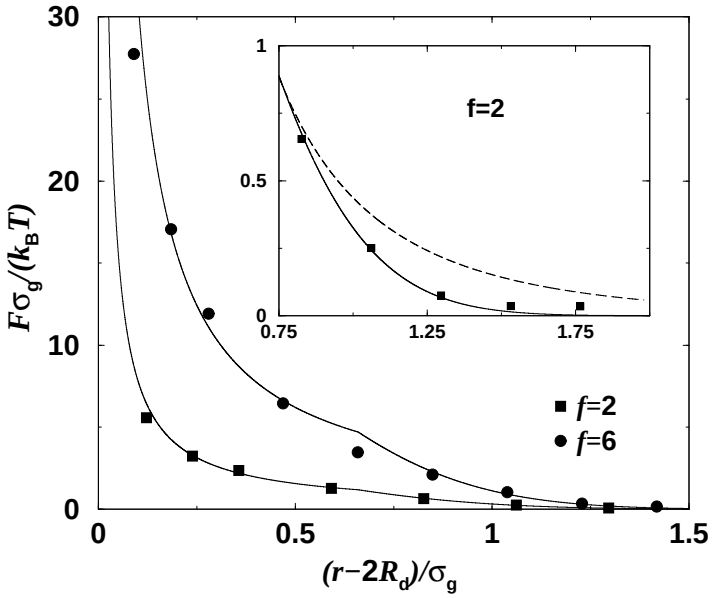

Figure 4.9: Effective force between two star polymers plotted against the center-to-center distance r for arm numbers $f = 2$ and $f = 6$. The simulation data (symbols) coincide with the logarithmic-Gauss expression (solid lines) of Eq. (4.30). In the inset, the outer distance region is enlarged in order to clearly show the validity of the Gaussian decay in this f-regime (solid line), whereas the Yukawa form (dashed line) produces poor agreement there.

with the potential in Eq. (4.30) above yields for the second virial coefficient of polymer solutions the value $B_2/R_g^3 = 5.59$, in agreement with the estimate $5.5 < B_2/R_g^3 < 5.9$ from renormalization group and simulations [134]. For $f = 5$ we find $\tau = 1.12$, which leads to $B_2/R_g^3 = 11.48$, in accordance with Monte Carlo simulation results [149, 29].

The very good agreement between the logarithmic-Gauss-potential of Eq. (4.30) and the simulation data for $f < 10$ can be seen in Fig. 4.9. In the inset of this Figure, it can also be seen that the Yukawa decay is way too slow there. Hence, the potential of Eq. (4.29), has a longer range than the true interaction for small f, a property that explains the discrepancies between the simulated and theoretical second virial coefficients based on this potential, which have been reported by Rubio and Freire [29] in their numerical study of low-functionality stars. At the same time, with increasing f, the roles of the Gaussian- and Yukawa-decays are reversed: in Fig. 4.10, we show simulation and theory results for $f = 10$. The original, logarithmic-Yukawa potential brings about better agreement now, as already established by earlier studies on stars with high arm numbers [28, 27, 136]. To summarize, we propose two analytic expressions for the effective star-star potential, valid in complementary regimes of the functionality f. The first one concerns the regime $f \lesssim 10$ with the validity of the logarithmic-Gauss-potential of Eq. (4.30) being established; in the second regime, $f \geq 10$, the logarithmic-Yukawa-potential of Eq. (4.29) holds. We remark that the ultimative decay

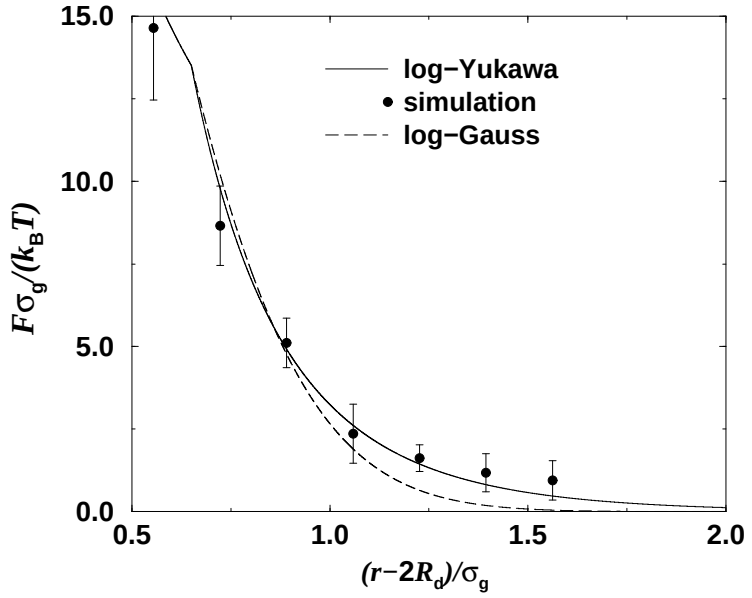

Figure 4.10: Effective force between two star polymers plotted against the center-to-center distance r for arm number $f = 10$. In contrast to Fig. 4.9, here the Yukawa form (solid line) gives an accurate description of the decay of the interaction at large separations, whereas the Gaussian form (dashed line) does not.

of the effective interaction for very long distances is still Gaussian even for very large f, but this is not relevant for B_2 as it occurs for much larger distances than the corona diameter.

4.4 Summary and concluding remarks

In summary, we have presented analytic results for the force between a colloid and a star polymer in a good solvent, accompanied with an analytic expression for the corresponding pair potential which is valid for size ratios $q \lesssim 0.3$. The validity of these expressions was established by direct comparison with Molecular Dynamics simulations. It should be noted that our theoretical approach is in principle generalizable to arbitrary geometrical shapes for the hard particle, thus opening up the possibility for studying effective forces between stars and hard ellipsoids, platelets etc. Further, a revised form for the star-star interaction for small functionalities has been presented, while at the same time the logarithmic-Yukawa form of this interaction remains valid for functionalities $f \gtrsim 10$.

The practical advantage of the present results is that they greatly facilitate the study of structural and thermodynamic properties of concentrated star polymer-colloid mixtures; a first attempt towards this has already been undertaken [34]. In this work, we limited ourselves to the case where the star is smaller than the colloid, i.e., $q < 1$. The study of the inverse case may be possible by applying the ideas presented here, however additional

complications arise through the possibility of the star to "surround" the smaller, colloidal particle, in which case one part of the arms acts to bring about a repulsion with the colloid and another causes an effective attraction between the two. Furthermore, a pair potential picture for the many-body system become more and more questionable for larger q as effective many-body forces [30] will play a more dominant role in this case.

Chapter 5

Conclusions and Outlook

In this work we presented two examples for the calculation of the effective interaction potential: between two PE-stars and between a star polymer and a colloidal particle. Both cases are examples for mesoscopic particles with internal structure. A knowledge of conformational properties like the size of the star or their monomer density profiles, is prerequisite for a creation of a convenient theoretical two-particle model which enables a calculation of the effective interaction. In turn, the knowledge of the effective interaction potential yields the possibility to investigate large scale phenomena, like the phase behavior of the according solutions. Structural studies are more convenient to compare theoretical predictions with experiments.

In the case of neutral star polymers, for which conformational properties are already known [12, 5, 20], the obtained results could be used in our interaction calculations, whereas in the case of PE-stars conformational informations were absent, and we had to create an own model of an isolated PE-star in order to obtain informations about its conformation.

Therefore, and to be familiar with some common terms in polymer theory, in Chapter 2 we illuminated the conformational aspect in more detail, and especially in terms of the reasons for the flexibility of polymer chains. Accordingly, we presented also some relevant parameters, which directly or indirectly influence the flexibility: in this context we investigated solvent and charge effects for the chain flexibility. The second part of this Chapter dealt with a statistical mechanics consideration of the effective interaction potential as a justification for their application in star-like systems. Following Ref. [53], we derived the pair-potential approximation from the exact expression of the effective Hamiltonian. The pair-potential approximation is especially valid for particles in dilute solutions. However, even for small distances it is a convenient approximation, as we showed for neutral star polymers in Appendix A, where triplet interactions are compared with the pair potential. In Section 2.2 we described the measurement of the effective interaction forces in MD simulations, since we use the link between theory and simulation for comparison purposes. We point out that all presented theoretical calculations in this work are verified by simulation results.

After this preliminary part the main subject of the work is presented in Chapter 3. It treats the considerations of PE-stars, the isolated as well as two stars. In contrast to neutral star polymers, we could not use cognitions about conformational properties of PE-stars. All known publications on this matter (see e.g. [45, 46, 47]), except of that of Klein Wolterink et al. [48] did not fit with our simulation results. Here, we note that simulations of PE-stars are presented at first in recent articles [54, 55]. Although our theoretical model is based on the idea of Klein Wolterink et al., their model is not convenient for the treatment of two PE-stars. We summarize the main features of our model, which have to be distinguished from all known conventional theoretical models of PE-stars:

- we took into account for the inhomogeneous behavior ($\approx r^{-2}$) of the density profile for the monomers *and* the counterions resulting from our computer simulations. This is in clear contrast to all other theories on this matter, where homogeneous charge distributions have been assumed [45, 46, 47, 48, 49].

- We distinguish three different regimes for the counterions with different density distributions: homogeneously distributed outside the star, inhomogeneously inside the star, and homogeneously distributed within hollow tubes around the PE-chains (condensed counterions).

- The determination of the radius of the star as well as for the numbers of counterions in their three different states by simultaneous minimization of the free energy.

All calculated quantities in the latter point show very good agreement with results obtained from monomer-resolved MD simulations regarding the counterions explicitly. We observed that almost all counterions (80-90%) are 'trapped' within the star and a significant amount of counterions are condensed along the almost fully stretched chains. We also considered the case of added salt and obtained similar agreements of theory and computer simulations. We note at this point that almost all coions remain outside the star, as predicted by theory and confirmed by simulations.

By expansion of the one-star model to a two star model we calculated the free energy difference between the free energy of two isolated stars and the free energy of two stars at distance D. The arising D-dependence in the free energy contributions occur mainly in the electrostatic part and especially in the entropic part of the counterions. We conclude that the electrostatic influence is much weaker, in odd with eventual intuitive expectations, but in line with Pincus' prediction, that the counterion entropy plays the major role for the effective interaction potential between PE-stars [49]. Nevertheless, electrostatics effects a large number of trapped counterions within the star, thus influencing the entropy enormously. In contrast to Pincus prediction, that the force is constant, we obtain a non-linear decay of the force. The curvature is weaker than in the effective potential between neutral stars [27, 28], but the force has a larger scale with a strong parametrical charge fraction dependence. The scale and curvature also depend on the salt concentration. The ensuing repulsive forces

decrease with adding salt. It should be emphasized that not the screening effect is responsible for the stronger curvature, and for the weaker scale of the force. It is rather a depletion effect of the ions (counter- and co-ions) outside the stars, which induce a decrease in the repulsive force between the stars. In order to offer a simple formula for the effective interaction potential we suggest an analytical expression, obtained by a fit with our simulation results. The expression is shared into two parts which are matched at $D = 2R$: a power-law potential at close separations $D \leq 2R$, and a Yukawa function that can be expected for larger distances beyond overlap $D \geq 2R$.

We hope to give stimulation for further experimental investigations on PE-star solutions. Furthermore, with a proposition of an effective interaction between the stars, we linked a microscopical consideration with a macroscopical treatment of the system by bridging the ensuing length scales. The only remained length scale is the radius of the PE-star R, in this sense we coarse-grained the system. It should now be possible to use our expression as an input quantity in liquid state theories [57] or simulations for further studies of PE-star solutions for different densities. This procedure of a systematic investigation of structural correlations has been already realized for the case of neutral star polymers [31, 32]. We already mentioned further possible future studies in PE-star solutions in Section 3.3; nevertheless we should repeat our suggestion of the study of spherical PE-brushes [42, 44] having a nonvanishing hard colloidal particle in the middle of the aggregate and a corresponding core-shell structure. Especially the possibility of comparing a modified theory, related to spherical PE-brushes, with experiments is enticing.

Principal interest in the field of star-like polyelectrolytes rests upon the combination of electrostatics and statistical mechanics, which is manifested in the competition of entropic and electrostatic effects. A final remark relating to PE-stars concern the inhomogeneity of charge distributions, that is often neglected in many charged polymeric systems. The presented system shows that the inhomogeneous charge distribution induce a curvature of the effective interaction potential. In the case of homogeneous distributions the interaction potential would decay linearly [49]. We stress that possible charge inhomogeneities should be regarded in future works.

The calculation of an effective interaction between a star polymer and a colloid presented in Chapter 4 is important for investigations in star-polymer-colloid mixtures. Our calculation of the effective force acting on a star polymer at a hard wall are based on an idea by Pincus [49] who determined the osmotic pressure of the monomers at the wall. From this quantity the force acting on the star can be derived, and an analytical expression were obtained, which showed excellent agreement with monomer resolved MD simulations. We expanded the model on curved spherical objects, in order to obtain the effective interaction potential between a star polymer and a colloid. As in the hard wall case theoretical calculations yield very good agreement with simulation data for a large scope of star-colloid size ratios $q < 1$, according to smaller stars than colloids. Further, a revised form for the star-star interaction for small functionalities has been presented, while at the same time the logarithmic-Yukawa

form of this interaction remains valid for functionalities $f \gtrsim 10$. The presented results greatly facilitate the study of structural and thermodynamic properties of concentrated star polymer-colloid mixtures [34, 56, 36]. As a future work, the case of $q \geq 1$, at which the star is larger than the colloid can be investigated. However, it can be expected that this situation is more complicated, since the arms are able to "surround" the colloid, and attractive contributions in the effective potential can be expected.

We hope to have enabled and stimulated further work in all of the presented subjects. Especially PE-star solutions offer a large field for further future studies.

List of Abbreviations

AFM	Atomic Force Microscopy
AO	Asakura-Oosawa (model)
CPU	Central Processing Unit (time)
DH	Debye-Hückel (screening)
DLVO	Derjaguin-Landau-Verwey-Overbeek (potential)
FFT	Fast Fourier Transformation
MC	Monte Carlo (simulation)
MD	Molecular Dynamics (simulation)
PE	Polyelectrolyte
PME	Particle Mesh Ewald (method)
RAM	Random Access Memory (space)
RW	Random Walk (model)
SALS	Small-Angle Light Scattering
SANS	Small-Angle Neutron Scattering
SAXS	Small-Angle X-Ray Scattering
SCF	Self-Consistent Field (calculation)
SFA	Surface Force Apparatus
TIRM	Total Internal Reflection Microscopy

Appendix A

Triplet interactions in star polymer solutions

In the following we want to give an example for many-body forces which we mentioned in Section 2.2.2. Here we restrict our consideration in the analysis of the effective triplet interactions between the centers of star polymers in a good solvent. In fact, we intend to calculate the expression of Eq. (2.48) for star polymers.

In general, while the pair interactions are the central focus and the typical input of any many-body theory, much less is known about triplet and higher-order many body interactions. For rare gases, the Axilrod-Teller triplet interaction [150] has been found to become relevant in order to describe high-precision measurements of the structure factor [151]. For charged colloids, the effective triplet forces are generated by nonlinear counterion screening. This was investigated by theory and simulations [152]. For star polymer solutions in a good solvent such studies are missing. In all three cases, the effective triplet forces originate from formally integrating out microscopic degrees of freedom, as is shown in Section 2.2.2. For rare gases, these are the fluctuations of the outer-shell electrons while for charged colloids the classical counterions play the role of additional microscopic degrees of freedom.

Usually one starts from an effective pair potential which is valid for large particle separation. The range of this effective pair potential involves a certain length scale ℓ which is the decay length of the van-der-Waals attraction, the Debye-Hückel screening length or the diameter of gyration $2R_g$, for rare gases, charged colloids, and star polymers, respectively. Triplet forces, i.e. three star forces, not forces between monomers, become relevant with respect to the pairwise forces if the typical separations between the particles are smaller than this typical length scale ℓ. This implies a triple overlap of particle coronae drawn as spheres of diameter ℓ around the particle centers. The triple overlap volume is an estimate for the magnitude of the triplet forces. Hence a three-particle configuration on an equilateral triangle is the configuration where triplet effects should be most pronounced.

This Appendix is organized as follows: In the next Section A.1 we briefly present theoretical predictions resulting from scaling theory. A detailed description of the theory can be

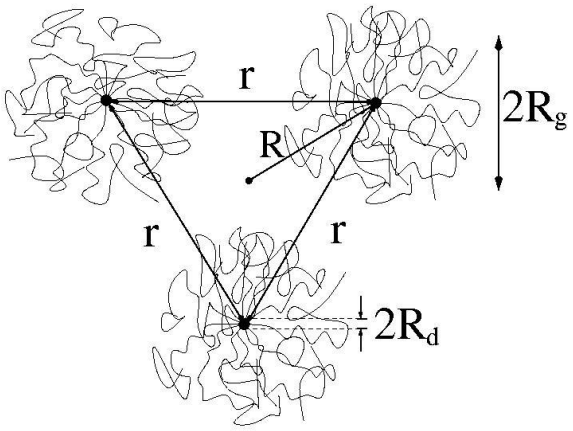

Figure A.1: Three star polymers at mutual distance r. The cores of the stars (with radius R_d) are located at the corners of an equilateral triangle. The distance from the center is R. The mean radius of gyration of a single star is R_g.

found in Ref. [30]. Afterwards we compare the theoretical predictions with results obtained from Molecular Dynamics simulations.

A.1 Theoretical predictions for three stars

We consider a symmetric situation in which the three cores of the polymer stars are located on the corners of an equilateral triangle (see Fig. A.1). The distance between the cores is r while their distance to the center of the triangle is R. We assume that the radius of gyration R_g of the star polymers is much larger than their mutual distance $R_g \gg r$.

Let us specify the result for the symmetric situation of three equivalent stars, each consisting of arm numbers $f_1 = f_2 = f_3 = f$. Coming back to the effective pair potential of star polymers, presented in Eq. (3.52), we should notice the nature of the interaction part for close distances. The inner part has a logarithmic form with a prefactor $\Theta^{(2)}_{ff} = \frac{5}{18} f^{3/2}$ and stems from scaling theory [5].

In the case of three stars only the prefactor of the logarithm $\Theta^{(3)}_{fff}$ changes due to a different scaling exponent of the according partition function. The three-star contact exponent $\Theta^{(3)}_{fff}$ can be written as

$$\Theta^{(3)}_{fff} = \frac{3^{3/2} - 3}{2^{3/2} - 2} \frac{5}{18} f^{3/2} \,. \tag{A.1}$$

An effective potential of the system of the three stars at small distance R from the center may then be defined by

$$V^{(3)\mathrm{eff}}_{fff}(R) = -k_{\mathrm{B}} T \Theta^{(3)}_{fff} \ln(R/R_g) \,. \tag{A.2}$$

We now derive the corresponding three body force underlying this effective potential. Note

that the absolute value of the force is the same for all three stars. The relation of the potential to the force on the core of one star is then

$$V_{fff}^{(3)\mathrm{eff}}(R+dR) - V_{fff}^{(3)\mathrm{eff}}(R) = \sum_{i=1}^{3} \vec{F}_i \cdot d\vec{R}_i = 3F_{fff}^{(3)}(R)dR\,. \tag{A.3}$$

The final result for the total force on each of the stars that includes any three body forces is therefore

$$F_{fff}^{(3)}(R) = -k_{\mathrm{B}}T\Theta_{fff}^{(3)}/(3R)\,. \tag{A.4}$$

If one starts instead from a sum of two body forces, then one star experiences the sum of the two forces calculated for the star-star interaction. With the given geometry of the equilateral triangle this is easily calculated to give

$$F_{fff}^{(2)}(r) = |\hat{r}_{12}\Theta_{ff}^{(2)}/r_{12} + \hat{r}_{13}\Theta_{ff}^{(2)}/r_{13}| = -k_{\mathrm{B}}T\Theta_{ff}^{(2)}/R\,. \tag{A.5}$$

Here, $r = r_{12} = r_{13} = R\sqrt{3}$ denote the distance between two of the stars, while the $\hat{r}_{ij}$ are the unit vectors along the edges of the triangle (see Fig A.1). The relative deviation from the pair potential picture is then given by

$$\frac{\Delta F}{F_{fff}^{(2)}} = \frac{F_{fff}^{(3)}(r) - F_{fff}^{(2)}(r)}{F_{fff}^{(2)}(r)} = \frac{\Theta_{fff}^{(3)} - 3\Theta_{ff}^{(2)}}{3\Theta_{ff}^{(2)}}\,. \tag{A.6}$$

Using the cone approximation for the contact exponent [153] we finally obtain for the relative deviation caused by triplet forces alone

$$\frac{\Delta F}{F_{fff}^{(2)}} = \frac{3^{3/2}-3}{2^{3/2}-2} \approx -0.11\,. \tag{A.7}$$

This result is independent of the number of arms and valid in the full region that is described by the logarithmic potential. The results are in good agreement with results derived from the perturbation expansion of polymer field theory [154, 155, 156] checking the relation Eq. (A.7).

A.2 Comparison with simulation results

Molecular dynamics (MD) simulations were performed using exactly the model that we already described in Section 3.1.1 but modified for three neutral star polymers. In fact, all in Section 3.1.1 described potentials between the monomers are valid, except of the Coulomb charges. In the FENE potential we used for the parameters $k_{\mathrm{FENE}} = 30.0\epsilon_{\mathrm{LJ}}$ and $R_0 = 1.5\,\sigma_{\mathrm{LJ}}$. We note that this model had been originally proposed to study single star polymers [18, 20]. In this model the configuration of star polymer $i = 1, 2, 3$ is given by the coordinates $\vec{r}_m^{(i,j)}$ of the N monomers $m = 1, \ldots, N$ of the f chains $j = 1, \ldots, f$ and the position of its core $r_0^{(i)}$.

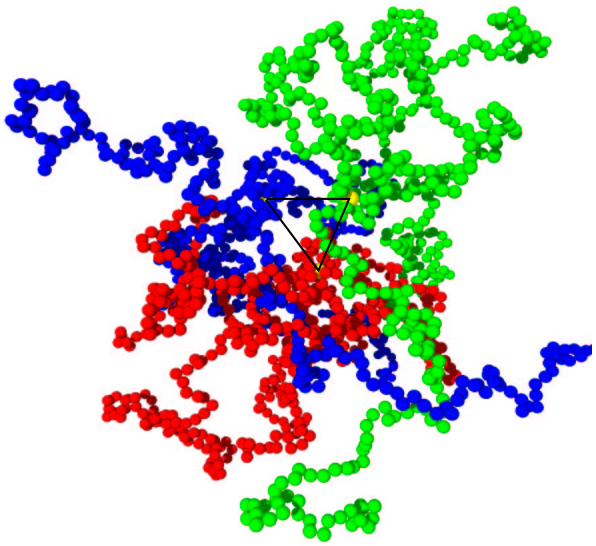

Figure A.2: Snapshot of the simulation of three stars with $f = 5$ arms each with $N = 100$ monomers. The cores are located at the corners of the equilateral triangle that is depicted in the center. The monomers that belong to the same star are represented by balls of the same color: either black, dark gray, or light gray.

The three cores of the stars were placed at the corners of an equilateral triangle, see again Fig. A.1 where also the core radius R_d is shown. A typical snapshot of the three star simulation is displayed in Fig. A.2 for a functionality of $f = 5$ and $N = 100$ monomers per chain. The force on the star core was averaged during the MD simulation for a number of edge lengths r of the triangle varying in the range between the diameter of the two cores $2R_d$ and the diameter of gyration $2R_g$ of a single star polymer. We have produced data for $f = 3, 5, 10, 18, 30$. For the smaller functionalities ($f = 3, 5, 10$) the number of monomers per chain was $N = 100$ while for $f = 10, 18, 30$ a number $N = 50$ was chosen. Note that the total system comprises between $900 - 4500$ mutually interacting particles. As equilibration is slow and the statistical average converges slowly, the simulation becomes increasingly time-consuming beyond such system sizes. As for reference data, we have also produced data for a two stars situation according to the calculations in Ref. [28].

Results of the computer simulation are compared to the theory in Figs. A.3a and A.3b. The reduced averaged force on a single star is shown versus the reduced triangle length for different arm numbers. As a reference case, also the corresponding results in a pair potential picture are shown, both within theory and simulation. For technical reasons we kept a small

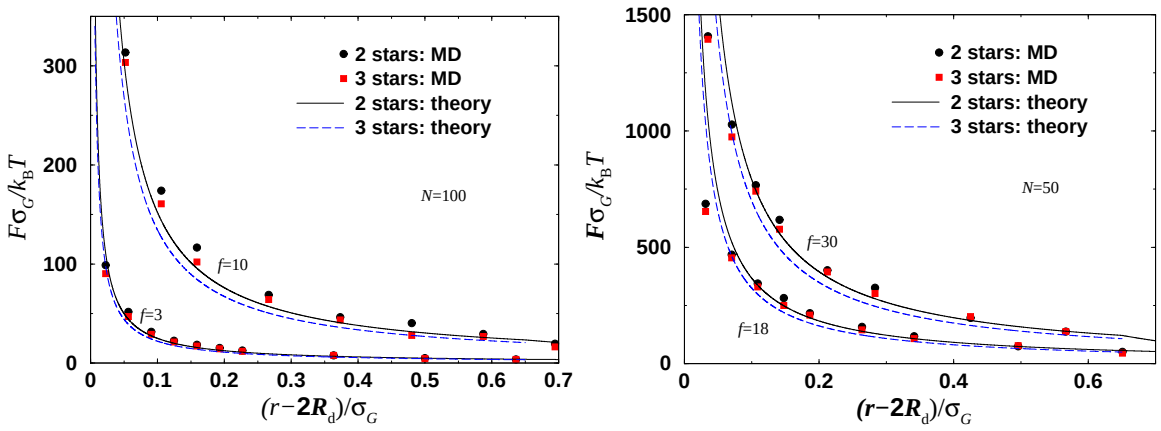

Figure A.3: a) Comparison of the force F measured in the three star MD with that calculated from a corresponding two star MD simulation for $f = 3$ and $f = 10$ with $N = 100$. Also the results predicted by the theory are plotted as a continuous line (only pair forces) and a broken line (including triplet forces). b) Same as Fig. 3a but for $f = 18$ and $f = 30$ with $N = 50$.

core radius R_d in the simulation, which is roughly 10% of the radius of gyration of the whole star. In the theory, on the other hand, the core size was zero. Hence, to compare properly [28], a shift $r - 2R_\mathrm{d}$ has to be performed. The values for R_d are listed in Table 4.1.

As expected, in both theory and simulation, the triplet forces become relevant only within the coronae. A comparison with pure pairwise forces leads to the first important observation that the triplet force is smaller, i.e. the pure triplet contribution is *attractive*. (Note that one has to multiply the pure two-star force by a factor of $\sqrt{3}$ for simple geometrical reasons.) The relative magnitude of the triplet term, however, is small. A quantitative comparison with theory and simulation leads to good overall agreement. The triplet contribution itself, however, is subjected to larger statistical errors of the simulation. Hence we resorted to a different strategy to check the theory by plotting the inverse force versus distance. If the theory is correct the simulation data should fall on a straight line both for the pure pairwise and the full triplet case. The slope should then give the theoretical prefactor of the logarithmic potential. The advantage of this consideration is that the slope bears a smaller statistical error as more data points are included. Such a comparison is shown in Fig. A.4 for $f = 10$. The first consequence is that the simulation data indeed fall on a straight line confirming the theory. In fact this is true for all other parameter combinations considered in the simulations. The slope is higher for the triplet and lower for the pair case, both in theory and simulation. The actual values in Fig. A.4 are in the same order of magnitude but a bit different.

In order to check this in more detail, we have extracted the slope for all simulation data. The result is summarized in Figure 5 where the relative differences of the slopes between the pair and triplet cases are plotted versus the arm number f. The theory predicts a constant

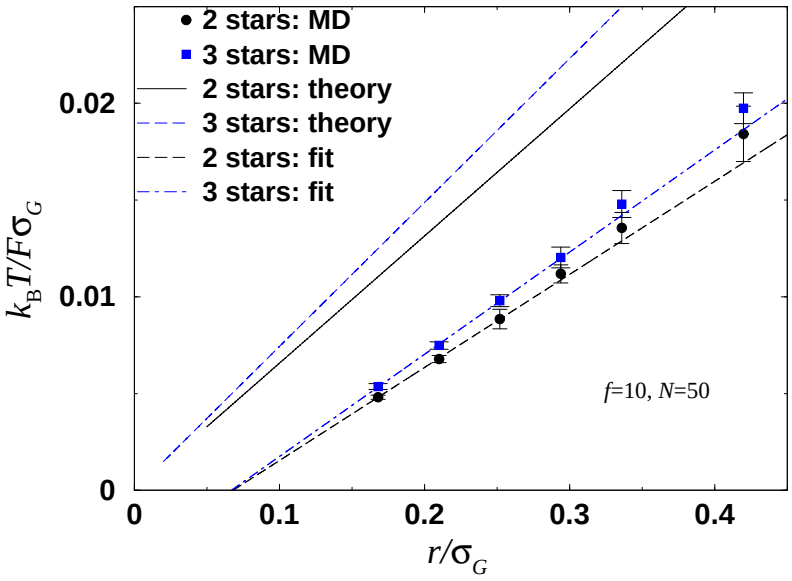

Figure A.4: Comparison of the inverse force $1/F$ measured in the three star MD with that calculated from a corresponding two star MD simulation for $f = 10$ with $N = 50$. The linear fits for the pair forces (small dashed line) and the full three body force (dash-dotted line) are shown together with the respective results predicted by the theory which are depicted by a continuous line (only pair forces) and a broken line (including triplet forces).

value of 0.11, see Eq. (A.5). The simulation data scatter a lot in the range between 0.05 and 0.15 due to the large statistical error but the theoretical value falls reasonably within the data. Consequently, the triplet contributions are found to be attractive and small even for nearly touching cores where the triplet overlap of the coronae is substantial.

A.3 Conclusions

In conclusion, we have calculated, by theory and computer simulations, the triplet interaction between star polymer centers in a good solvent positioned on the corners of an equilateral triangle. The triplet part was found to be attractive but only about 11% of the pairwise repulsion. Our calculations justify earlier investigations [32] where the pair potential framework was used even slightly above the star overlap concentration.

We finish with a couple of remarks: First, the scaling theory can also be performed for any triplet configurations beyond the equilateral triangle studied in this Appendix. Second, arbitrary higher-order many body forces can be investigated assuming a cluster of M stars. Such a calculation is given [30]. As a result, the deviations from the pair potential picture increase with the number M and even diverge for $M \to \infty$. This implies that the pair

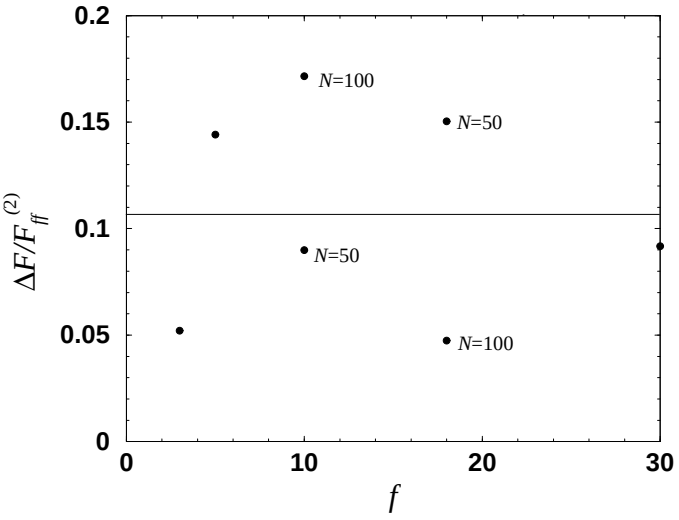

Figure A.5: The slopes of the linear fits to the data as shown in Fig. 4 were extracted from the simulation data for $f = 3, 5, 10, 18, 30$ and $N = 50, 100$ to calculate the relative deviation $\Delta F/F_{fff}^{(2)}$ induced by the triplet forces. The line at 0.11 corresponds to the analytic result.

potential picture breaks down for very high concentrations. This is expected as for high concentration a star polymer solution is mainly a semi-dilute solution of linear chains where it is irrelevant at which center they are attached to [113]. As far as further simulational work is concerned, there are many open problems left. Apart from the investigation for arbitrary triplet configurations and their extensions to an arbitrary number of stars, the most challenging problem is a full "ab initio"simulation of many stars including many-body forces from the very beginning. This is in analogy to Car-Parrinello simulations [157] which were also applied to colloidal suspensions [158]. A first attempt has been done [159], but certainly more work is needed here. Another (a bit less demanding) task is to study stars on a periodic solid lattice with periodic boundary conditions and extract the many body interactions from there.

It would be interesting to study the relevance of triplet forces for star polymers in a *poor* solvent near the Θ-point [135]. It can, however, be expected that the triplet forces here are even less important than for a good solvent as the effective interaction becomes stiffer in a poor solvent. Furthermore, the effect of polydispersity in the arm number which has been briefly touched in our scaling theory treatment should be extended since this is important to describe real experimental samples.

Appendix B

The Lekner method

The calculation of the Coulomb energy of an infinite periodic system is an important part of the numerical work in many applications. These systems are usually obtained by considering N charges in a central box and all their periodic images. The problem of simulating the movement of this charges is called *N-body problem*. Computing the forces among a set of N bodies can be done in a straightforward way by computing all N^2 pairwise interactions. There are various algorithms to increase the efficiency of the simulation regarding the CPU-time. However, all these algorithms are efficient under certain conditions. Before introducing the so-called Lekner method we first present shortly some of the most common methods:

An important class of the mentioned algorithms are the tree-based methods, which use a tree data structure to hierarchically group the bodies (or particles) into clusters, that is, groups of bodies that are fairly close to each other (see, e.g. [160, 161]). Those methods can calculate the forces between N particles in time proportional to $\mathcal{O}(N \log N)$ or even $\mathcal{O}(N)$. A detailed introduction into this methods is given by Hockney and Eastwood [162]. However, tree-based methods take use of physical approximations like multipoles which are accurate for a sufficient number of particles ($\gg 10\,000$).

For lower numbers of particles $N < 10\,000$ different algorithms are more accurate by summing the Coulomb forces between all particles. One of the main problems is the acceleration of the slow convergence of the occuring sums. The most common method to handle the convergence in a convenient way was proposed by Ewald [163, 164]. The basic idea is to split the sum of Coulomb interactions into two parts: a short-ranged contribution and a long-ranged contribution which accounts for the interaction between a certain particle and all other particles beyond a defined cutoff distance inclusive the periodic images. The long-ranged part is calculated via Fourier-transformation which leads to a fast variant of the Ewald summation, the particle-mesh Ewald (PME) algorithm [165] which uses the Fast Fourier transformation. These methods scale also up to $\mathcal{O}(N \log N)$ with a sufficient accuracy. However, the mentioned scaling can be achieved only if the system is essentially homogeneous distributed. The cutoff radius at which the short- and the long- ranged contributions are split, a strongly inhomogeneous system scales with N^2 even by using the above

methods, if almost all particles are concentrated in a certain region which size is in the order of the cutoff radius.

Since the simulated PE-stars contains strongly inhomogeneous distributed charges we have to use an N^2-scaling algorithm. Rather than the Ewald summation we use the so-called Lekner summation of the Coulomb sum [58]. Lekner rederived some of the identities which are in essence contained in the pioneering work by Madelung [166] who calculated the Coulomb sum. Lekner accelerated the convergence of the Coulomb sum without using accuracy. This is achieved with less terms than in the Ewald summation, and it avoids the introduction of a cutoff radius with a reasonable value. We now present the basic feature of the Lekner method [58, 167], which were used in all our simulations of PE-stars. The method was previously applied in [168, 169].

For an assembly of N ions in a central cubic cell of dimension L, the Coulomb force $\boldsymbol{F}_i^{(c)}$ exerted onto particle i by particle j, and by all repetitions of particles j in the periodic system, is

$$\boldsymbol{F}_i = \frac{q_i q_j}{\epsilon} \sum_{\text{all cells}} \frac{\boldsymbol{r}_i - \boldsymbol{r}_j}{|\boldsymbol{r}_i - \boldsymbol{r}_j|^3}, \tag{B.1}$$

where q_i is the charge of the ith particle and ϵ denotes the permittivity of the dielectric medium.

Because of the x, y, z symmetry it is sufficient to consider only one component of the force. For the x-component we obtain

$$F_{ix} = \frac{q_i q_j}{\epsilon L^2} \sum_{l,m,n=-\infty}^{\infty} \frac{\xi + l}{[(\xi + l)^2 + (\eta + m)^2 + (\zeta + n)^2]^{3/2}}, \tag{B.2}$$

where we used the reduced components $\xi L \equiv x_i - x_j$, $\eta L \equiv y_i - y_j$ and $\zeta L \equiv z_i - z_j$ with the condition $|\xi|, |\eta|, |\zeta| \leq 1$. The last sum can be transformed in three mathematical steps:

1. Euler transformation:

$$x^{-\nu} = \frac{1}{\Gamma(\nu)} \int_0^\infty \mathrm{d}t t^{\nu-1} \mathrm{e}^{-xt}, \tag{B.3}$$

   with the Γ-function $\Gamma(\nu)$;

2. Poisson-Jacobi identity:

$$\sum_{l=-\infty}^{\infty} \mathrm{e}^{-(\xi+l)^2 t} = \sqrt{\frac{\pi}{t}} \sum_{l=-\infty}^{\infty} \mathrm{e}^{-\frac{\pi l^2}{t}} \cos(2\pi l \xi); \tag{B.4}$$

3. modified Bessel function of zero order

$$K_0(2\pi|lm|) = \frac{1}{2} \int_0^\infty \frac{\mathrm{d}t}{t} \mathrm{e}^{-\frac{(\pi l)^2}{t} - m^2 t}. \tag{B.5}$$

If we use in step 2 the partial derivation of the Poisson-Jacobi identity with respect to ξ we rewrite Eq. (B.2).

$$F_{ix} = 8\pi \frac{q_i q_j}{\epsilon L^2} \sum_{l=1}^{\infty} l \sin(2\pi l \xi) \sum_{m,n=-\infty}^{\infty} K_0 \left(2\pi \left[(\eta + m)^2 + (\zeta + n)^2 \right]^{1/2} \right) . \qquad \text{(B.6)}$$

In the first sum we took use of the point-symmetry of the sin-function.

For pair of particles not aligned parallel to x-axis the convergence of the sum in Eq. (B.6) is fast. Thus an evaluation of just 20 terms in the sum is enough to get a part-per-million accuracy: $m, n = -2, \ldots, 2$, $l = 1, \ldots l_{\max}$, with $l_{max} = 2(\eta^2 + \zeta^2)^{-1/2}$ [58].

The convergence becomes worse if simultaneously $|\eta L| < \delta$ and $|\zeta L| < \delta$ ($\delta \approx \sigma_{\mathrm{LJ}} \ll L$) for the case $m = n = 0$. The number of terms needed in the sum for a desired accuracy increases rapidly with increasing δ. If the particles are aligned parallel to the x-axis such that $|\eta| + |\zeta| \equiv 0$, the sum in (B.6) diverges with $m = n = 0$. For this particular case F_{ix} is [170]

$$\begin{aligned} F_{ix} &= 8\pi \frac{q_i q_j}{\epsilon L^2} \sum_{l=1}^{\infty} l \sin(\pi l \xi) \\ &\quad \times \sum_{m=-\infty}^{\infty} \left[K_0 \left(2\pi l \left| \frac{\xi}{2} + m \right| \right) + (-1)^l K_0 \left(2\pi l \left| \frac{\xi}{2} + m - \frac{1}{2} \mathrm{sign}(\xi L) \right| \right) \right] . \end{aligned} \qquad \text{(B.7)}$$

We finally summarize the different cases:

- case 1: $|\xi| L, |\eta| L, |\zeta| L > \delta \;\rightarrow$ Lekner summation using Eq. (B.6).
- case 2: $|\xi| L > \delta$, $|\eta| L, |\zeta| L \leq \delta \;\rightarrow$ Lekner summation using Eq. (B.7).
- case 3: $|\xi| L, |\eta| L, |\zeta| L \leq \delta \;\rightarrow$ full Coulomb force between both particles only, without their periodic images.

The Lekner forces (B.6) and (B.7) were calculated on a lattice in the beginning of the simulation. The grid distance b was chosen as $b \approx 0.15\sigma_{\mathrm{LJ}}$. The forces were tabulated inducing a large memory space usage (RAM-space $>$ 60 Mbyte, depending on the size of the simulation box). Although there are some methods enabling the save of RAM space by dynamical variation of the grid distance during the simulation, we renounced these methods in order to save CPU time.

Appendix C

Calculation of the electrostatic potential for a chopped sphere

In this Appendix we present the technical details for the calculation of the electrostatic potential of the two fused spheres of radius R, each carrying a charge Q_* and having a charge density $\varrho(\boldsymbol{r'})$ that decays as $(r')^{-2}$ with the distance r' from its center and is abruptly cut off at the mid-plane, as given by Eqs. (3.32) and (3.34). In other words, we show the steps for the calculation of the electrostatic potential $\Phi_{\rm in}(\boldsymbol{r})$ of Eq. (3.35).

C.1 Calculation of the electrostatic potential $\Phi_{\rm in}$

The electrostatic potential $\Phi(\boldsymbol{r})$ due to the charge density $\varrho(\boldsymbol{r})$ in a dielectric medium of permittivity ϵ is given by

$$\Phi(\boldsymbol{r}) = \frac{1}{\varepsilon}\int \frac{\varrho(\boldsymbol{r'})}{|\boldsymbol{r'}-\boldsymbol{r}|}\mathrm{d}^3r'. \tag{C.1}$$

In order to calculate the integral above, we now take the two inner fused spheres shown in Fig. 3.8 and introduce infinitesimally thin discs of thickness $\mathrm{d}z'$ that are perpendicular to the z-axis and cover the whole pattern, as shown in Fig. C.1. There, we show for clarity only one of the two fused spheres, cut in the mid-plane, which we call a 'chopped sphere' and which can be figured as a succession of discs, each carrying an elementary charge $\mathrm{d}Q$. It is a straightforward calculation to show that this elementary charge is given by

$$\mathrm{d}Q = \frac{Q_*}{2R}\ln\left(\frac{R}{c}\right)\frac{1}{1+\cos\theta_0\,[1-\ln(\cos\theta_0)]}\mathrm{d}z', \tag{C.2}$$

i.e., it depends on the geometry through $\cos\theta_0 = D/(2R)$ as well as on the position of the disc-center C along the z-axis. As shown in Fig. C.1, c is the distance (OC) between the disc center and the center of the chopped sphere, which is taken to be the origin of the coordinate axes. With $C = (x', y', z')$ we have therefore

$$c = |z'|, \tag{C.3}$$

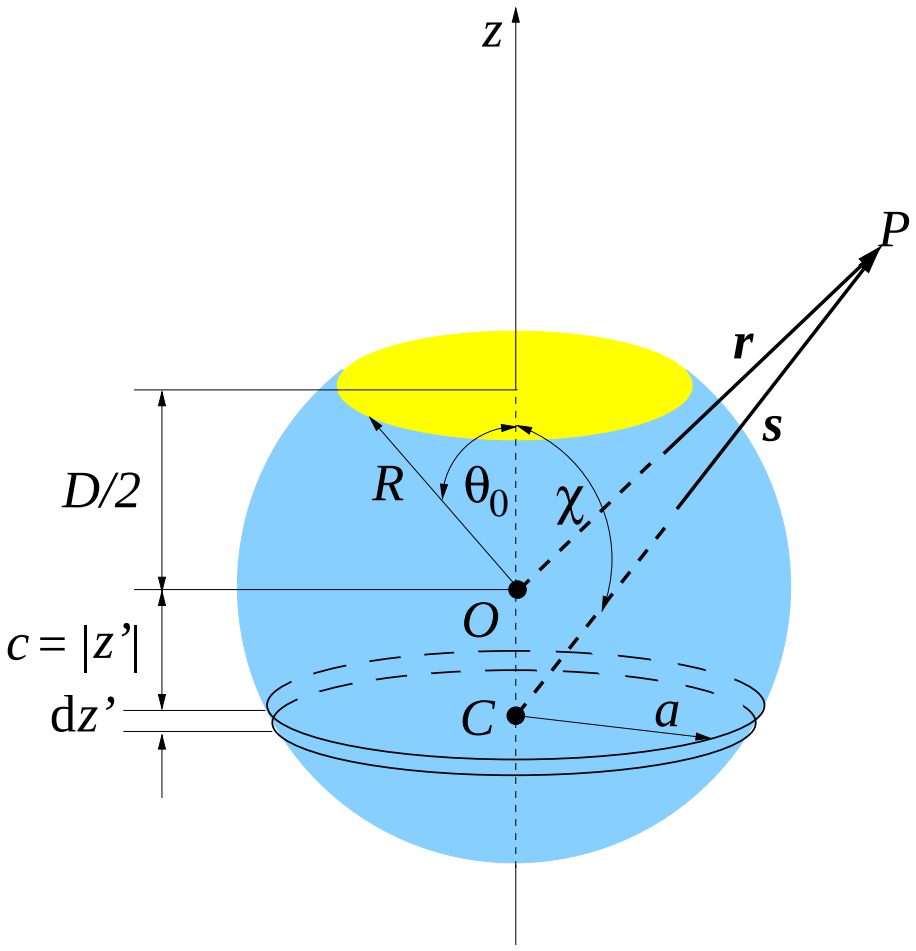

Figure C.1: A sketch of the chopped sphere showing the geometry of the problem and demonstrating the procedure used for the calculation of the electrostatic potentials.

whereas the radius a of the disc is given by

$$a = \sqrt{R^2 - z'^2}. \tag{C.4}$$

The elementary contribution of the disc to the electrostatic potential at the point P, $\mathrm{d}\Phi_{\mathrm{disc}}(\boldsymbol{r}; z')$, depends parametrically on the disc-center location z'. Its calculation follows from further decomposing the disc into concentric rings of radius ξ centered at C, making use of the known results for the electrostatic potential of a charged ring [171, 172], and integrating thereafter from $\xi = 0$ to $\xi = a$. Note that, due to the inhomogeneous, $\propto (r')^{-2}$ dependence of the charge density inside the sphere, we are now dealing with discs that have inhomogeneous charge densities as function of ξ themselves, and which vary as $\propto (\xi^2 + c^2)^{-1}$. The integration over the rings can be nevertheless carried out analytically.

We employ cylindrical coordinates and also introduce the vector $\boldsymbol{s}$ connecting the disc center with the observation point P, see Fig. C.1. We have, evidently, $\boldsymbol{r} = (\rho, \phi, z)$ and $\boldsymbol{s} =$

$(\rho, \phi, z-z')$, with the distance from the z-axis ρ and the azimuthal angle ϕ. Due to azimuthal symmetry, it holds $\mathrm{d}\Phi_{\rm disc}(\boldsymbol{r}, z') = \mathrm{d}\Phi_{\rm disc}(\rho, z; z')$. It is convenient as an intermediate step to express the sought-for potential in a shifted system of axes, whose origin lies at the center C of the disc, and in which the potential is expressed by another function $\mathrm{d}\Phi'$, i.e., we write:

$$\mathrm{d}\Phi_{\rm disc}(\rho, z; z') = \mathrm{d}\Phi'(\rho, z - z'; z'), = \mathrm{d}\Psi(s, \chi; z'). \tag{C.5}$$

Here, s is the magnitude of the vector $\boldsymbol{s}$ and χ is the angle between $\boldsymbol{s}$ and the z-axis. The coordinates s and χ are related to the original ones through:

$$s = \sqrt{\rho^2 + (z - z')^2}; \tag{C.6}$$

$$\cos\chi = \frac{z - z'}{\rho^2 + (z - z')^2}. \tag{C.7}$$

The function $\mathrm{d}\Psi(s, \chi; z')$ can be obtained analytically through the integration over rings mentioned above. The result reads as follows.

$$\mathrm{d}\Psi(s, \chi; z') = \begin{cases} \mathrm{d}\Psi_<(s, \chi; z') & \text{for } s \le a; \\ \mathrm{d}\Psi_>(s, \chi; z') & \text{for } s > a. \end{cases} \tag{C.8}$$

The term $\mathrm{d}\Psi_<(s, \chi; z')$ is given by:

$$\mathrm{d}\Psi_<(s, \chi; z') = \frac{2\,\mathrm{d}Q}{\varepsilon \ln[1 + (a/c)^2]} \frac{1}{c} \sum_{k=0}^{\infty} P_{2k}(0) P_{2k}(\cos\chi)\, \left[A_k(s; z') + B_k(s; z')\right], \tag{C.9}$$

where $P_m(x)$ is the Legendre polynomial of order m,

$$A_k(s; z') = \left(\frac{s}{c}\right)^{-(2k+1)} \left\{ \frac{(-1)^k}{2} \ln\left[1 + \left(\frac{s}{c}\right)^2\right] + \sum_{j=1}^{k} \frac{(-1)^{j+k}}{2j} \left(\frac{s}{c}\right)^{2j} \right\}, \tag{C.10}$$

and

$$B_k(s; z') = \left(\frac{s}{c}\right)^{2k} \left\{ (-1)^k \left[\tan^{-1}\left(\frac{a}{c}\right) - \tan^{-1}\left(\frac{s}{c}\right)\right] - \sum_{j=1}^{k} \frac{(-1)^{j+k}}{2j-1} \left[\left(\frac{c}{a}\right)^{2j-1} - \left(\frac{c}{s}\right)^{2j-1}\right] \right\}. \tag{C.11}$$

The term $\mathrm{d}\Psi_>(z, \boldsymbol{s})$ is given by:

$$\begin{aligned} \mathrm{d}\Psi_>(s, \chi; z') &= \frac{2\,\mathrm{d}Q}{\varepsilon \ln[1 + (a/c)^2]} \frac{1}{c} \\ &\times \sum_{k=0}^{\infty} P_{2k}(0) P_{2k}(\cos\chi) \left(\frac{c}{s}\right)^{2k+1} \left\{ \sum_{j=1}^{k} \frac{(-1)^{j+k}}{2j} \left(\frac{a}{c}\right)^{2j} + \frac{(-1)^k}{2} \ln\left[1 + \left(\frac{a}{c}\right)^2\right] \right\}. \end{aligned} \tag{C.12}$$

The electrostatic potential caused by the *single* chopped sphere, $\Phi_{\rm chop}(\boldsymbol{r})$ at point P can be obtained by a z'-integration

$$\Phi_{\rm chop}(\boldsymbol{r}) = \int_{z'=-R}^{z'=D/2} \mathrm{d}\Phi_{\rm disc}(\rho, z; z') = \int_{z'=-R}^{z'=D/2} \mathrm{d}\Psi\left(s(\rho, z; z'), \chi(\rho, z; z'); z'\right). \tag{C.13}$$

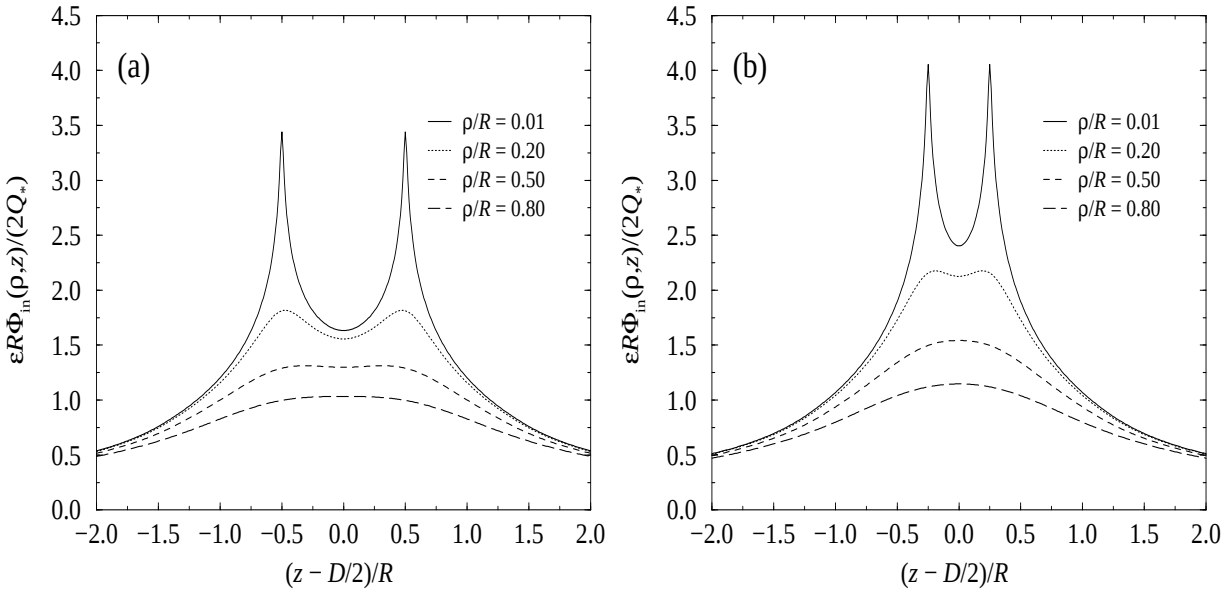

Figure C.2: The electrostatic potential $\Phi_{\rm in}(\boldsymbol{r})$ for two inhomogeneously charged, chopped fused spheres of radius R, plotted as a function of z along paths of fixed distance ρ from the z-axis. (a) Center-to-center distance $D = R$; (b) $D = R/2$. The curves are shown in the cylindrical coordinates introduced in Fig. C.1. The centers of the spheres are located at the z-positions for which the upper curves have sharp peaks.

Due to symmetry, the *total* electrostatic potential $\Phi_{\rm in}(\boldsymbol{r})$ caused by *both* fused spheres at the observation point P is given as

$$\Phi_{\rm in}(\boldsymbol{r}) = \Phi_{\rm chop}(\boldsymbol{r}) + \Phi_{\rm chop}(\boldsymbol{D} - \boldsymbol{r}), \tag{C.14}$$

where $\boldsymbol{D} = D\hat{\boldsymbol{e}}_z$. In Fig. C.2, we show representative results for $\Phi_{\rm in}(\boldsymbol{r})$ obtained with this procedure.

The integral in Eq. (C.13) cannot be carried out analytically and one has to resort to a simple, one-dimensional numerical integration. In performing this integral by using Eqs. (C.8) - (C.12) together with Eqs. (C.2) - (C.7), all k- and j-sums appearing there must be made manifestly convergent, i.e., the sums have to be expressed in terms of a variable $x < 1$ raised to positive powers. For this purpose, it is necessary, depending on whether $s < c$ or $s > c$, to make expansions of the logarithmic and/or the inverse tangent functions in Eqs. (C.10) and (C.11). The expressions suitable for the numerical integration are given below for completeness and convenience.

Case I: $s < c < a$ or $s < a < c$.

$$\mathrm{d}\Psi_<(s,\chi;z') = \frac{2\,\mathrm{d}Q}{\varepsilon \ln[1+(a/c)^2]}\,\frac{1}{c}\sum_{k=0}^{\infty} P_{2k}(0)P_{2k}(\cos\chi)\,\left[C_k(s;z') + D_k(s;z') + E_k(s;z')\right], \tag{C.15}$$

where

$$C_k(s;z') = \sum_{j=k+1}^{\infty} \frac{(-1)^{j+k+1}}{2j} \left(\frac{s}{c}\right)^{2(j-k)-1}; \tag{C.16}$$

$$D_k(s;z') = \left(\frac{s}{c}\right)^{2k} (-1)^k \left[\tan^{-1}\left(\frac{a}{c}\right) - \tan^{-1}\left(\frac{s}{c}\right)\right]; \tag{C.17}$$

$$E_k(s;z') = \sum_{j=1}^{k} \frac{(-1)^{j+k+1}}{2j-1} \left(\frac{s}{c}\right)^{2(k-j)+1} \left[\left(\frac{s}{a}\right)^{2j-1} - 1\right]. \tag{C.18}$$

Case II: $c < s < a$.

$$\mathrm{d}\Psi_<(s,\chi;z') = \frac{2\,\mathrm{d}Q}{\varepsilon \ln[1+(a/c)^2]} \frac{1}{c} \sum_{k=0}^{\infty} P_{2k}(0) P_{2k}(\cos\chi)\ [F_k(z,s) + G_k(z,s) + H_k(z,s)]\,, \tag{C.19}$$

where

$$F_k(s;z') = \left(\frac{c}{s}\right)^{2k+1} \frac{(-1)^k}{2} \ln\left[1 + \left(\frac{s}{c}\right)^2\right]; \tag{C.20}$$

$$G_k(s;z') = \sum_{j=1}^{k} \frac{(-1)^{j+k}}{2j} \left(\frac{c}{s}\right)^{2(k-j)+1}; \tag{C.21}$$

$$H_k(s;z') = \sum_{j=k+1}^{\infty} \frac{(-1)^{j+k}}{2j-1} \left(\frac{c}{s}\right)^{2(j-k)-1} \left[\left(\frac{s}{a}\right)^{2j-1} - 1\right]. \tag{C.22}$$

Case III: $a < s < c$.

$$\begin{aligned} \mathrm{d}\Psi_>(s,\chi;z') &= \frac{2\,\mathrm{d}Q}{\varepsilon \ln[1+(a/c)^2]} \frac{1}{c} \\ &\times \sum_{k=0}^{\infty} P_{2k}(0) P_{2k}(\cos\chi) \sum_{j=k+1}^{\infty} \frac{(-1)^{j+k+1}}{2j} \left(\frac{a}{s}\right)^{2j} \left(\frac{s}{c}\right)^{2(j-k)-1}. \end{aligned}$$

Case IV: $c < a < s$.

$$\mathrm{d}\Psi_>(s,\chi;z') = \frac{2\,\mathrm{d}Q}{\varepsilon \ln[1+(a/c)^2]} \frac{1}{c} \sum_{k=0}^{\infty} P_{2k}(0) P_{2k}(\cos\chi)[I_k(s;z') + J_k(s;z')], \tag{C.23}$$

where

$$I_k(s;z') = \sum_{j=1}^{k} \frac{(-1)^{j+k}}{2j} \left(\frac{a}{s}\right)^{2(k-j)+1} \left(\frac{c}{s}\right)^{2j}; \tag{C.24}$$

$$J_k(s;z') = \frac{(-1)^k}{2} \ln\left[1 + \left(\frac{a}{c}\right)^2\right] \left(\frac{c}{s}\right)^{2k+1}. \tag{C.25}$$

Case V: $a < c < s$. Here, $\mathrm{d}\Psi_>(s,\chi;z')$ can be taken directly from Eq. (C.12), as all parameters appearing in the sums are smaller than unity.

C.2 Calculation of the electrostatic potential Φ_{out}

In order to calculate the electrostatic potential $\Phi_{\text{out}}(\boldsymbol{r})$, caused by the hollow fused spheres of the free counterions that reside in the volume V_{out} (see Fig. 3.8), we employ the superposition principle. Thereby, the aforementioned hollow region of uniform charge density $\varrho_{\text{out}}(\boldsymbol{r})$ is apprehended as the superposition of two fused spheres of radius R_W with charge density $\varrho_{\text{out}}(\boldsymbol{r})$ and of two smaller fused spheres, of radius R, with charge density $-\varrho_{\text{out}}(\boldsymbol{r})$. In this way, the problem is reduced to the calculation of the electrostatic potential of two fused spheres with uniform charge density. The geometrical setup as well as the method of calculation are identical to those presented in Appendix C.1. Thereby, the electrostatic potential $\mathrm{d}\Phi_{\text{disc}}(\boldsymbol{r})$ is still given by expressions of the form (C.5)-(C.8), however Eqs. (C.2), (C.9) and (C.12) have to be replaced by their counterparts valid for homogeneous charge distributions. The corresponding expressions for spheres of radius R are given below.

$$\mathrm{d}Q = \pi Q_* \left(R^2 - z'^{\,2}\right) \left\{ \frac{2\pi R^3}{3} \left[1 + \frac{3}{2}\left(\frac{D}{2R}\right) - \frac{1}{2}\left(\frac{D}{2R}\right)^3 \right] \right\}^{-1} \mathrm{d}z', \tag{C.26}$$

$$\mathrm{d}\Psi_<(s,\chi;z') = \frac{2\,\mathrm{d}Q}{\varepsilon a} \sum_{k=0}^{\infty} P_{2k}(0) P_{2k}(\cos\chi) \left[\frac{4k+1}{2(k+1)(2k-1)} \left(\frac{s}{a}\right) - \frac{1}{2k-1} \left(\frac{s}{a}\right)^{2k} \right], \tag{C.27}$$

and

$$\mathrm{d}\Psi_>(s,\chi;z') = \frac{2\,\mathrm{d}Q}{\varepsilon s} \sum_{k=0}^{\infty} \frac{P_{2k}(0) P_{2k}(\cos\chi)}{2(k+1)} \left(\frac{a}{s}\right)^{2k}. \tag{C.28}$$

The substitution $R \to R_W$ yields the corresponding ones for the fused spheres of radius R_W. Note that the term in the curly brackets in Eq. (C.26) is the volume of the chopped sphere.

Bibliography

[1] D. Frenkel and B. Smit, *Understanding Molecular Simulation*, Academic Press, San Diego, 1996.

[2] M. P. Allen and D. J. Tildesley, *Computer Simulation of Liquids*, Clarendon Press, Oxford, 1987.

[3] S. Asakura and F. Oosawa, *J. Chem. Phys.* **22**, 1255 (1954).

[4] P. J. Flory and W. R. Krigbaum, *J. Chem. Phys.* **18**, 1086 (1950).

[5] T. A. Witten, P. A. Pincus, and M. E. Cates, *Europhys. Lett.* **2**, 137 (1986).

[6] P. J. Flory, *Principles of Polymer Chemistry*, Cornell University Press, Ithaca, 1953.

[7] P. G. de Gennes, *Scaling Concepts in Polymer Physics*, Cornell University Press, Ithaca, 1979.

[8] J. des Cloizeaux and G. Jannink, *Polymers in Solution*, Clarendon Press, Oxford, 1990.

[9] M. Doi, *Introduction to Polymer Physics*, Clarendon Press, Oxford, 1996.

[10] M. Doi and S. F. Edwards, *The Theory of Polymer Dynamics*, Clarendon Press, Oxford, 1986.

[11] G. S. Grest, L. J. Fetters, J. S. Huang, and D. Richter, *Adv. Chem. Phys.* **XCIV**, 67 (1996).

[12] M. Daoud and J. P. Cotton, *J. Physique* **43**, 531 (1982).

[13] J. L. Alessandrini and M. A. Carignano, *Macromolecules* **25**, 1157 (1992).

[14] D. Richter, O. Jucknischke, L. Willner, L. J. Fetters, M. Lin, J. S. Huang, J. Roovers, C. Toporowski, and L. L. Zhou, *J. Physique IV Suppl.* **3**, 3 (1993).

[15] C. Gay and E. Raphael, *J. Phys. II France* **6**, 587 (1996).

[16] A. P. Gast, *Curr. Opinion Coll. Int. Sci.* **2**, 258 (1997).

[17] J. Stellbrink, J. Allgaier, M. Monkenbusch, D. Richter, A. Lang, C. N. Likos, M. Watzlawek, H. Löwen, G. Ehlers, and P. Schleger, *Progr. Coll. Polym. Sci.* **115**, 88 (2000).

[18] G. S. Grest, K. Kremer, and T. A. Witten, *Macromolecules* **20**, 1376 (1987).

[19] K. Ohno, *Phys. Rev. A* **40**, 1524 (1989).

[20] G. S. Grest, *Macromolecules* **27**, 3493 (1994).

[21] A. Forni, F. Ganazzoli, and M. Vacatello, *Macromolecules* **29**, 2994 (1996).

[22] J. J. Freire, *Adv. Polym. Sci.* **143**, 35 (1999).

[23] L. A. Molina and J. J. Freire, *Macromolecules* **32**, 499 (1999).

[24] J. Roovers, *Macromolecules* **27**, 5359 (1994).

[25] D. Vlassopoulos, T. Pakula, G. Fytas, M. Pitsikalis, and N. Hadjichristidis, *J. Chem. Phys.* **111**, 1760 (1999).

[26] D. Vlassopoulos, T. Pakula, G. Fytas, J. Roovers, K. Karatasos, and N. Hadjichristidis, *Europhys. Lett.* **39**, 617 (1997).

[27] C. N. Likos, H. Löwen, M. Watzlawek, B. Abbas, O. Jucknischke, J. Allgaier, and D. Richter, *Phys. Rev. Lett.* **80**, 4450 (1998).

[28] A. Jusufi, M. Watzlawek, and H. Löwen, *Macromolecules* **32**, 4470 (1999).

[29] A. M. Rubio and J. J. Freire, *Comp. Theor. Polymer Sci.* **10**, 89 (2000).

[30] C. von Ferber, A. Jusufi, C. N. Likos, H. Löwen, and M. Watzlawek, *Eur. Phys. J. E* **2**, 311 (2000).

[31] M. Watzlawek, H. Löwen, and C. N. Likos, *J. Phys.: Condens. Matter* **10**, 8189 (1998).

[32] M. Watzlawek, C. N. Likos, and H. Löwen, *Phys. Rev. Lett.* **82**, 5289 (1999).

[33] C. von Ferber, A. Jusufi, M. Watzlawek, C. N. Likos, and H. Löwen, *Phys. Rev. E* **62**, 6949 (2000).

[34] J. Dzubiella, A. Jusufi, C. N. Likos, C. von Ferber, H. Löwen, J. Stellbrink, J. Allgaier, D. Richter, A. B. Schofield, P. A. Smith, W. C. K. Poon, and P. N. Pusey, *Phys. Rev. E* **64**, 010401(R) (2001).

[35] A. Jusufi, J. Dzubiella, C.N.Likos, C. von Ferber, and H. Löwen, *J. Phys.: Cond. Matt.* **13**, 6177 (2001).

[36] J. Dzubiella, C. N. Likos, and H. Löwen, Phase behavior and structure of star-polymer–colloid mixtures, submitted to The Journal of Chemical Physics, 2002.

[37] G. S. Manning, *J. Chem. Phys.* **51**, 924 (1969).

[38] H. Schiessel and P. Pincus, *Macromolecules* **31**, 7953 (1998).

[39] B. V. Derjaguin and L. D. Landau, *Acta Physicochim. USSR* **14**, 633 (1941).

[40] E. J. W. Verwey and J. T. Overbeek, *Theory of the Stability of Lyophobic Colloids*, Elsevier, Amsterdam, 1948.

[41] M. Heinrich, M. Rawiso, J. G. Zilliox, P. Lesieur, and J. P. Simon, *Eur. Phys. J. E* **4**, 131 (2001).

[42] X. Guo and M. Ballauff, *Langmuir* **16**, 8719 (2000).

[43] Q. de Robillard, X. Guo, M. Ballauff, and T. Narayanan, *Macromolecules* **33**, 9109 (2000).

[44] X. Guo and M. Ballauff, *Phys. Rev. E* **64**, 051406 (2001).

[45] O. V. Borisov, *J. Phys. II (France)* **6**, 1 (1996).

[46] O. V. Borisov and E. B. Zhulina, *J. Phys. II (France)* **7**, 449 (1997).

[47] O. V. Borisov and E. B. Zhulina, *Eur. Phys. J. B* **4**, 205 (1998).

[48] J. Klein Wolterink, F. A. M. Leermakers, G. J. Fleer, L. K. Koopal, E. B. Zhulina, and O. V. Borisov, *Macromolecules* **32**, 2365 (1999).

[49] P. Pincus, *Macromolecules* **24**, 2912 (1991).

[50] M. J. Stevens and K. Kremer, *Phys. Rev. Lett.* **71**, 2228 (1993).

[51] M. J. Stevens and K. Kremer, *J. Chem. Phys.* **103**, 1669 (1995).

[52] U. Micka, C. Holm, and K. Kremer, *Langmuir* **15**, 4033 (1999).

[53] C. N. Likos, *Phys. Rep.* **348**, 267 (2001).

[54] A. Jusufi, C. N. Likos, and H. Löwen, *Phys. Rev. Lett.* **87**, 018301 (2002).

[55] A. Jusufi, C. N. Likos, and H. Löwen, *J. Chem. Phys.* **116**, 11011 (2002).

[56] J. Dzubiella and A. Jusufi, *Cond. Matt. Phys.* **5** (2002).

[57] J.-P. Hansen and I. R. McDonald, *Theory of Simple Liquids*, Academic Press, London, second edition, 1986.

[58] J. Lekner, *Physica A* **176**, 524 (1991).

[59] *Physik der Polymere*, volume **22** of *IFF-Ferienkurs*, (1991).

[60] B. Zimm, W. H. Stockmayer, and M. Fixman, *J. Chem. Phys.* **21**, 1716 (1953).

[61] W. H. Stockmayer, *Macromol. Chem.* **35**, 54 (1960).

[62] J. Zinn-Justin, *Phys. Rep.* **70**, 101 (1981).

[63] P. Grassberger, R. Hegger, and L. Schäfer, *J. Phys. A: Math. Gen.* **27**, 7265 (1994).

[64] S. T. Sun, I. Nishio, G. Swislow, and T. Tanaka, *J. Chem. Phys.* **73**, 5971 (1980).

[65] H. Dautzenberg, W. Jaeger, J. K"otz, B. Philipp, C. Seidel, and D. Stscherbina, *Polyelectrolytes - Formation, Characterization and Applications*, Hanser Publishers, Munich, 1994.

[66] F. Oosawa, *Polyelectrolytes*, Marcel Decker, New York, 1970.

[67] T. Odijk and A. H. Houwaart, *J. Polym. Sci., Polym. Phys.* **16**, 627 (1978).

[68] J.-L. Barrat and J. Joanny, *Adv. Chem. Phys* **103**, 1 (1995).

[69] J. S. Higgins and H. C. Benoît, *Polymers and Neutron Scattering*, Clarendon Press, Oxford, 1994.

[70] O. Gratter and O. Kratky, *Small Angle X-Ray Scattering*, Academic Press, New York, 1982.

[71] C. Caccamo, J.-P. Hansen, and J. Rychaert, editors, *New Approaches to Problems in Liquid State Theory*, Kluwer Academic, Dordrecht, 1999.

[72] M. Dijkstra, R. van Roij, and R. Evans, *Phys. Rev. Lett* **81**, 2268 (1998).

[73] M. Dijkstra, R. van Roij, and R. Evans, *Phys. Rev. Lett* **82**, 117 (1999).

[74] M. Dijkstra, R. van Roij, and R. Evans, *Phys. Rev. E* **59**, 5744 (1999).

[75] P. N. Pusey, in *Les Houches, Session LI, Liquids, Freezing and Glass Transition*, North-Holland, Amsterdam, 1991, ed. by J.-P. Hansen, D. Levesque and J. Zinn-Justin.

[76] H. Löwen and G. Kramposthuber, *Europhys. Lett.* **23**, 673 (1993).

[77] Y. Kamiyama and J. Israelachvili, *Macromolecules* **25**, 5081 (1992).

[78] N. Kawanishi, H. K. Christenson, and B. W. Ninham, *J. Phys. Chem.* **94**, 4611 (1990).

[79] P. Richetti and P. Kekicheff, *Phys. Rev. Lett.* **68**, 1951 (1992).

[80] A. Milling and S. Biggs, *J. Coll. Int. Sci.* **170**, 604 (1995).

[81] D. C. Prieve, F. Luo, and F. Lanni, *Faraday Discuss. Chem. Soc.* **83**, 297 (1987).

[82] D. C. Prieve and J. Y. Walz, *Appl. Opt.* **32**, 1629 (1993).

[83] A. Sharma, S. N. Tan, and J. Y. Walz, *J. Coll. Int. Sci.* **191**, 236 (1997).

[84] D. C. Prieve, *Adv. Coll. Int. Sci.* **82**, 93 (1999).

[85] P. L. D. Rudhardt, C. Bechinger, *Phys. Rev. Lett.* **81**, 1330 (1998).

[86] M. Watzlawek, *Phase Behavior of Star Polymers*, Shaker-Verlag, Aachen, 2000.

[87] A. Yethiraj and C.-Y. Shew, *Phys. Rev. Lett.* **77**, 3937 (1996).

[88] A. Yethiraj, *Phys. Rev. Lett.* **78**, 3789 (1997).

[89] N. V. Brillantov, D. V. Kuznetzov, and R. Klein, *Phys. Rev. Lett.* **81**, 1433 (1998).

[90] R. G. Winkler, M. Gold, and P. Reineker, *Phys. Rev. Lett.* **80**, 3731 (1998).

[91] R. M. Nyquist, B.-Y. Ha, and A. Liu, *Macromolecules* **32**, 3481 (1999).

[92] Y. Kantor and M. Kardar, *Phys. Rev. Lett.* **83**, 745 (1999).

[93] R. Golestanian, M. Kardar, and T. B. Liverpool, *Phys. Rev. Lett.* **82**, 4456 (1999).

[94] L. Harnau and P. Reineker, *J. Chem. Phys.* **112**, 437 (2000).

[95] V. V. Vasilevskaya, A. R. Khokhlov, and K. Yoshikawa, *Macromol. Theory Simul.* **9**, 600 (2000).

[96] J.-F. Joanny, *Eur. Phys. J. E* **5**, 3 (2001).

[97] F. Vongoeller and M. Muthukumar, *Macromolecules* **28**, 6608 (1995).

[98] R. Hariharan, C. Biver, J. Mays, and W. B. Russel, *Macromolecules* **31**, 7506 (1998).

[99] E. B. Zhulina, J. Klein Wolterink, and O. V. Borisov, *Macromolecules* **33**, 4945 (2000).

[100] F. S. Csajka and C. Seidel, *Macromolecules* **33**, 2728 (2000).

[101] F. S. Csajka, R. R. Netz, C. Seidel, and J.-F. Joanny, *Eur. Phys. J. E* **4**, 505 (2001).

[102] P. Pincus, *Macromolecules* **24**, 2912 (1991).

[103] W. Groenenwegen, A. Lapp, S. U. Egelhaaf, and J. R. C. van der Maarel, *Macromolecules* **33**, 4080 (2000).

[104] W. Groenenwegen, S. U. Egelhaaf, A. Lapp, and J. R. C. van der Maarel, *Macromolecules* **33**, 3283 (2000).

[105] W. Essafi, F. Lafuma, and C. E. Williams, *J. Phys. II (France)* **5**, 1269 (1995).

[106] P. Guenoun, F. Muller, M. Delsanti, L. Auvray, Y. J. Chen, J. W. Mays, and M. Tirell, *Phys. Rev. Lett.* **81**, 3872 (1998).

[107] M. Deserno, C. Holm, and S. May, *Macromolecules* **33**, 199 (2000).

[108] E. Y. Kramarenko, A. R. Khokhlov, and K. Yoshikawa, *Macromol. Theory Simul.* **9**, 249 (2000).

[109] J.-P. Hansen and H. Löwen, *Ann. Rev. Phys. Chem.* **51**, 209 (2000).

[110] E. H. Lieb, *Rev. Mod. Phys.* **48**, 553 (1976).

[111] Y. Levin and M. E. Fisher, *Physica A* **225**, 164 (1996).

[112] M. N. Tamashiro, Y. Levin, and M. Barbosa, *Physica A* **258**, 341 (1998).

[113] T. A. Witten and P. A. Pincus, *Macromolecules* **19**, 2509 (1986).

[114] A. R. Denton, unpublished.

[115] A. Lang, C. N. Likos, M. Watzlawek, and H. Löwen, *J. Phys.: Condens. Matter* **12**, 5087 (2000).

[116] C. N. Likos, A. Lang, M. Watzlawek, and H. Löwen, *Phys. Rev. E* **63**, 031206 (2001).

[117] A. A. Louis, P. G. Bolhuis, J.-P. Hansen, and E. J. Meijer, *Phys. Rev. Lett.* **85**, 2522 (2000).

[118] A. A. Louis, P. G. Bolhuis, and J.-P. Hansen, *Phys. Rev. E* **62**, 7961 (2000).

[119] C. N. Likos, M. Schmidt, H. Löwen, M. Ballauff, D. Pötschke, and P. Lindner, *Macromolecules* **34**, 2914 (2001).

[120] A. A. Louis, *Philos. Trans. Ros. Soc. A* **359**, 939 (2001).

[121] A. J. Archer and R. Evans, *Phys. Rev. E* **64**, 041501 (2001).

[122] A. J. Archer and R. Evans, Wetting in the binary Gaussian core model, in press, J. Phys.: Condens. Matter (2002).

[123] C. N. Likos and H. M. Harreis, Star polymers: from conformations to interactions to phase diagrams, in press, Cond. Matt. Phys. (2002).

[124] P. Ziherl and R. D. Kamien, *Phys. Rev. Lett.* **85**, 3528 (2000).

[125] P. Ziherl and R. D. Kamien, *J. Phys. Chem. B* **105**, 10147 (2001).

[126] M. Dijkstra, J. M. Brader, and R. Evans, *J. Phys.: Condens. Matter* **11**, 10079 (1999).

[127] S. M. Ilett, A. Orrock, W. C. K. Poon, and P. N. Pusey, *Phys. Rev. E* **51**, 1344 (1995).

[128] A. Moussaïd, W. C. K. Poon, P. N. Pusey, and M. F. Soliva, *Phys. Rev. Lett.* **82**, 225 (1999).

[129] H. N. W. Lekkerkerker, W. C. K. Poon, P. N. Pusey, A. Stroobants, and P. B. Warren, *Europhys. Lett.* **20**, 559 (1992).

[130] A. A. Louis, R. Finken, and J.-P. Hansen, *Europhys. Lett.* **46**, 741 (1999).

[131] M. Fuchs and K. S. Schweizer, *Europhys. Lett.* **51**, 621 (2000).

[132] S. Asakura and F. Oosawa, *J. Polymer Sci.* **33**, 183 (1958).

[133] A. Vrij, *Pure Appl. Chem.* **48**, 471 (1976).

[134] P. G. Bolhuis, A. A. Louis, J.-P. Hansen, and E. J. Meijer, *J. Chem. Phys.* **114**, 4296 (2001).

[135] C. N. Likos, H. Löwen, A. Poppe, L. Willner, J. Roovers, B. Cubitt, and D. Richter, *Phys. Rev. E* **58**, 6299 (1998).

[136] J. Stellbrink, B. Abbas, J. Allgaier, M. Monkenbusch, D. Richter, C. N. Likos, H. Löwen, and M. Watzlawek, *Progr. Coll. Polym. Sci.* **110**, 25 (1998).

[137] K. Shida, K. Ohno, M. Kimura, and Y. Kawazoe, *Macromolecules* **33**, 7655 (2000).

[138] E. Eisenriegler, *Polymers Near Surfaces*, World Scientific, Singapore, 1993.

[139] T. Bickel, C. M. Marques, and C. Jeppesen, *Phys. Rev. E* **62**, 1124 (2000).

[140] E. Eisenriegler, *Phys. Rev. E* **55**, 3116 (1997).

[141] R. J. Hunter, *Foundations of Colloid Science*, volume I, Clarendon Press, Oxford, 1986.

[142] S. Dietrich and H. W. Diehl, *Z. Phys. B* **43**, 315 (1981).

[143] K. Ohno and K. Binder, *J. Phys. France* **49**, 1329 (1988).

[144] H. W. Diehl and M. Shpot, *Nucl. Phys. B* **528**, 595 (1998).

[145] R. Hegger and P. Grassberger, *J. Phys. A: Math. Gen.* **27**, 4069 (1994).

[146] A. Y. Grosberg, P. G. Khalatur, and A. R. Khokhlov, *Makromol. Chem. Rapid Commun.* **3**, 709 (1982).

[147] L. Schäfer and A. Baumgärtner, *J. Phys. (Paris)* **47**, 1431 (1986).

[148] B. Krüger, L. Schäfer, and A. Baumgärtner, *J. Phys. (Paris)* **50**, 3191 (1989).

[149] K. Ohno, K. Shida, M. Kimura, and Y. Kawazoe, *Macromolecules* **29**, 2269 (1996).

[150] B. M. Axilrod and E. Teller, *J. Chem. Phys.* **11**, 229 (1943).

[151] M. Tau, L. Reatto, R. Magli, P. A. Egelstaff, and F. Barrochi, *J. Phys.: Condens. Matter* **1**, 7131 (1989).

[152] H. Löwen and E. Allahyarov, *J. Phys.: Condens. Matter* **10**, 4147 (1998).

[153] J. des Cloizeaux, *J. Phys. (Paris)* **36**, 281 (1975).

[154] C. von Ferber, *Nucl. Phys. B* **490**, 511 (1997).

[155] C. von Ferber and Y. Holovatch, *Europhys. Lett.* **39**, 31 (1997).

[156] C. von Ferber and Y. Holovatch, *Phys. Rev. E* **56**, 6370 (1997).

[157] R. Car and M. Parinello, *Phys. Rev. Lett.* **55**, 2471 (1985).

[158] H. Löwen, P. A. Madden, and J.-P. Hansen, *J. Chem. Phys.* **98**, 3275 (1993).

[159] T. Pakula, D. Vlassopoulos, G. Fytas, and J. Roovers, *Macromolecules* **31**, 8931 (1998).

[160] J. E. Barnes and P. Hut, *Nature* **324**, 446 (1986).

[161] L. Greengard and V. Rokhlin, *J. Comp. Phys.* **73**, 325 (1987).

[162] R. W. Hockney and J. W. Eastwood, *Computer Simulation Using Particles*, McGraw-Hill International, New York, 1981.

[163] P. P. Ewald, *Ann. Phys.* **64**, 253 (1921).

[164] S. W. de Leeuw, J. W. Perram, and E. R. Smith, *Proc. R. Soc. London* **A373**, 27 and 57 (1980).

[165] T. Darden, D. M. York, and L. G. Pedersen, *J. Chem. Phys.* **98**, 10089 (1993).

[166] E. Madelung, *Phys. Zeitschrift* **19**, 524 (1918).

[167] R. Sperb, *Mol. Sim.* **20**, 179 (1997).

[168] R. J. Mashl and N. Grønbech-Jensen, *J. Chem. Phys.* **109**, 4617 (1998).

[169] N. Grønbech-Jensen, G. Hummer, and K. M. Beardmore, *Mol. Phys.* **92**, 941 (1997).

[170] E. Allahyarov and H. L"owen, *Phys. Rev. E* **62**, 5542 (2000).

[171] J. D. Jackson, *Classical Electrodynamics*, Wiley, New York, 2nd edition, 1975.

[172] W. K. H. Panofsky and M. Phillips, *Classical Electricity and Magnetism*, Addison-Wesley, Reading, 2nd edition, 1962.

Acknowledgement

I wish to thank cordially Professor Dr. Hartmut Löwen for his confidence for providing me the opportunity to perform this work and for his excellent support during the past years. He was always available for discussions and gave me very valuable advises for my future perspectives.

Special thanks I owe HSdoz. Dr. Christos N. Likos for his extreme valuable, friendly support. He inspired me with great ideas and showed me even in scientific problematic situations the right way-out. His confidence gave me the motivation to overcome also difficult times; he has been always right in his optimism. His contributions were indispensable for a successful completion of the work.

I am deeply grateful to Joachim Dzubiella with whom I spent the past three years in a office. With our scientific discussions, his humour and music he cared about a very friendly atmosphere in our office (and the whole department).

I wish to thank also Dr. Christian von Ferber for successful and very friendly research collaborations, as well as Dr. Martin Watzlawek who helped me especially in the beginning of my scientific work. He is a source of fruitful inspiration and gave me confidence for a successful execution of the work.

Special thanks for helpful discussions and valuable hints appertain to Dr. Elshad Allahyarov, Professor Dr. Rainer Grauer, Professor Dr. Eckhard Rebhan, and especially to Dr. Helmut Schiessel for supplying me his phase diagram .

I am very grateful to Ansgar Esztermann, Cord Kielhorn and Alexander Schlensog for ensuring of a "smooth" simulation run on the computer systems. Their tireless work were essential for a successful completion of the simulations.

I wish also to thank the other members of the department for Theoretical Physics II at the Heinrich-Heine-University of Düsseldorf, especially I acknowledge to Holger Harreis, Dr. Martin Heni, Norman Hoffmann, Ralf Pierre and Dr. Matthias Schmidt.

With Jina Nahavandi I could always find the needful distance to the work. She has always supported me in the good as well as in the difficult times; I am very grateful for her tireless patient.

I am also indebted to my parents and my sister for their continous support. They have always kept me grounded and I thank especially my parents who gave me the opportunity for study (shum faleminderit për përkrahjën).

Last, but not least, I would like to thank all my friends, as well as my colleagues from SCR Cambridge for a very nice leisure time I could spent, giving me the needed force for further work (except the day after).

I gratefully acknowledge for financial and collegial support from the Graduiertenkolleg "Hochtemperatur-Plasmaphysik" of the Deutsche Forschungsgemeinschaft.